FORSCHUNGSZENTRUM JÜLICH GmbH

KFA

Projektträger Biologie, Energie, Ökologie (BEO)
International Energy Agency IEA

Implementing Agreement for a Programme of Research and Development on Wind Energy Conversion Systems – Annex XI

23rd Meeting of Experts – Fatigue of Wind Turbines

Golden, Colorado, October 1992

Organized by:
Project Management Organization Biology, Energy, Ecology BEO
Research Centre Jülich GmbH

On behalf of the
Federal Minister for Research and Technology,
The Fluid Mechanics Department
of the Technical University of Denmark

Scientific Coordination:
M. Pedersen (Techn. Univ. of Denmark)
R. Windheim (BEO-KFA Jülich)

Implementing Agreement for a Programme of Research and Development on Wind Energy Conversion Systems – Annex XI

23rd Meeting of Experts – Fatigue of Wind Turbines

Golden, Colorado, October 1992

Organized by:
Project Management Organization Biology, Energy, Ecology BEO
Research Centre Jülich GmbH

On behalf of the
Federal Minister for Research and Technology,
The Fluid Mechanics Department
of the Technical University of Denmark

Scientific Coordination:
M. Pedersen (Techn. Univ. of Denmark)
R. Windheim (BEO-KFA Jülich)

CONTENTS

Meeting Objective

The objective of this meeting is to exchange relevant information concerning wind turbine fatigue, design, analysis, inspection and evaluation.

Wind turbines are subjected to demanding fatigue loads for 10^8 cycles or more throughout their lives. Engineers must design components which are both economic and able to survive for the life of the turbine. Fatigue life predition is an essentiel part of designing viable wind turbine components. High cycle material fatigue properties, full blade fatigue life predictions and verification testing are all critically important in designing a structurally sound turbine system.

Many different groups have been conducting independent research and tests in each of these areas. Past IEA fatigue experts meetings have focused on coupon material testing. This is one of the most important pieces of information the designer must have before he or she can design an efficient struture. Before the design process is complete, the designs must also predict and verify the full fatigue life. For this reason, full blade fatigue testing and certification testing have been added to the relevant topics to be discussed at this meeting. In addition, as large numbers of machines are deployed, it will become important to access fatigue damage using non-destructive techniques in order to certify the safety of turbines as they age.

Bristol Polytechnic
Faculty of Engineering
Coldharbour Lane
Frenchay
Bristol BS16 1QY

IEA - FATIGUE EXPERTS MEETING, October 15-16 1992
NREL, Golden, Colorado, USA

FATIGUE PROPERTIES OF WINGBLADE MATERIALS AND COMPONENTS MANUFACTURED BY THE TRANSVERSE FILAMENT WINDING PROCESS

by

G A Lowe and N D Satterly,
Faculty of Engineering, Bristol Polytechnic, UK*

Abstract

Bristol Polytechnic's main task within the EC JOULE Programme has been to test glass reinforced polyester coupons and D-spars manufactured using the transverse filament winding process. Associated research work funded by the UK Department of Energy has investigated the effect of changing the manufacturing technique in order to improve the design and production process particularly with regard to large wind turbine blades.

Apart from standard static and fatigue testing to characterise the material, the work has also concentrated on examining the relationship between the results obtained from tests of spar samples (components) and spar coupons produced by typical Blade Manufacturers, with those from tests on representative coupons extracted from laboratory produced flat plates.

In order to compare the effect of cyclic loading on small specimens and large structural components manufactured by the same method, various damage accumulation techniques have been incorporated into the test programme. The measurement of damage using reduction of flexural stiffness, hysteresis looping, surface temperature, infra-red inspection and changes in natural frequency are all techniques used or being developed in the work.

The Structures Testing Facility at the Polytechnic is capable of testing fairly large components, up to 8 metres in length and any new spar or blade development can be tested, in perhaps a modified form, to check the fatigue strength.

*now changing to: University of the West of England, Bristol

Introduction

The rotor blades of a wind turbine generator can expect to be subjected to over 100 million fatigue cycles in their lifetime. Thus the choice of materials and an adequate knowledge of their static and fatigue properties are essential elements of rotor design.

Glass-reinforced polyester resins have been used widely for blade manufacture in a form of construction comprising hand-laid aerofoil shells over a machine-wound load-bearing spar. The continued development of these materials is the subject of a collaborative JOULE project [1] being undertaken by a ten partner consortium from Germany, the Netherlands, Belgium, Denmark, Sweden, Norway and the UK.

While actively participating in the main CEC-funded programme, Bristol Polytechnic has also been undertaking supplementary work within a UK Department of Energy research contract. The main tasks here have been to wind spars under different conditions, characterise the material by coupon testing and perform full scale fatigue tests on the spars, in order to compare the results from spars and coupons made using the transverse filament winding process [2]

In all the test work, various NDT methods have been used to measure damage accumulated during the fatigue cycling of the specimen, mainly changes in flexural stiffness, hysteresis area and surface strain, but temperature has also proved to be a sensitive indicator of damage accumulation. Other methods are also being investigated.

Testing of Plate and Coupon Material

Flat plates have been manufactured, in house, using transverse filament tape in order to compare material produced under laboratory conditions with that produced using bulk manufacturing techniques. Two metre lengths of spar were especially manufactured for this purpose at O L Boats in Denmark, coupons being extracted and tested for material characterisation. Coupons were also extracted from a complete 9m spar purchased from O L Boats. In all cases samples were manufactured from Transverse Filament glass Tape (TFT) and isophthalic polyester resin. Note that the tape used consisted of glass fibres woven or knitted with polyester yarn, tests being carried out on samples manufactured from both types representing, respectively, the traditional and more developed tape construction

Three point bend tests in fatigue [3] were performed on all samples, using a Schenck Pulser mechanical resonance machine. Static properties were obtained for each different material to allow the results to be normalised. Figure 1 shows a comparison of fatigue stress with life to failure (severe damage or 10% loss of stiffness) for plate and spar coupon specimens.

It can be seen from the comparison of results in Figure 1 that the flat plate specimens exhibited a better life, as expected, than the tape wound examples. The coupons from the tape wound section lives are not in general quite as good as the laboratory made flat plates, but the coupons extracted from the spar reached considerably lower lives. One key reason for this could be the poor quality of the spar manufacture with misalignment of the fibres with respect to the flexural axis. Nevertheless, this spar was made by a wind turbine blade manufacturer and so the results should be taken seriously. The comparison clearly indicates

a big difference between specially made laboratory samples and production wound material which should not be ignored by designers basing their calculations on data obtained from specially produced samples.

Figure 2 shows a comparison of the Bristol Polytechnic fatigue results on samples tested under three point bending with Riso filament wound material tested in tension. The comparison of testing methods shows similar trends with only a small difference in the two sets of results at high lives.

NDT techniques were used to measure damage accumulated during testing, mainly periodic measurement of stiffness, hysteresis area, surface temperature and change in resonance frequency of the test machine. A plot of these changes during a typical test, taken from the data monitoring system, is shown in Figure 3.

Spar Tests

The inner 5.5 metres of the 9m O L Boats spar was mounted horizontally off the strong wall of the Structures Testing Rig, as shown diagrammatically in Figure 4. A vertical cyclic jack load was applied (R= 0.25) at the end of the cantilever and data logging equipment used to monitor on-line the damage accumulated during test via measurement of strain, stiffness, hysteresis looping and rise of temperature.

The spar was cycled at a load to give a maximum stress consistent with a reasonable life (10^6 cycles), as predicted from coupon data. The frequency was approximately 0.5 Hertz. After only 55000 cycles clear damage was evident in the tension surface at the critical section, and small cracks developed quickly to give fibre failure and a much larger crack in just 100 more cycles. This failure mechanism was recorded with a video camera. Figure 5 shows a view of the spar at failure, where extensive bending is evident under the high loading condition. A further 8000 cycles were applied, at a much reduced load, to measure general degradation of the spar and study more closely accumulation of damage in the cracked region.

The results from this (first) spar test indicated that under a stress ratio of approximately 35%, fatigue failure of the critical tension zone in the spar occurred in the order of 60000 cycles. This result has been high lighted for comparison with the coupon data in Figure 1 and shows a much lower life, which is cause for concern even allowing for the poor quality of the spar.

The overall stiffness of the spar was measured using a displacement transducer mounted at the free end. During the main test the data monitoring system indicated an 8% reduction in stiffness from start of test to failure. It was also found that once the initial damage had been located, by infra-red scanning [4], strain gauges, etc, the measurement of temperature change appeared to correlate reasonably well with the development of the damage.

A second (larger) spar, manufactured by Polymarin in Holland, has now been tested and is shown in Figure 6. The result from this test also indicates a much reduced life compared with coupon data. Only 100000 cycles were achieved but again the applied loading was high, in order to accelerate the fatigue, with corresponding maximum strains well above the normal working strains experienced in practice. The fatigue failure, in this case, started at tape lap joints in the critical strain region and the type of failure is shown in Figures 7 and 8. In order to check the effect of the joint more representative coupon tests are now being undertaken.

Two further spars have been wound at Polymarin and these will be used to further investigate the damage tolerance of the material and structural integrity of spars made using this winding method. In addition, the effect of tape tension is also being considered within the manufacturing process and with a special comparison testing programme.

General comments on the Research Results to date

A useful fatigue testing facility for fibrous composite turbine blade materials and structures has now been developed at Bristol Polytechnic. Considerable experience has also been gained on the measurement of damage accumulated during the testing, but further work is in progress to find better, and more accurate, ways of measuring the damage - particularly at lower testing loads and strains.

There is a clear indication that the fatigue life of spars made using the tape winding process is considerably lower than the life obtained from testing small coupon specimens used to characterise the material. This is cause for concern and more work is scheduled in order to verify this trend. It is clear, however, that the production quality of the material and manufacturing process for the component is extremely important in achieving a good fatigue life.

References

[1] R M Mayer "Fatigue and Design of Wing Blades for Wind Turbines"
Proc EWEC 1991 Conf, Amsterdam.

[2] B J Johansen, M Lilholt and A Lystrup, "Wing Blades of Glass Fibre Reinforced Polyester for a 630 Kw Wind Turbine, Design, Fabrication and Material Testing"
ICCM-3, Paris, August 1980.

[3] G D Sims, "A Vamas Round Robin on Fatigue Test Methods for Polymer Matrix Composites Part 1 - Tensile and Flexural Tests of Unidirectional Material"
NPL Report No DMA(A)180, April 1989

[4] A G Dutton, A D Irving, G M Smith and B R Clayton "Condition Monitoring Techniques for Composite Wind Turbine Blades"
BWEA/DTI Workshop, University of Nottingham, Sept 1992.

Figure 1 SN DATA FOR GRP COMPOSITES

Woven Material

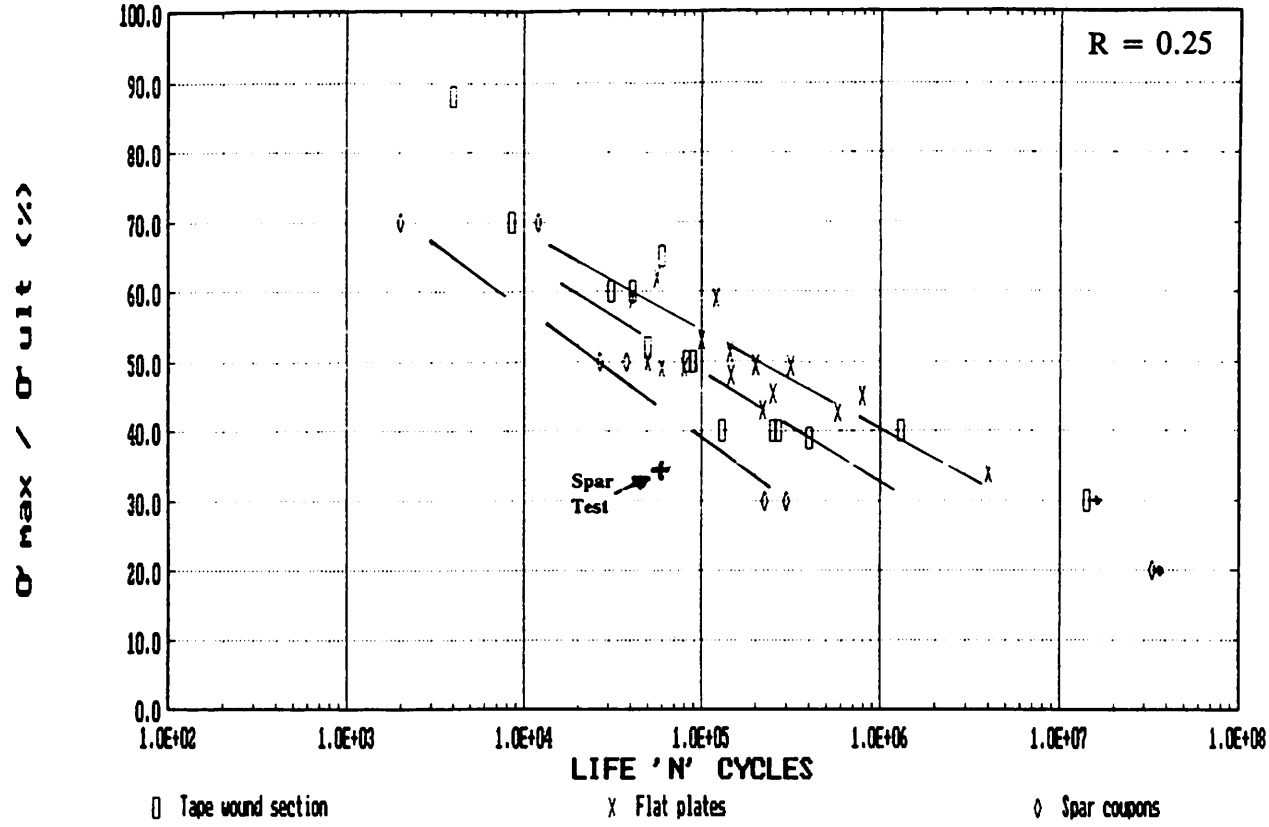

Figure 2 SN DATA FOR GRP COMPOSITES

Woven Material/Riso Filament Wound

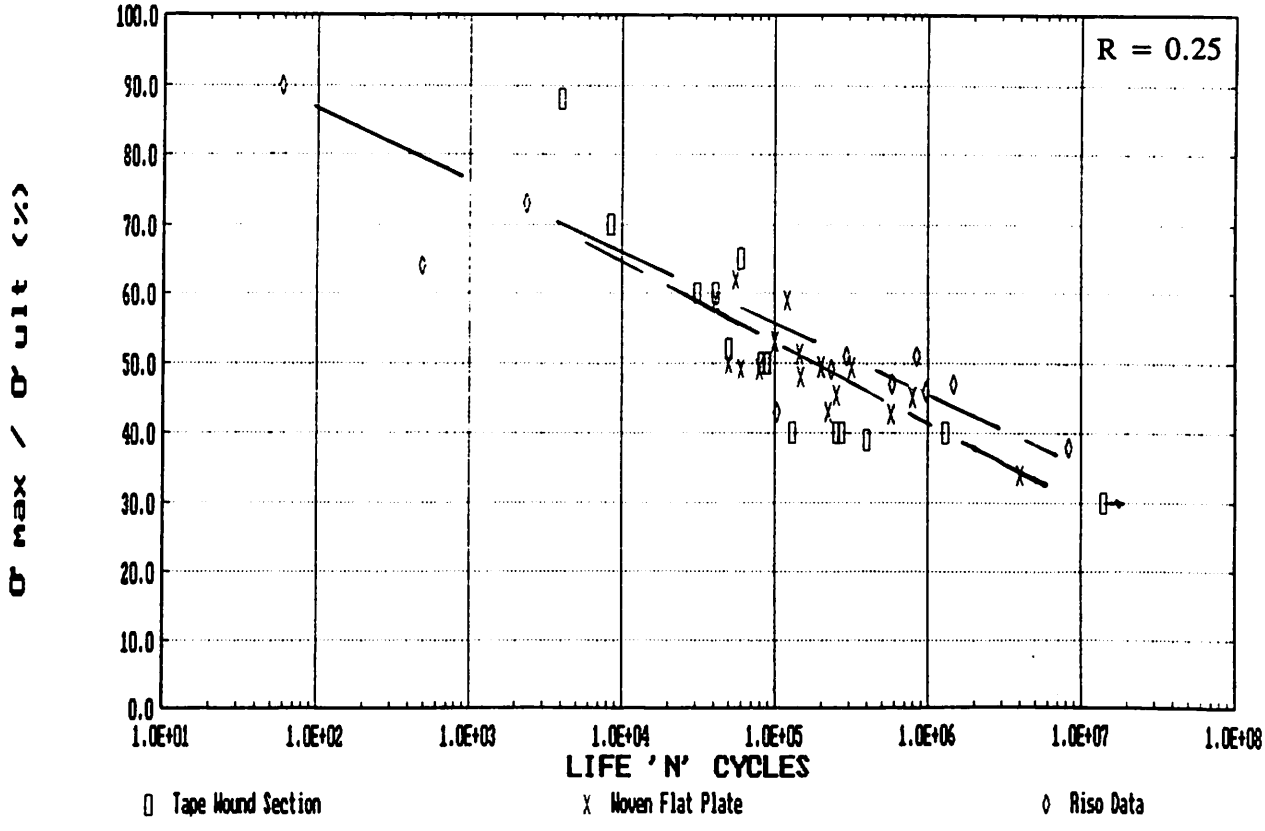

Figure 3 MEASUREMENT OF DAMAGE ACCUMULATION DURING COUPON TESTING

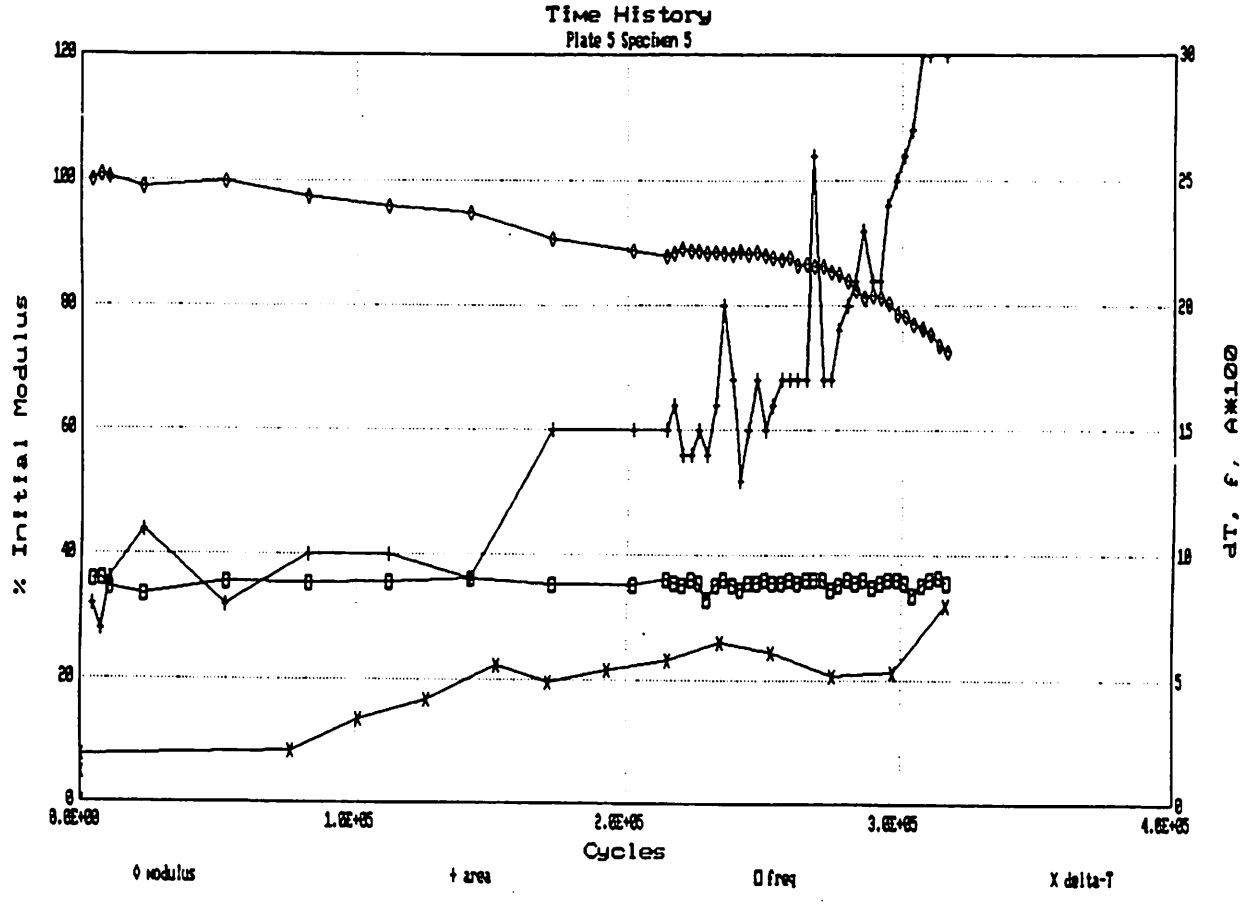

Figure 4 SPAR TEST
General Arrangement

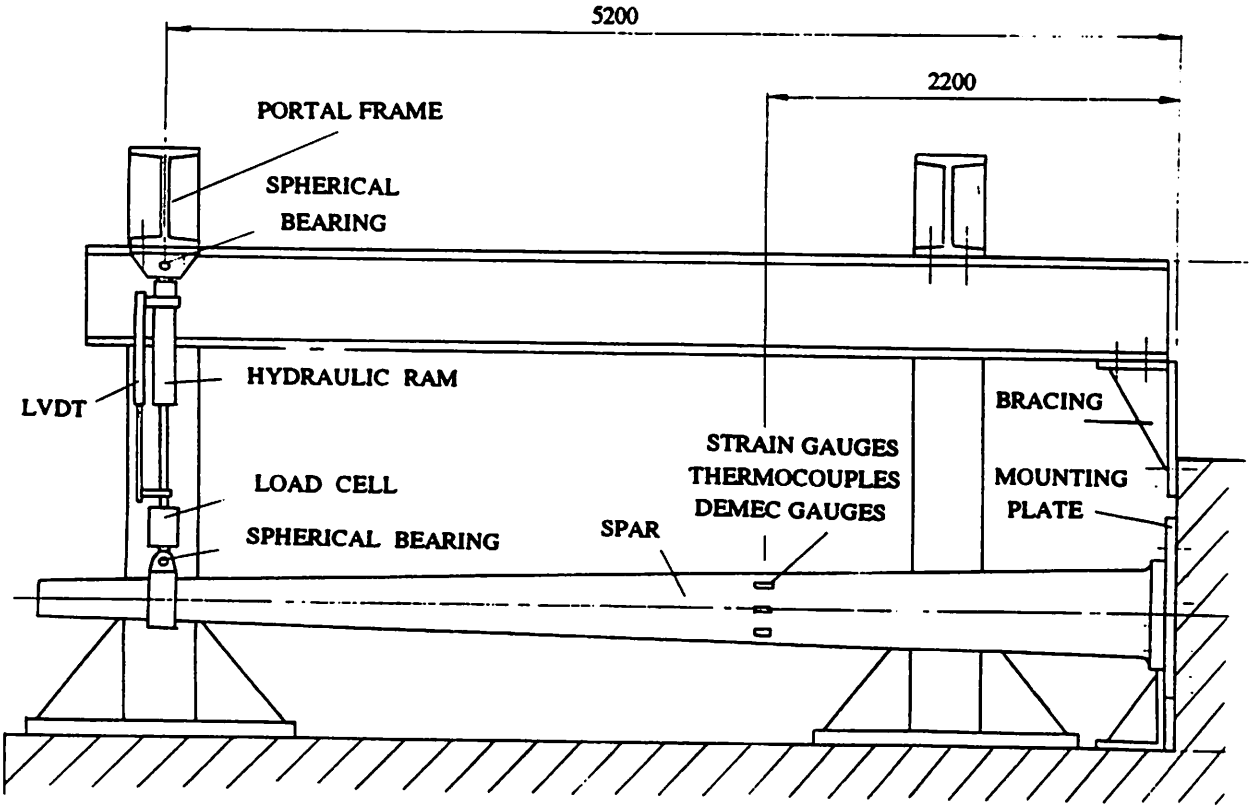

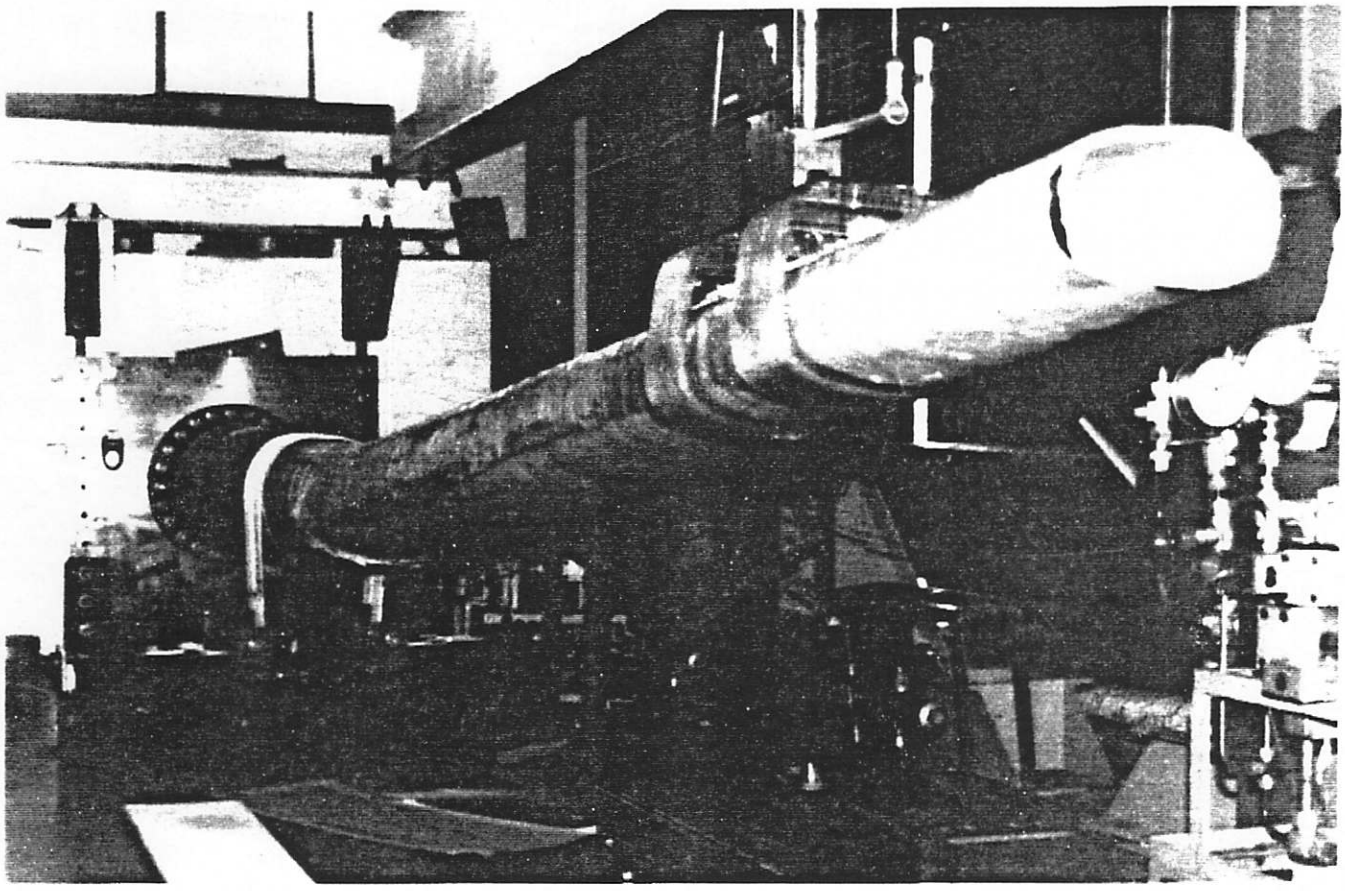

Figure 5. **Fatigue Test of the First Spar - View at Failure**

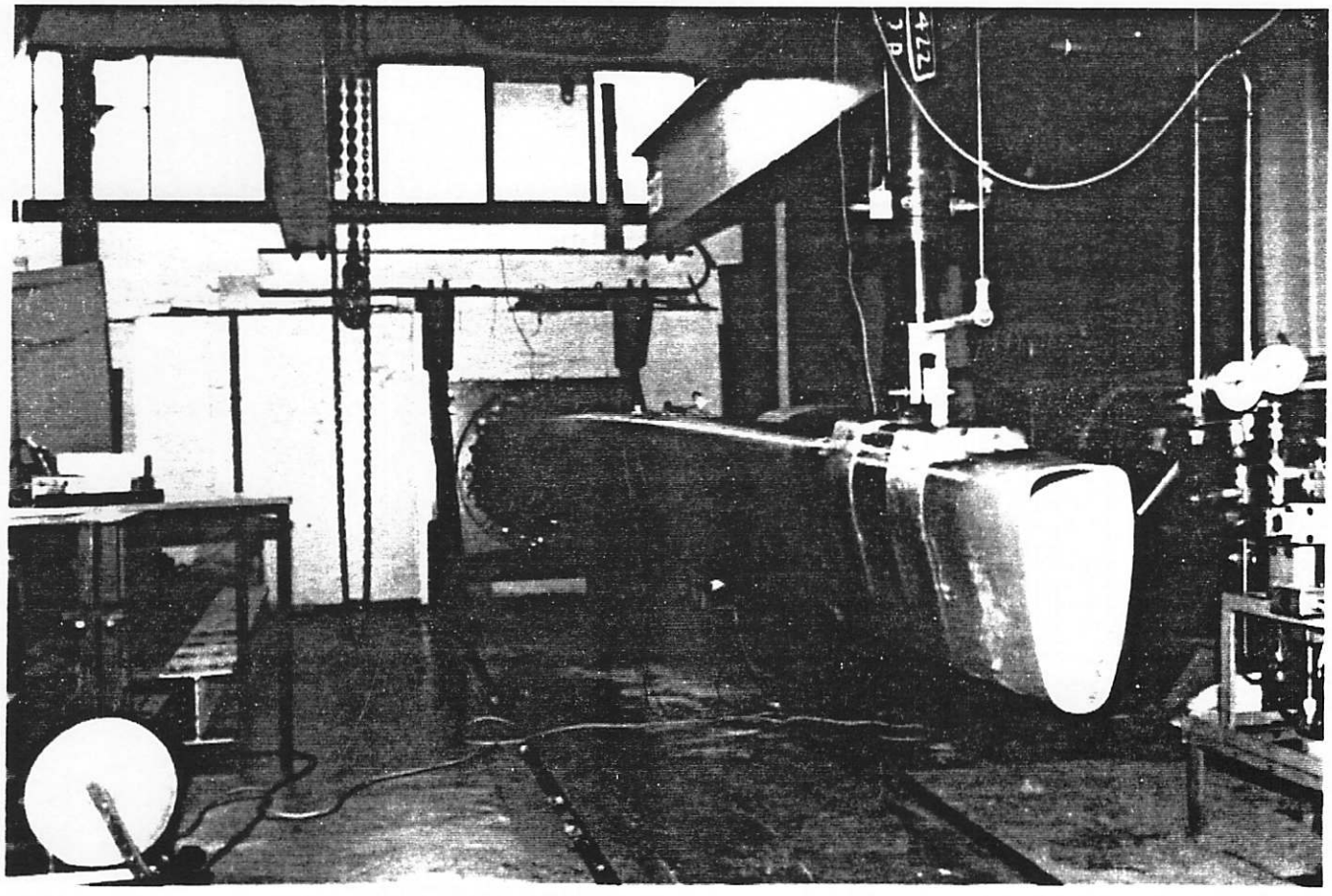

Figure 6. **View of the Second Spar During Test**

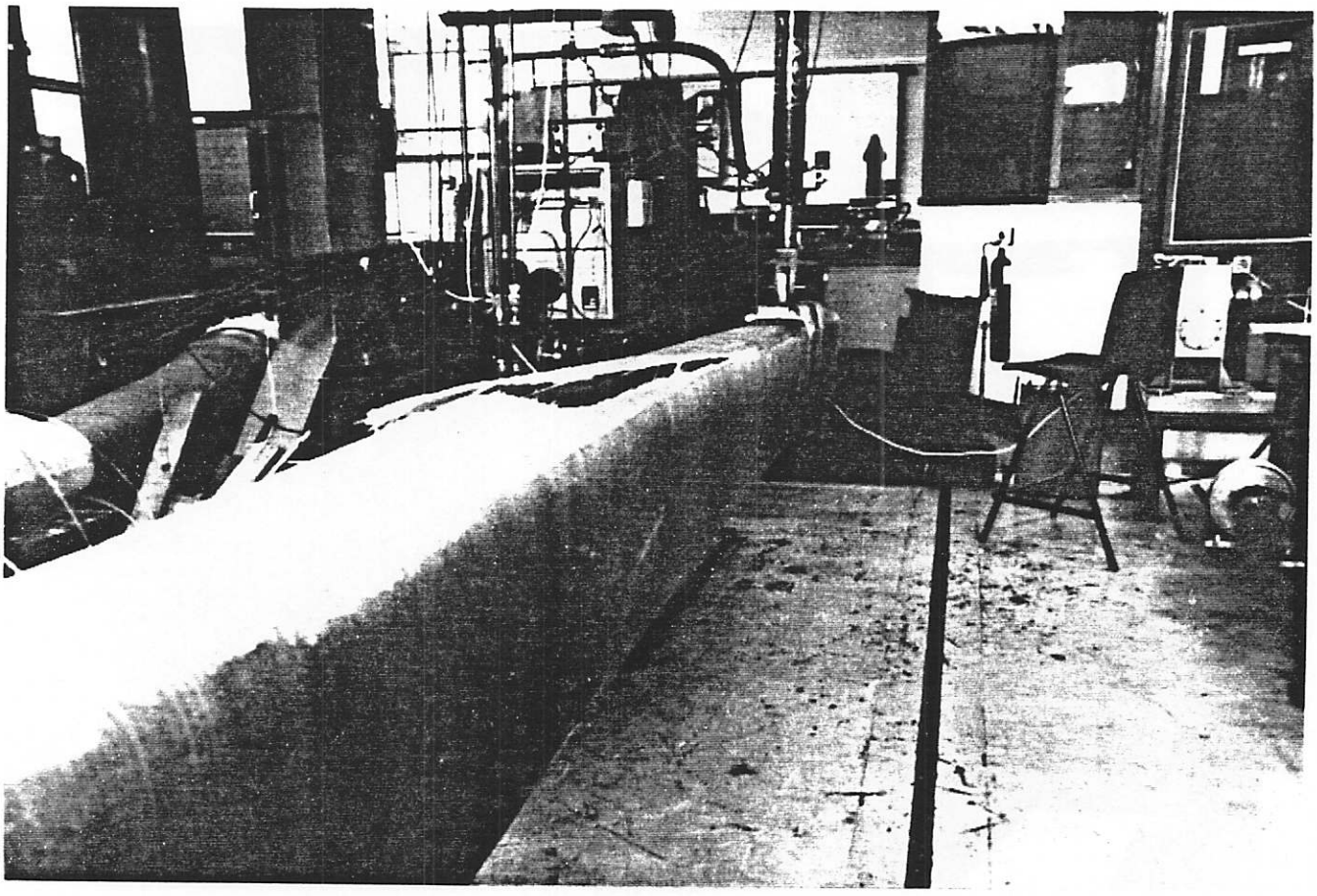

Figure 7. **Failure of the Second Spar**

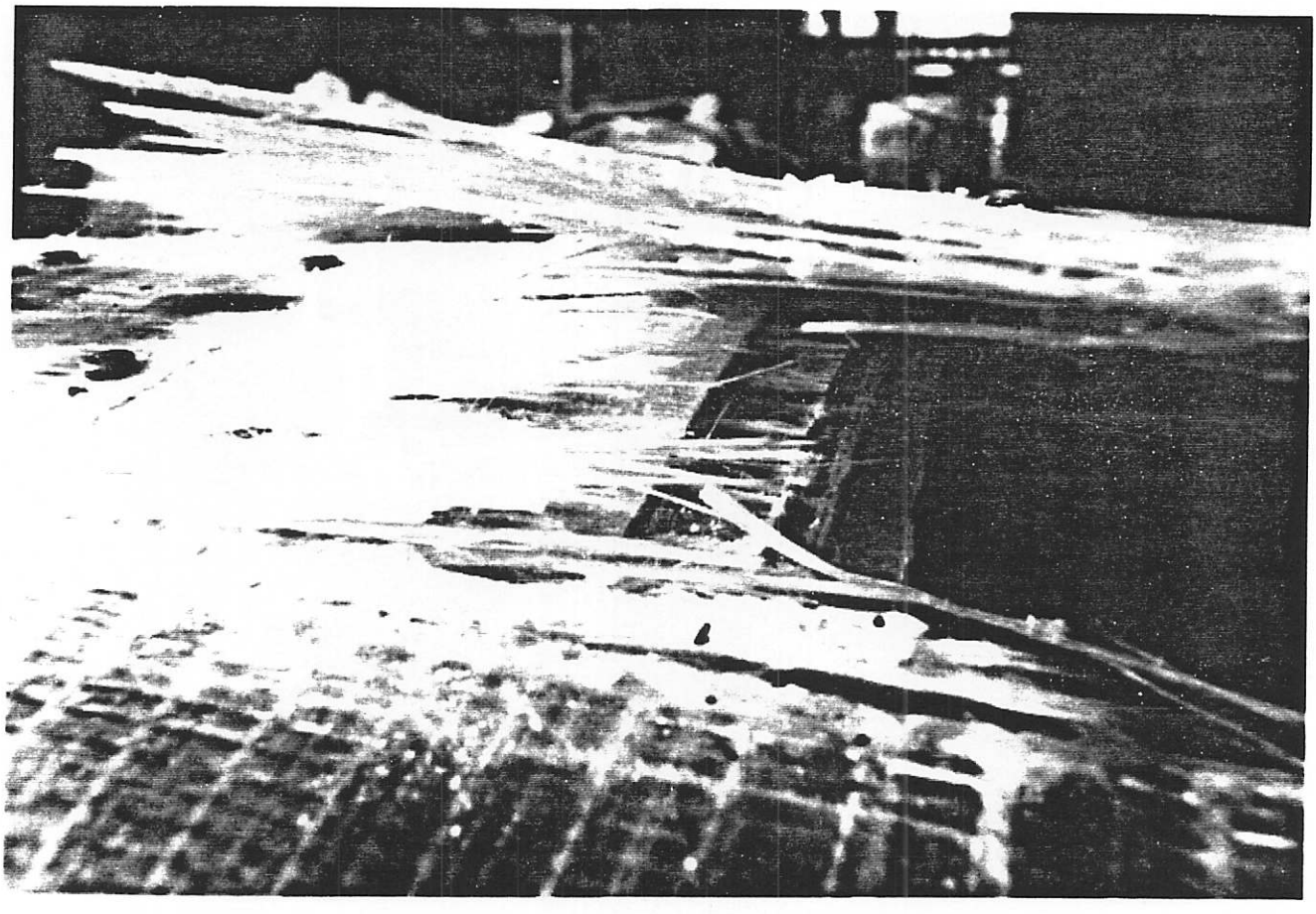

Figure 8. **Detail of the Fatigue Failure in the Second Spar**

FATIGUE PERFORMANCE OF WIND TURBINE BLADE COMPOSITE MATERIALS

by
John F Mandell, Robert M. Reed
Daniel D. Samborsky and Qiong (Rena) Pan

Department of Chemical Engineering
Montana State University
Bozeman, Montana 59715

ABSTRACT

The fatigue behavior has been explored for a variety of generic materials used in wind turbine blades. Coupon testing was carried out under constant amplitude tensile fatigue loading to beyond 10^7 cycles for most materials. Unidirectional materials preformed close to expectations despite fiber misalignment. Materials with triaxial (0/±45) reinforcement showed greater fatigue sensitivity than expected, but lifetime trends flattened at high cycles. The Uniaxial and trialial materials could be normalized to a single S-N lifetime trend for each case. Results include the effects of differing matrix materials, manufacturing methods, reinforcement structure, loading conditions, and specimen edge effects.

This work was supported by the U.S. Department of Energy and Sandia National Laboratories under subcontract 40-8875, and the National Renewable Energy Lab under subcontract XF-1-11009-5. Materials were supplied by Phoenix Industries and U.S Windpower.

INTRODUCTION

The high cycle fatigue resistance of composite materials used in wind turbine rotor blades has been recognized as a major uncertainty in predicting the reliability of wind turbines over their design lifetime [1]. Blades are expected to experience 10^8 to 10^9 significant fatigue cycles over a 20 to 30 year lifetime, well beyond the cycle range where the fatigue behavior of composites has previously received attention. For the lower cost glass fiber composites used in wind turbine blades, there exists neither an adequate data base at high cycles [1], nor an adequate lifetime prediction methodology proven for composite structures in general [2].

BACKGROUND

The fatigue behavior of composite materials has been the subject of several reviews [1-7], and is distinguished by several important general features [2, 3]:

1. Failure is usually progressive, resulting from the gradual accumulation and interaction of dispersed damage, rather than by the nucleation and growth of a dominant crack.
2. As damage accumulates, the constitutive relations of the material may change significantly.
3. A number of distinct damage modes can be identified, including fiber dominated tension and compression, matrix dominated cracking parallel to the fibers, and interlaminar cracking between plies. Some of these may produce failure directly, particularly fiber dominated modes, while modes such as matrix cracking may have an indirect effect on failure by causing load transfer onto the fibers.
4. Under tensile loading the strains to produce matrix cracking in off-axis plies (with thermoset resin composites) are generally well below those to produce fiber failure. As a consequence, in multidirectional composites, cracking tends to initiate first in domains (plies) where the fibers are at the greatest orientation relative to the maximum tensile stress. Cracking then accumulates in these domains (such as 90^0 plies), followed by domains of lesser orientation (such as 45^0 plies). Delamination between piles may also occur at cut edges, ply terminations, or at the intersection of matrix cracks in adjoining plies. Finally, gross failure often occurs by fiber breakage in any domains oriented nearly parallel to the maximum stress (such as 0^0 plies). Under compressive loading the strains to produce matrix cracking in off-axis domains are often comparable to those for fiber dominated failure, so damage development in a matrix dominated mode may also produce gross failure.
5. Large-scale delamination between plies has been a significant failure mode for

composite structures, particularly with out-of-plane loads. Classical linear elastic fracture mechanics has proven applicable to delamination problems under different modes of crack extension and for both static and fatigue loading.

6. Theoretical models for damage progression and failure are under development, but no general approach to lifetime prediction for composites is widely accepted. Only delamination failures have a well developed theoretical context through classical fracture mechanics.

7. Few results are available for lifetimes greater than 10^6 cycles for any composite systems. Cumulative damage effects from varying load histories have been studied in only a few cases, and no general theoretical framework (such as linear damage laws) is accepted.

While these features are common to a broad range of fiber and matrix systems with continuous or chopped strand reinforcement, the actual sensitivity to fatigue loads depends strongly on the material system used, particularly the type of fiber and style of reinforcement (parallel aligned layers, woven, chopped, etc.). S-N lifetime data (maximum stress vs. cycles to failure) can follow a variety of trends [8,9], but the most simple and frequently observed are of the form

$$S/S_0 = 1-b \log N \qquad (1)$$

or

$$S/S_0 = N^{-(1/m)} \qquad (2)$$

Where S is the maximum stress, S_0 is the single cycle strength, N is the number of cycles to failure, and m and b are constants. Eq.(1) yields a linear S-N curve on a plot of S vs. log N while Eq.(2) is linear on a log-log plot. Eq.(2) derives from integration of the Paris fatigue crack growth law

$$da/dN = A\,(K_{max})^m \qquad (3)$$

where a is the crack length, K_{max} is the maximum stress intensity factor (K is more commonly used) and A is a constant; m should be the same as in Eq. 2.

Empirical findings are that S-N data for composites may show a better fit to either Eq.(1) or (2) depending on the material system, and in many cases it is difficult to distinguish which is the more representative form. Composites with well aligned fibers either parallel to the (uniaxial) load direction, or at some orientation, tend to follow Eq. (1) closely, as do composites with multi-directional reinforcement where the lifetime is clearly dominated by one orientation [8].

However, more complex cases such as woven fabrics and chopped strand composites tend to have somewhat nonlinear S-N curves on a semi-log plot, and the most appropriate curve fit is unclear. Woven fabric reinforcements show an even more nonlinear trend on a semi-log plot, with a steep curve at

low to moderate cycles associated with delamination at the weave cross-over points [5], while the curves tend to flatten at higher cycles; significant high cycle data are not available.

Fatigue crack growth data for thermoset composites and neat resins tend to show very high exponents, m (Eq.3), compared with most metals, representing increased fatigue resistance. Values reported for m for both the neat matrix materials and opening mode delamination are often in the 10-20 range. For Mode II the exponents tend to be in the range of 10-12 [8].

EXPERIMENTAL METHODS

Materials were supplied by U.S. wind industry blade manufacturers, molded as flat sheets using preparation methods representative of blade manufacturing. This involved hand layup using nonwoven (stitched) E-glass fabrics having either unidirectional or triaxial (0/$\pm$45) fibers. The triaxial reinforcement contained unidirectional layers stitched together, having differing amounts of 0^0 and $\pm 45^0$ material. The directions given refer to the angle of the fibers relative to the direction of the uniaxial stress which is applied to test specimens cut from the sheets, so that the 0^0 indicates that the fibers are approximately parallel-aligned in the direction of the applied stress.

Table 1 gives a description of each material used in this study. The materials were intended to be as representative of wind turbine blades as possible, including typical fiber misalignments. However, to maintain reasonable specimen to specimen consistency, regions of material with greater than 4^0 fiber misalignment were excluded in preparing test specimens.

The materials in Table 1 contain several different reinforcement styles, two generic types of matrix materials (unsaturated polyester and unsaturated vinylester), and differing processing methods from the two manufacturers. Materials F, G, H and J also contain ply terminations to represent regions of blades which taper in thickness, the results of which will be reported elsewhere.

Flat coupons were used throughout the study, following ASTM D 3039-76 as closely as possible. The flat rectangular specimens were cut with a diamond-edged saw from larger sheets supplied by blade manufactures. Tabs for gripping were bonded to the ends with an epoxy adhesive cured at room temperature or 140^0F. (The original material sheets experienced exotherms in excess of 140^0 and some were post cured at 140^0F.) A variety of adhesives and tab materials were investigated. Most of the specimens were prepared with epoxy electrical vector board (Radio Shack Protoboard) which worked well in most cases. Compression and reversed loading tests used a similar geometry, but with a much shorter gage length.

Particular gage lenghts were empirically selected to prevent elastic buckling in the undamaged state. No side constrant was used.

Tests were run on a 50 kip capacity MTS 880 servohydraulic testing machine using hydraulic grips. A constant amplitude, force control, sine waveform loading was used in all cases. The frequency was varied approximately inversely with the maximum stress level to maintain a constant load rate. The frequency at low cycles was a few Hz, varying up to 15 Hz for the highest cycle tests. This frequency range was the fastest possible without overheating the specimens. Fatigue lifetime is generally not found to be sensitive to frequency in the absence of thermal runaway hysteretic heating [8].

Strain measurement at higher cycles was a problem. Bonded strain gages failed, and fatigue extensometers did not always remain well seated. Cyclic stress-strain and modulus data were obtained by interrupting the tests and replacing the extensometer; thus, the cumulative strain, which was very small in cases where it was measured, was usually not included. Other test interruptions occurred due to power failures. These were common in very long tests, and the testing equipment did not generally overload the specimens significantly during shut-downs. Peak loads during shut-downs were recorded.

All tests were conducted in ambient laboratory air. This is generally low humidity with temperatures between 65 and 80^{0}F.

Further details of the results of this study can be found in Ref. 9.

RESULTS AND DISCUSSION

Unidirectional Materials

Materials A, B, and L are unidirectional, loaded in the longitudinal (fiber) direction. A and B differ only in matrix material (polyester vs vinylester); L is constructed with slight inherent fiber misalignment between strands and layers, and has a higher fiber content.

Figure 1 gives S-N data for material B. The arrows on the points at 40 x 10^6 cycles indicate run out tests which did not fail. Several aspects of Figure 8 are significant:

1. The data at higher stresses fall below Eq. 1 with a slope, b, of 0.1 (10%/decade).
2. The power law fit of Eq. 2 is in good agreement with the data for an exponent, m, of 13.5.
3. There is no apparent effect of specimen width for the 1.0 and 2.0-inch-wide specimens tested.
4. The initial strain value given on the right, 0.68%, corresponds to the 20 ksi stress level. The actual strain increases slightly during the specimen lifetime.

Materials A, B and L are compared in Figure 2, with the maximum stress, S, normalized by the static strength, S_0. Again, Eq.(2) with a power law exponent in the range of m=13.5

fits the data well. Little difference between unidirectional Materials A, B, and L is noted, despite the differences in matrix material and manufacturing details. The vinylester matrix typically yields a slightly higher static strength (Fig. 2, Material A vs. B), but little difference in fatigue, particularly at higher cycles.

Problems with failures in the tab area were common with unidirectional specimens, and clear tab failures were deleted from the plotted data. Edge splitting was also a common problem, as misaligned fibers were cut along the specimen edges, particularly notable with Material L but also a problem with A and B. Splits often occurred early in the lifetime, so that most of the lifetime was consumed with a reduced cross-sectional area and other complications such as nonsymmetry. The tabs often showed some delamination as well, particularly where the splits reached the tab area. The unidirectional materials showed some matrix cracking normal to the stress direction, particularly along the stitch lines; this was also observed in the run-out specimens.

As noted earlier, Eq. (1) has an empirical basis in a broad range of materials with well aligned fibers, where b=0.1 for E-glass strands and composites. Eq.(2) is generally applicable where the lifetime is associated with growing cracks, as in delamination studies [8], where Eq. (3) describes the crack growth behavior. Delamination tests on Materials H and J [9] produce a power law behavior following Eq. (3), with the same exponent, m=13.5, which fits the unidirectional S-N data well. This implies that the lifetime of the unidirectional materials is dominated by the matrix crack growth, edge splitting process. However, the data in Fig. 8 are also not far from the expected trend of Eq. (1) with b=0.1, and more high-cycle data will be required to adequately test either prediction.

Extrapolation to 10^9 cycles of the trend lines given in Fig. 1 for Eqs. (1) vs. (2) shows a great deal of sensitivity to the assumed model. the expected stress or strain level to produce 10^9 cycle failures is only half as great if Eq. (1) is assumed, as compared with Eq. (2). Again, more high-cycle data are required before a 10^9 cycle stress or strain level can be projected with any confidence.

Triaxial Reinforcement

Materials F/G, H/J, M and N contain 0/±45 layers of reinforcement with differing stacking sequence, relative amounts of 0 and ± 45 material, and strand sizes. These material showed consistently poorer fatigue resistance than did the unidirectional materials. Figure 3 compares S-N data for all of the triax materials on a normalized stress plot. Despite the differences in matrix, manufacturing, and percent 0^0 material all of the data sets overlap, and all show a clear

flattening trend at high cycles. The F/G and H/J data shown are for specimens without ply terminations (joints or tapers) in the gage section, or for specimens which fail away from the ply terminations.

The triax materials showed distinctly different failure patterns from the unidirectional materials. Figure 4 shows failed triax specimens. Generally, the $\pm 45^0$ layers failed separately, and may delaminate from the 0^0 material. No significant tab problems were observed with most of these materials, and failures were usually in the gage section. The failure sequence usually showed cracking in the $\pm 45^0$ layers, often associated with matrix cracks normal to the load in matrix rich areas around the 0^0 material. Prior to total failure, local severe damage zones were observed to nucleate and grow. For F/G materials these appear as in Fig 4a, while more distinct failures along with stitch lines were seen in Materials M and N. These zones often, but not always, initiated at the edges. The failure zones in Materials M and N included cracks along the $\pm 45^0$ strands and broken 0^0 strands right at the fabric stitch lines (Fig. 4(b)).

Strain Data

Figure 5 compares higher cycle strain data for the unidirectional and triax materials. The initial strains for the unidirectional materials were in the range of 0.8% to produce failure at 10^7 cycles, while for the triax materials the strain was in the range of 0.3 to 0.4%. the latter range is already well below the extrapolated unidirectional strains at 10^8 to 10^9 cycles, and so the triax results are very disappointing in terms of allowable strain levels. Also notable on Figure 5 are data for the N triax tested in the transverse direction, $(90/\pm 45)$. These failure strains are in the same range as for the 0^0 direction. It is apparent that all of the triax materials fail soon after the $\pm 45^0$ layers crack, and are not dominated by the 0^0 layer strain capability. Figure 5 gives a comparison of 0^0 and 90^0 oriented S-N data for Material N.

An approximate prediction of what should happen when the $\pm 45^0$ layers fail can be obtained from classical laminate theory [9]. If the $\pm 45^0$ ply stiffness is then assumed to be zero, in Materials M and N, for example, the overall modulus should decrease by about 25%, raising the strain on the 0^0 material by a factor 1.25. From Figure 5, even the extreme assumption of zero stiffness in the cracked plies, $\pm 45^0$ ply failure should not lead to the observed failure of the 0^0 layers at the lower strain levels. As noted earlier, carbon fiber composites fabricated from prepreg tend to follow to 0^0 ply fatigue trends under these conditions [8]. Thus, the triax performance in tension is much poorer than expected either from experience with other composites or from

simple calculations. Current modelling of this problem suggests that matrix and off-axis cracks generate much higher stress concentrations in the 0^0 E-glass materials than from carbon lepoy. This is particularly significant when the off-axis material is bound very tightly to the off-axis plies.

Complex Laminate Structures

Material P is a more complex laminate constructed of layers of triax, mat, and unidirectional material (about 50% unidirectional). Figure 6 compares the normalized fatigue trend for material P with that of the pure triax materials. The failure mode for this laminate showed initial fracture zones in the triax like Fig. 4(a), followed by delamination from the undirectional layers. While this appears to be the desired failure sequence to protect the more structural and fatigue resistant unidirectional layers, the lifetime trend and failure strains were similar to those of the other triax materials. This disappointing result again indicates the need for improved modelling and more fatigue resistant triax reinforcement.

Specimen Edge Effects

Figures 7 and 8 give S-N data for materials T and V and U and W, respectively. These are comparisons of standard coupons of two different triax materials with special coupons fabricated without cut edges (all specimens were 2-inches wide). The latter specimens were molded with the triax wrapped at the edges to present cut edge effects. No significant difference was observed in either the lifetime data or the failure modes when the wrapped edges were used. Similar test comparisons are being carried out with unidirectional materials. The results given here suggest that conventional material coupons may give results which are not significantly affected by the presence of free (cut) edges, for triax reinforcement.

Compression and Reversed Loading

Compression and reversed loading fatigue tests have been carried out on materials N and P, containing triax and triax/mat/unidirectional reinforcement. These tests were exploratory in nature, but provide meaningful trends for the geometries and constraint conditions used. Compression tests are recognized [2] as producing results which depend on the test conditions, such as buckling restraints, load introduction details, and thickness. These tests used tabbed coupons clamped in hydraulic grips with no lateral gage section restraints. The gage lengths of 1/4 to 1.0 inches prevented elastic buckling at the maximum compressive load, but out-of-plane deflections were commonly observed after damage was well developed, close to the failure condition. Other exploratory static data showed that the static strength in compression was significantly (up to 50%)

lighter if the thickness was doubled. Thus, caution must be used in interpretation these results.

Figures 9 and 10 show the S-N data for materials N and P at R values of 0.1 (tension-tension), -1.0 (reversed), and 10 (compression-compression). The static compression strengths are lower than for tension, but the compression fatigue trends are less steep than for tension (b is higher in Eq. (1)). The values of b observed in compression are similar to literature data for other glass and carbon fiber composites [8]. Reversed loading results generally follow the lower of the tension or compression trends for the cycle range in question, with a slightly reduced lifetime as compared to the pure tension or compression curve. The data in Fig. 9 and 10 suggest a transition from compression to tension dominated failures as the cycle range increases and the stress level decreases; this may be relevant to bending conditions in blade tests or service loading.

Comparison With Other Studies

Several wind energy related programs in Europe have reported significant fatigue data for materials of the general type studied here [10-14]. Data for unidirectional fiberglass composites in tensile fatigue (R=0.1) show failure strains in the 10^6 to 10^8 cycle range which are very similar to those in this study, around 0.8% at 10^7 cycles [10,11]. The S-N data for predominantly unidirectional material at R= 0.1 in Ref.11 approximately follow Eq. (1) with b= 0.1, with the data falling slightly above the predicted lifetimes (with some uncertainty about the static test load rate effects). No fatigue limit is found out to 10^8 cycles. Data for spectrum loading (WHISPER spectrum) are reasonably predicted by a linear damage law combined with the constant amplitude results. However, testing at two stress levels tended to extend the life at the second (lower) level, contrary to linear damage expectations. Reversed loading (R= -1) produces lower failure stress levels, but is presumably related to the nature of any bucking constraints in compression.

Results in Ref. 12 were generally similar to those found here in trend and strain levels for unidirectional material at R= 0.1. Compression data and R= -1.0 data are generally at similar strains to those in Ref. 10, despite the use of an antibuckling device which appeared to raise the static compressive values. Spectrum fatigue results (WHISPX) showed approximate agreement with linear damage law predictions in tensile dominated fatigue, but less agreement in compression [13].

With regard to the effects of vinylester vs. polyester matrix materials, data in Ref. 14 support the findings in the present study. Materials with woven roving and mat reinforcement showed some advantage for vinylesters over

orthopthalic polyesters at high stresses (above where matrix cracking occurs on the first cycle), but S-N data (R= -1.0) for all matrix systems converged at lower stresses/longer lifetimes. This has also been observed in automotive SMC composites with various matrix modifications [8]. Data reported in Ref. 15 for flexural fatigue appear to show similar convergence at high cycles for vinlyester and polyester matrices, but the vinylester showed a greater advantage at lower cycles than found in other data sets.

CONCLUSIONS

The unidirectional materials performed close to expected trends despite significant fiber misalignment; a power law trend appeared to provide the best fit to most of the data. This may imply that the lifetime is dominated by matrix cracking along misoriented fibers, as the power law exponent correlates with the exponent obtained in ply delamination tests. Triaxial materials showed a more steep S-N data trend at higher stresses, which tended to flatten at lower stress. Data from several material types with differing matrix (vinylester and polyester), percent 0^0 material, and manufacturing method could be normalized to a single S-N curve. Failure of the triaxial material appears to be dominated by cracking in the $\pm 45^0$ plies, which was not anticipated. Data are also given in Ref. 9 for changes in laminate stiffness and temperature during cycling.

Results for more complex laminates containing uniaxial as well as triaxial plies showed a triax-dominated behavior in tension. Compression fatigue produced a lower static strength, but also less fatigue sensitivity, than for tension. Reversed loads followed the lower of the tension or compression trend lines. Special triax coupons with wrapped edges showed similar results to coupons with machined edges.

References

1. "Assessment of Research Needs for Wind Turbine Rotor Technology", Report of the Committee on Assessment of Research needs for Wind Turbine Rotor Materials Technology, National Research Council, National Academy Press, Washington D.C. (1991).

2. "Life Prediction Methodologies for Composite Materials", Report of the Committee on Life Prediction Methodologies for Composite Materials Advisory Board, NRC, National Academy Press, Washington D.C. (1991).

3. K.L. Reifsnider, Ed., Fatigue of Composite Materials, Vol. 4 Composite Materials Series, Ed. R. B. Pipes, Elsevier Publishing Co., London (1991).

4. A.H. Chardon and G. Verchery, Eds., Durability of Polymer Based Composite Systems for Structural Applications, Elsevier Applied Science, London (1991).

5. J.F. Mandell, "Fatigue Behavior of Fiber-Resin Composites", Developments in Reinforced Plastics-2, G. Pritchard, Ed., Applied Science Publishers, London, p. 67 (1982).

6. R. Talreja, "Fatigue of Composite Materials", Technomic, Lancaster, PA (1987).

7. M.J. Owen, In Short Fiber Reinforced Composite Materials, ASTM STP 772 B. A. Sanders, Ed., ASTM, Phil. p. 64 (1982).

8. J.F. Mandell, "Fatigue Behavior of Short Fiber Composite Materials", The Fatigue Behavior of Composite Materials, K.L. Reifsnider, Ed., Ch. 7, Elsevier Science Publishing, London (1991).

9. J.F. Mandell, R.M. Reed, and D.D. Samborsky, "Fatigue of Fiberglass Wind Turbine Blade Materials," Contractor Report SAND92-7005, Sandia National Laboratories, Albuquerque, N.M.

10. P.W. Bach, "High Cycle Fatigue Testing of Glass Fiber Reinforced Polyester and Welded Structural Details" , ECN Report C-91-010, ECN, Petten, The Netherlands (1991).

11. R.H.F. Tikkemeijer and P.A. Joosse, "Fatigue of Wind Turbine Materials", NOVEM Contract 24.300/0550, NOVEM Utrecht, 3503 R.E. Utrecht, The Netherlands (1991).

12. Ch. W. Kensche and T. Kalkuhl, "Fatigue Testing of GL-EP in Wind Turbine Rotor Blades", Proc. European Community Wind Energy Conf., Madrid (1990).

13. Ch. W. Kensche, Institute for structure and Design, DLR Stuttgart, Germany, Personal Communication (1991).

14. A.T. Echtermeyer, L. Buene, B. Engh, and O.E. Sund, "Significance to Damage Caused by Fatigue on Mechanical Properties of Composite Laminates", Proc. ICCM 8, Honolulu (1991)

15. P. Burrell, T. McCabe, and R. de la Rosa, "Cycle Test Evaluation of Various Polyester Types and a Mathematical Model for Projecting Flexural Fatigue Endurance," Proc. 41st Ann. Tech. Conf. Reinforced Plastic/Composite Inst., Society of the Plastics Industry, Paper 7-D (1986).

TABLE 1

FIBERGLASS MATERIALS TESTED

MATERIAL	V_f	PLY GEOMETRY	MATRIX	THICKNESS (INCHES)	LOAD DIRECTION	DESCRIPTION
A	0.30	$[0]_5$	polyester	0.16	0°	12 oz unidirectional fabric
B	0.30	$[0]_5$	vinylester	0.16	0°	12 oz unidirectional fabric
F	0.36	$[(\pm 45/0)_n]_s$	polyester	0.19/0.28	0°	33 oz Triax (48% 0's,26% +45's, 26% -45's) 6 plies reduced to four at central ply termination
G	0.36	$[(0/\pm 45)_n]_s$	polyester	0.19/0.28	0°	Same as material F
H	0.37	$[(\pm 45/0)_3]_s$	polyester	0.25	0°	32 oz Triax (70% 0's, 15% +45's, 15% -45's) 6 plys with ply joint in central 2 plys
J	0.37	$[(0/\pm 45)_3]_s$	polyester	0.25	0°	Same as material H
L	0.50	$[0]_n$	polyester	0.13	0°	Non-woven uniaxial fibers
M	0.38	$[0/\pm 45]_n$	vinylester	0.15	0°	Triaxial reinforcement (Same percentages as F)
N	0.38	$[0/\pm 45]_n$	polyester	0.15	0°, 90°	Same as material M
P	0.40	[T/M/U/M/T]	vinylester	0.15	0	Combined (0/+-45) Triax(T), chopped strand mat(M) and unidirectional(U) plies.
R	0.39	$[0/\pm 45]_n$	polyester	0.14	0	Separate 0° and ±45° plies. 50 % 0, 50 % ±45

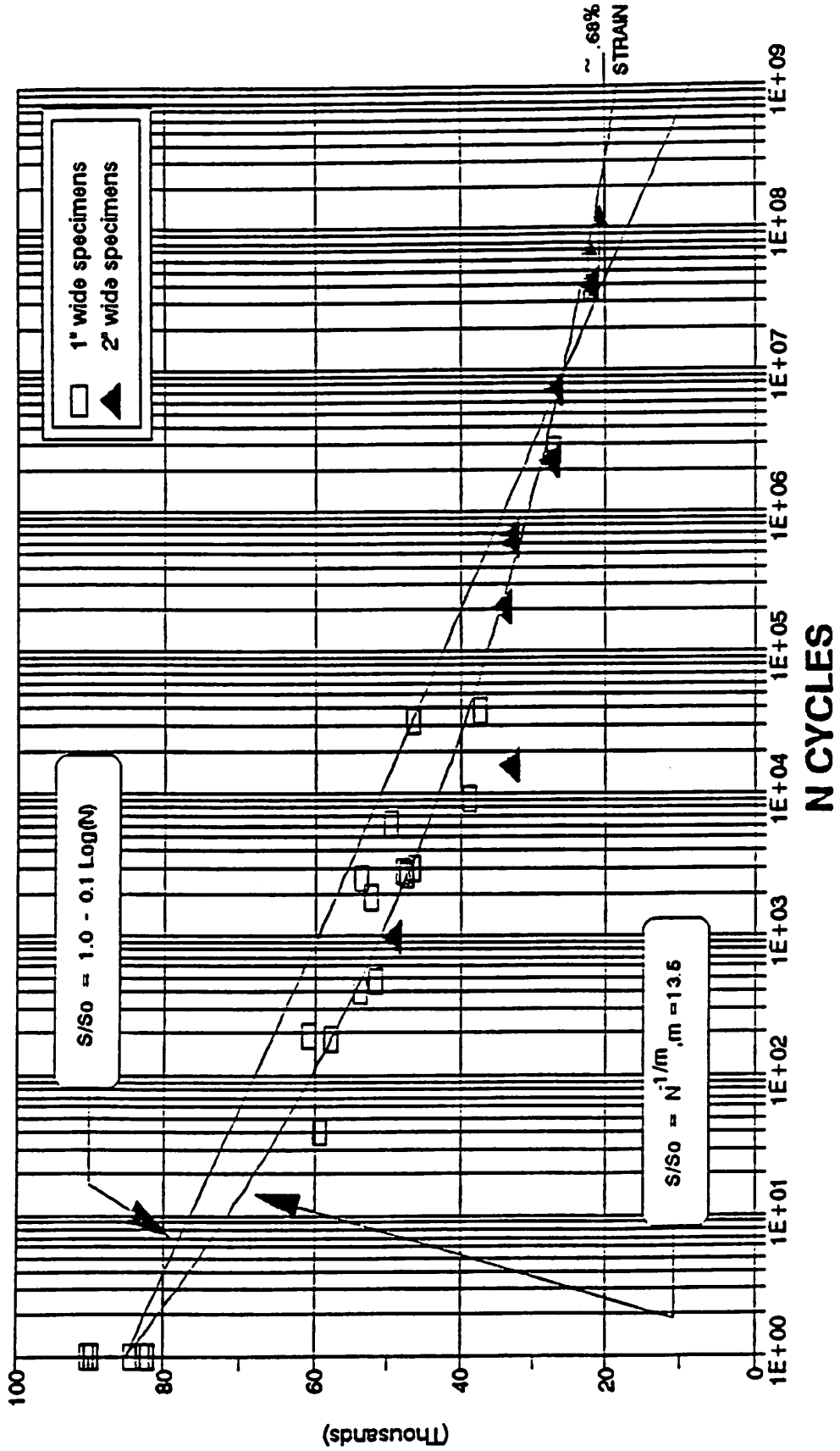

FIGURE 1 S-N Data For Material B (Unidirectional)

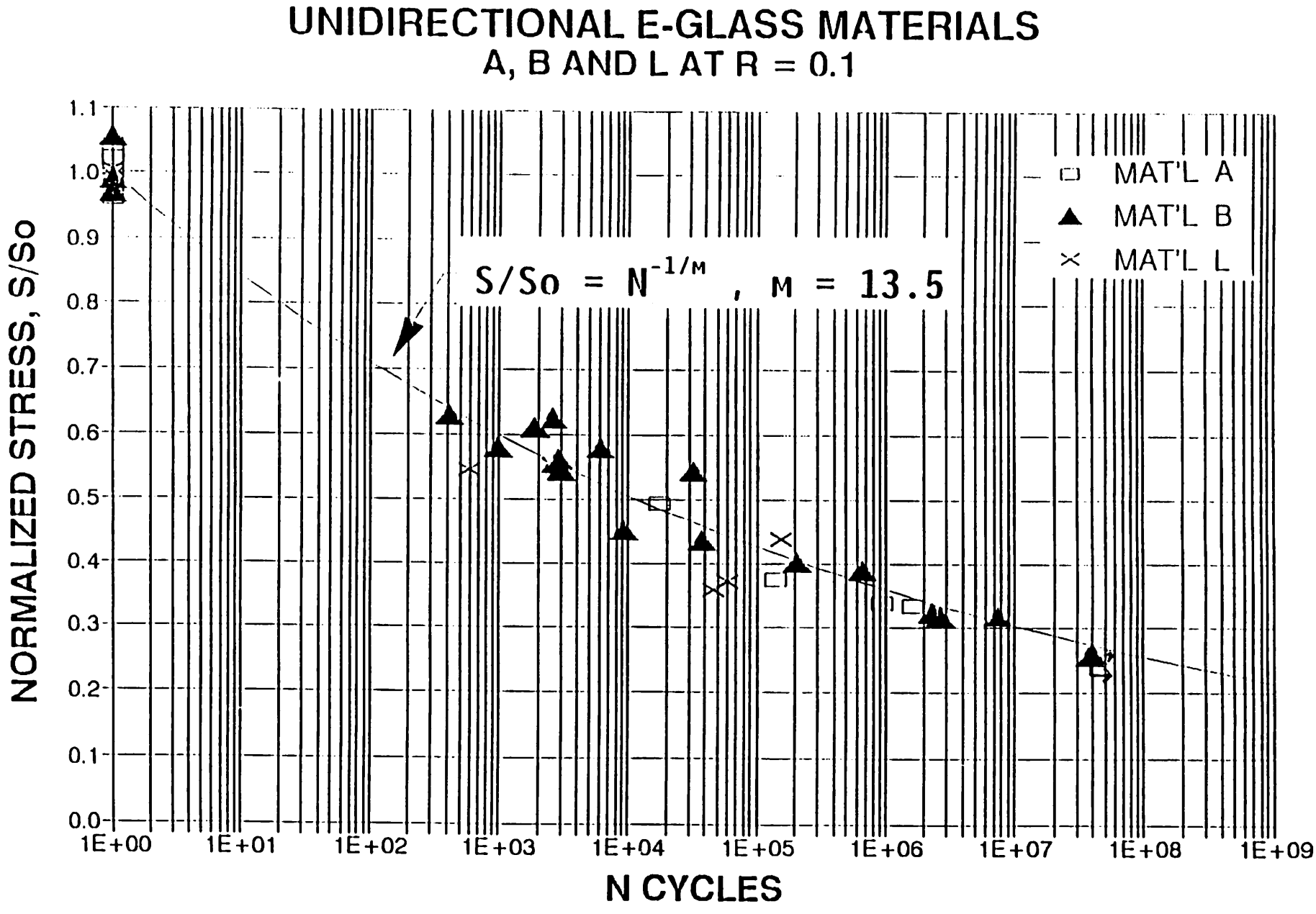

FIGURE 2 Comparison of Normalized S-N Data for Unidirectional Materials A, B, and L

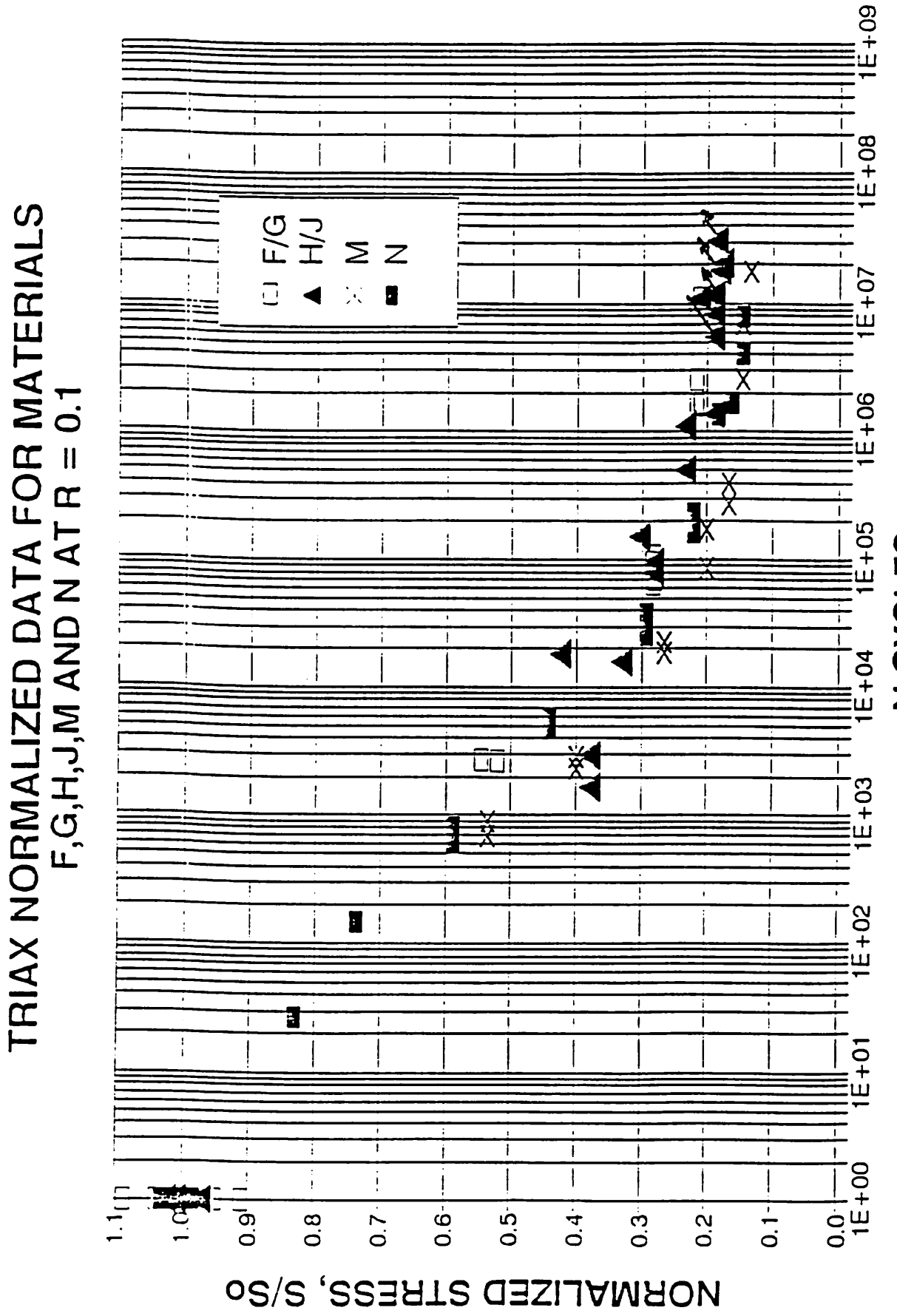

FIGURE 3 Normalized S-N Data for All Triax Materials

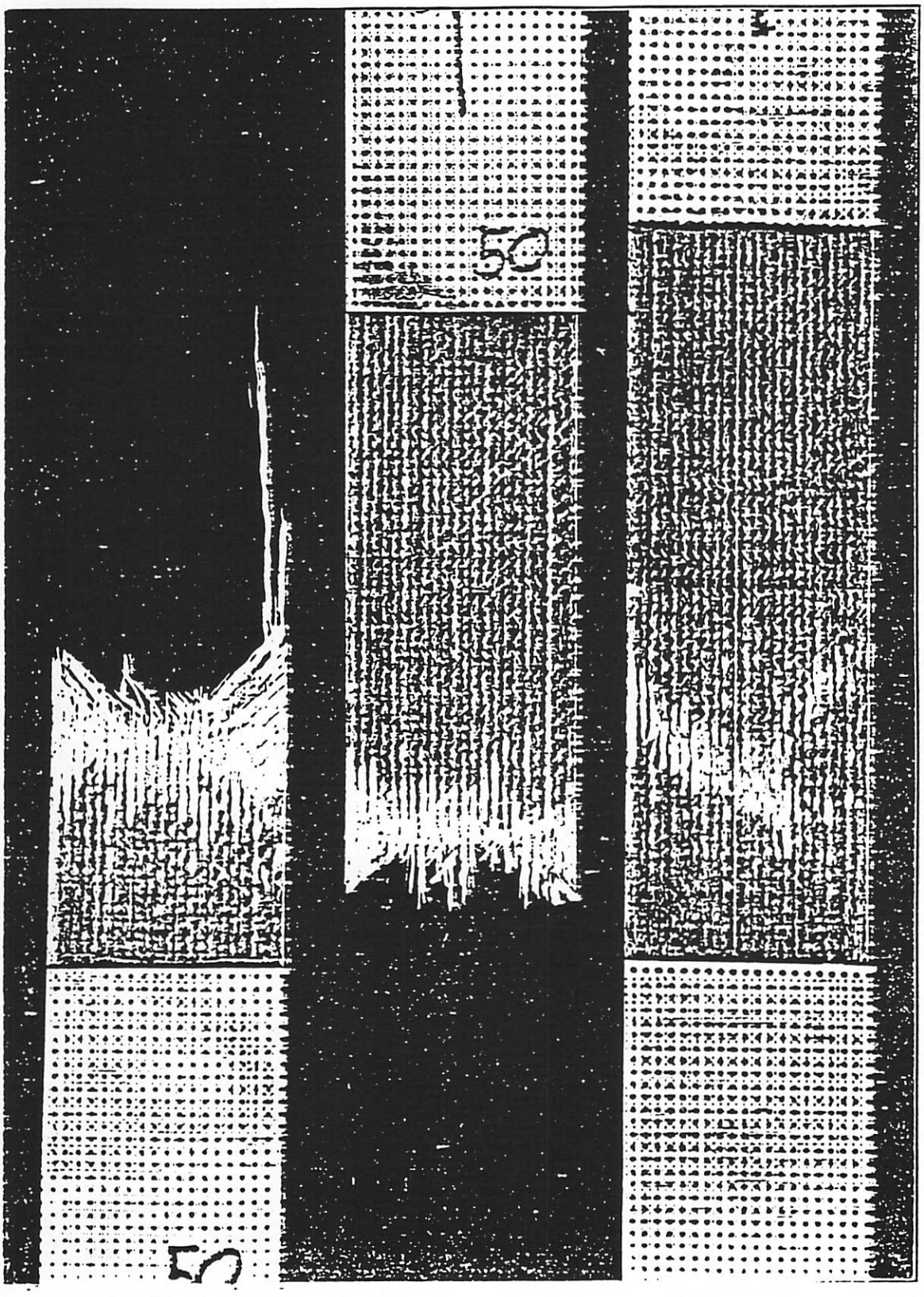

FIGURE 4a Damage Growth and Failure, Materials F/G

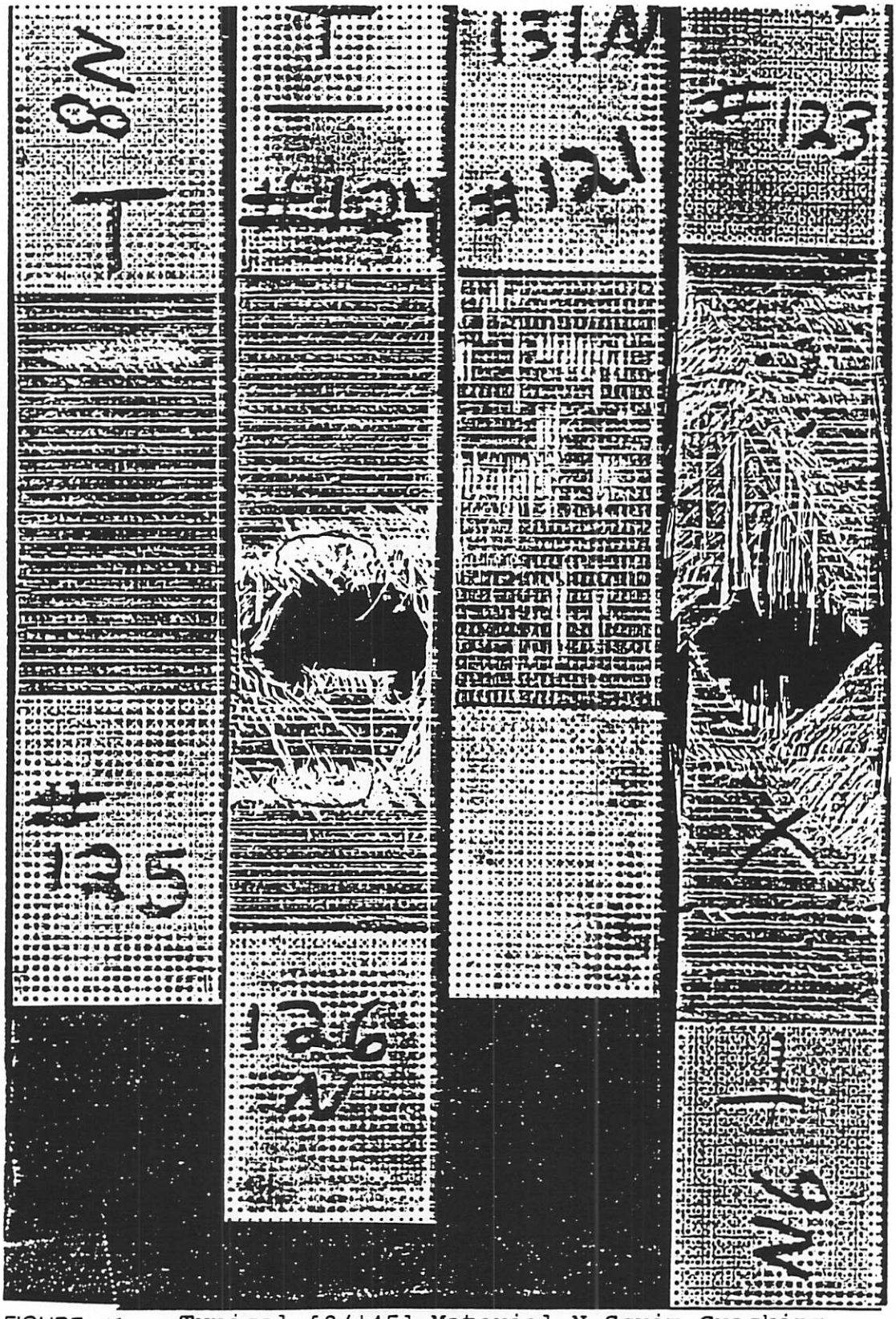

FIGURE 4b Typical [0/±45] Material N Scrim Cracking, and ±45 Damage Region Failure Modes.

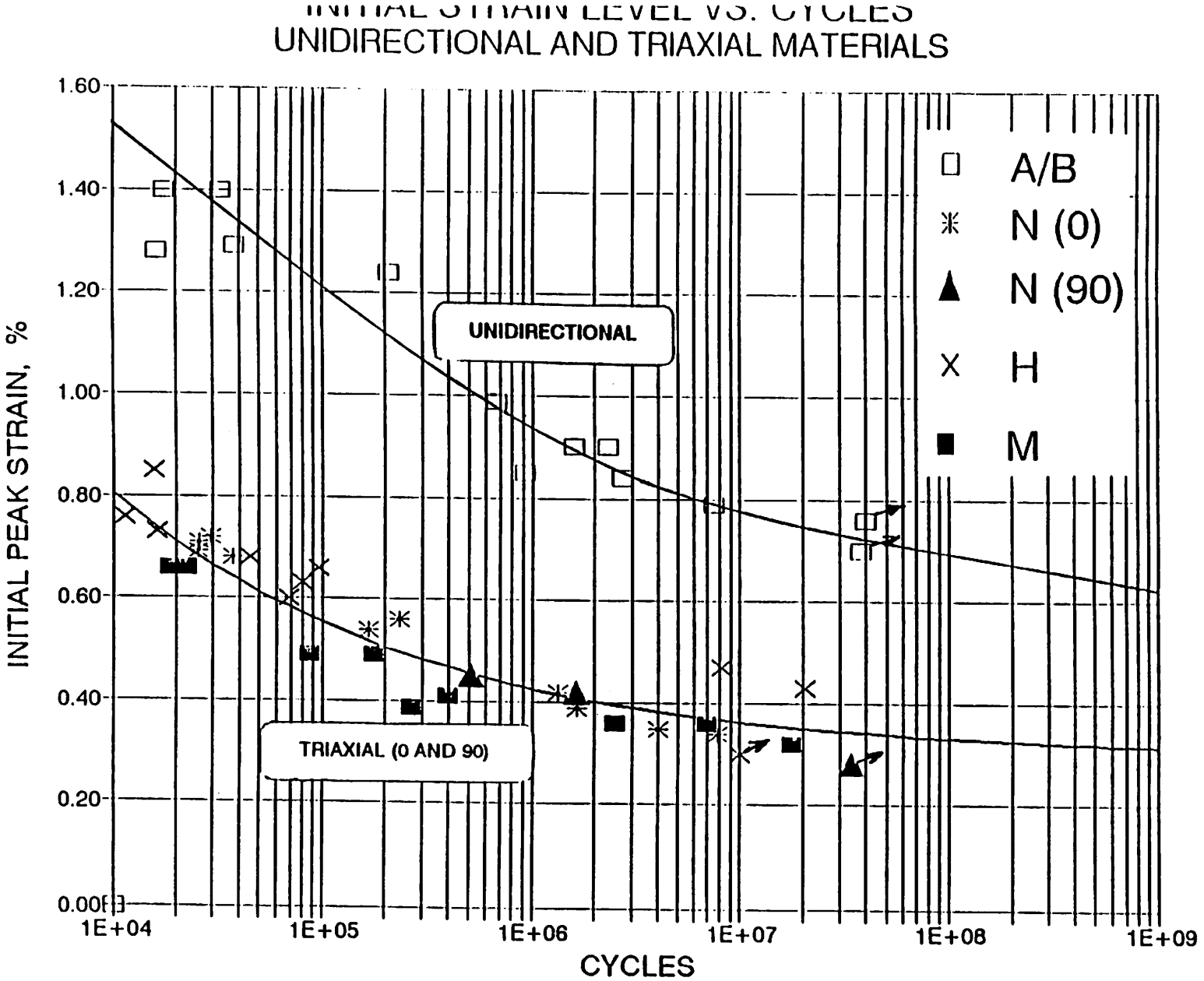

FIGURE 5 **Initial Strain vs. Cycles to Failure, Unidirectional and Triaxial Materials**

FIGURE 6

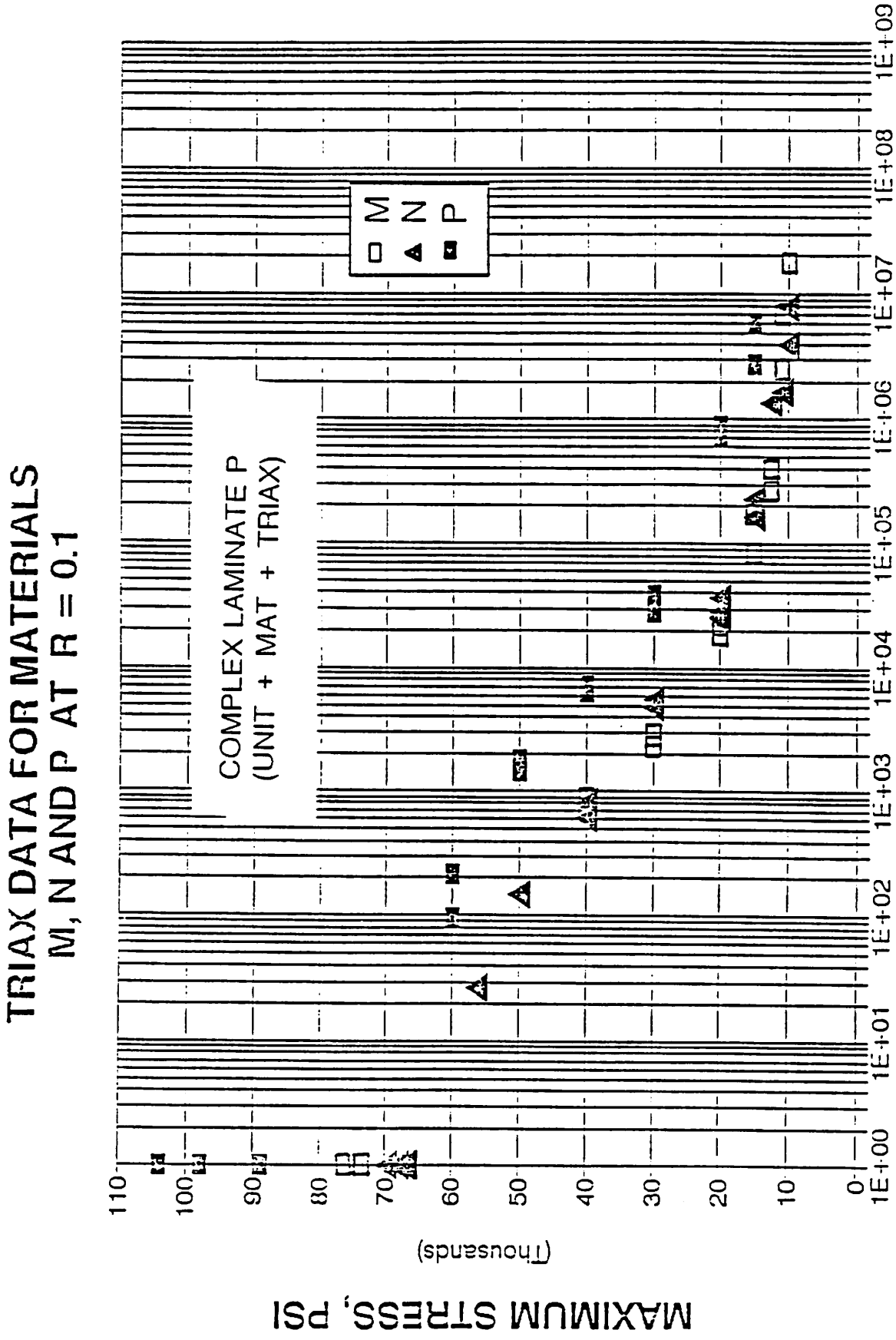
TRIAX DATA FOR MATERIALS
M, N AND P AT R = 0.1
COMPLEX LAMINATE P
(UNIT + MAT + TRIAX)
M
N
P
MAXIMUM STRESS, PSI
(Thousands)
110
100
90
80
70
60
50
40
30
20
10
0
1E+00
1E+01
1E+02
1E+03
1E+04
1E+05
1E+06
1E+07
1E+08
1E+09
N CYCLES

FIGURE 7

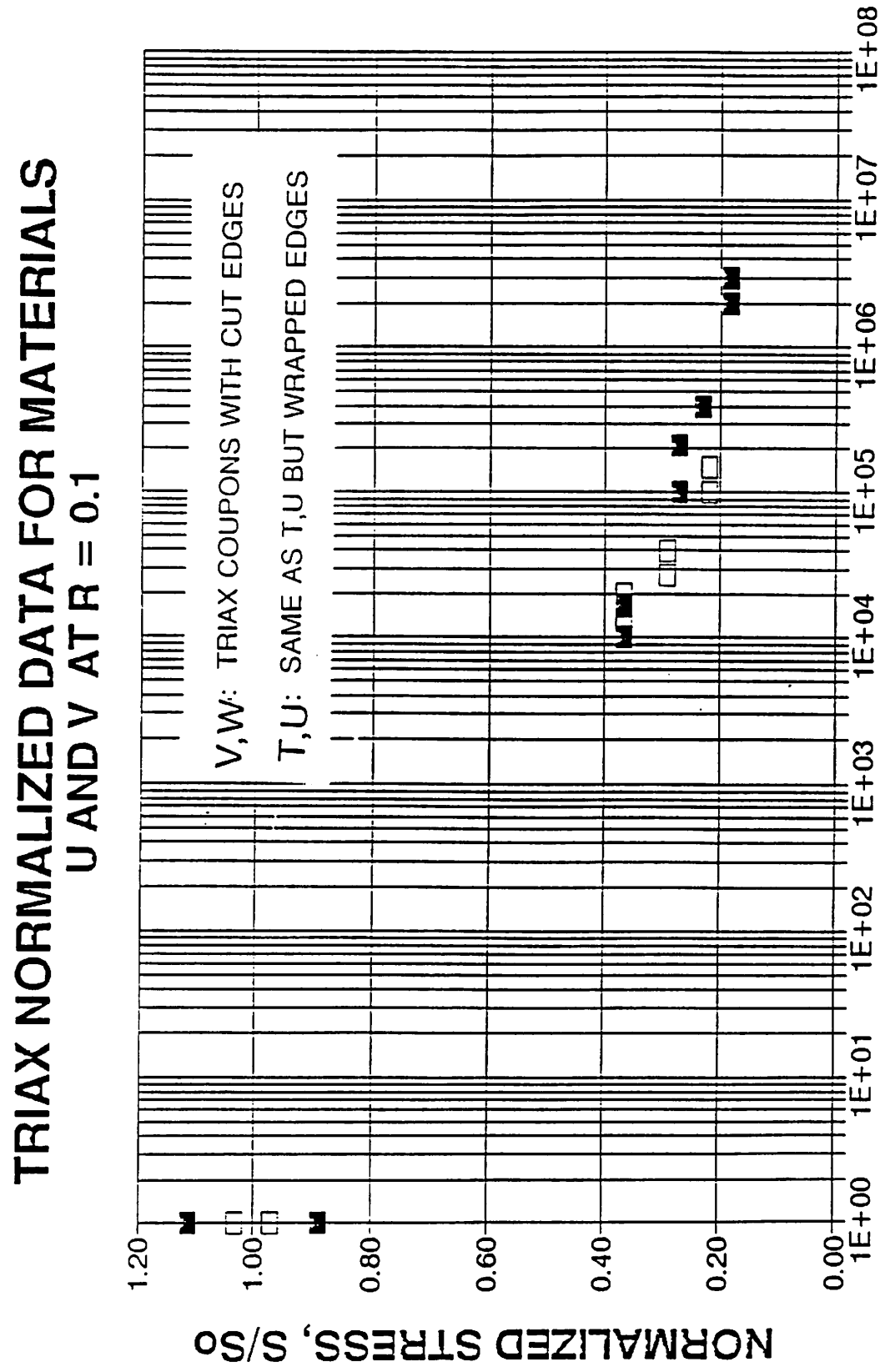
TRIAX NORMALIZED DATA FOR MATERIALS
U AND V AT R = 0.1
V,W: TRIAX COUPONS WITH CUT EDGES
T,U: SAME AS T,U BUT WRAPPED EDGES
NORMALIZED STRESS, S/So
1.20
1.00
0.80
0.60
0.40
0.20
0.00
1E+00
1E+01
1E+02
1E+03
1E+04
1E+05
1E+06
1E+07
1E+08
N CYCLES
MATERIAL U
MATERIAL V

FIGURE 8

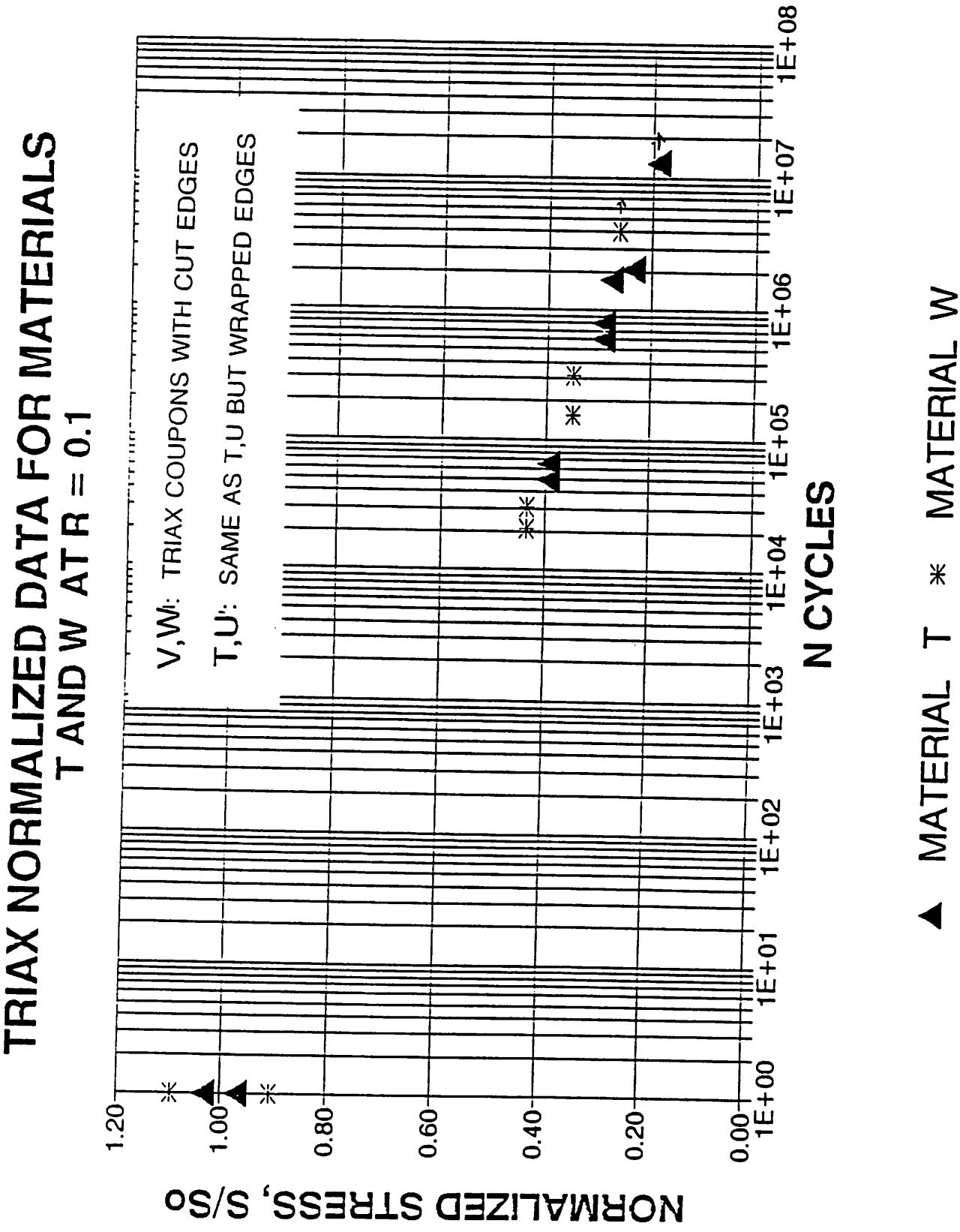
TRIAX NORMALIZED DATA FOR MATERIALS
T AND W AT R = 0.1
V,W: TRIAX COUPONS WITH CUT EDGES
T,U: SAME AS T,U BUT WRAPPED EDGES
NORMALIZED STRESS, S/So
1.20
1.00
0.80
0.60
0.40
0.20
0.00
1E+00
1E+01
1E+02
1E+03
1E+04
1E+05
1E+06
1E+07
1E+08
N CYCLES
▲ MATERIAL T
✳ MATERIAL W

FIGURE 9

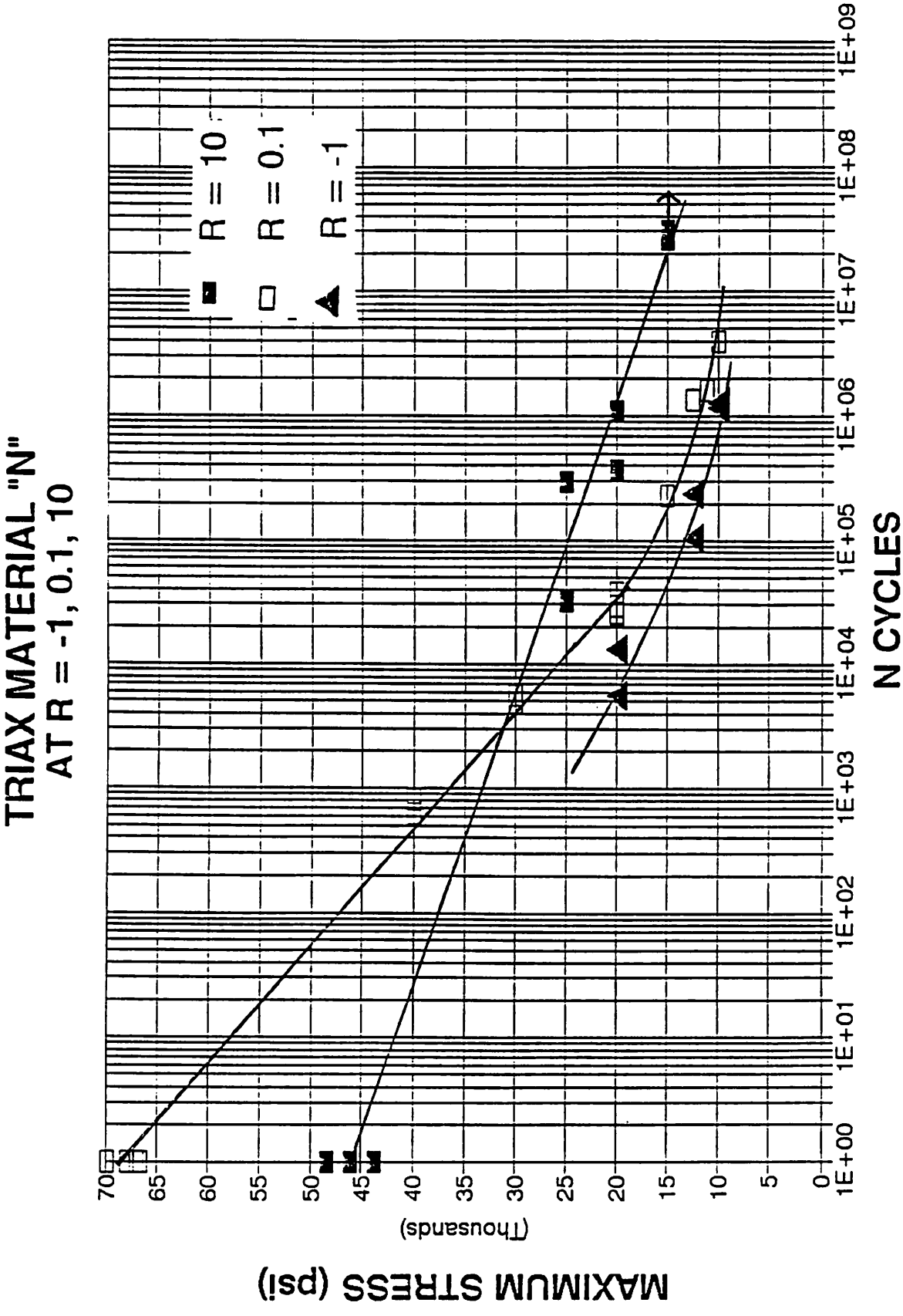
TRIAX MATERIAL "N"
AT R = -1, 0.1, 10
R = 10
R = 0.1
R = -1
MAXIMUM STRESS (psi)
(Thousands)
70
65
60
55
50
45
40
35
30
25
20
15
10
5
0
1E+00
1E+01
1E+02
1E+03
1E+04
1E+05
1E+06
1E+07
1E+08
1E+09
N CYCLES

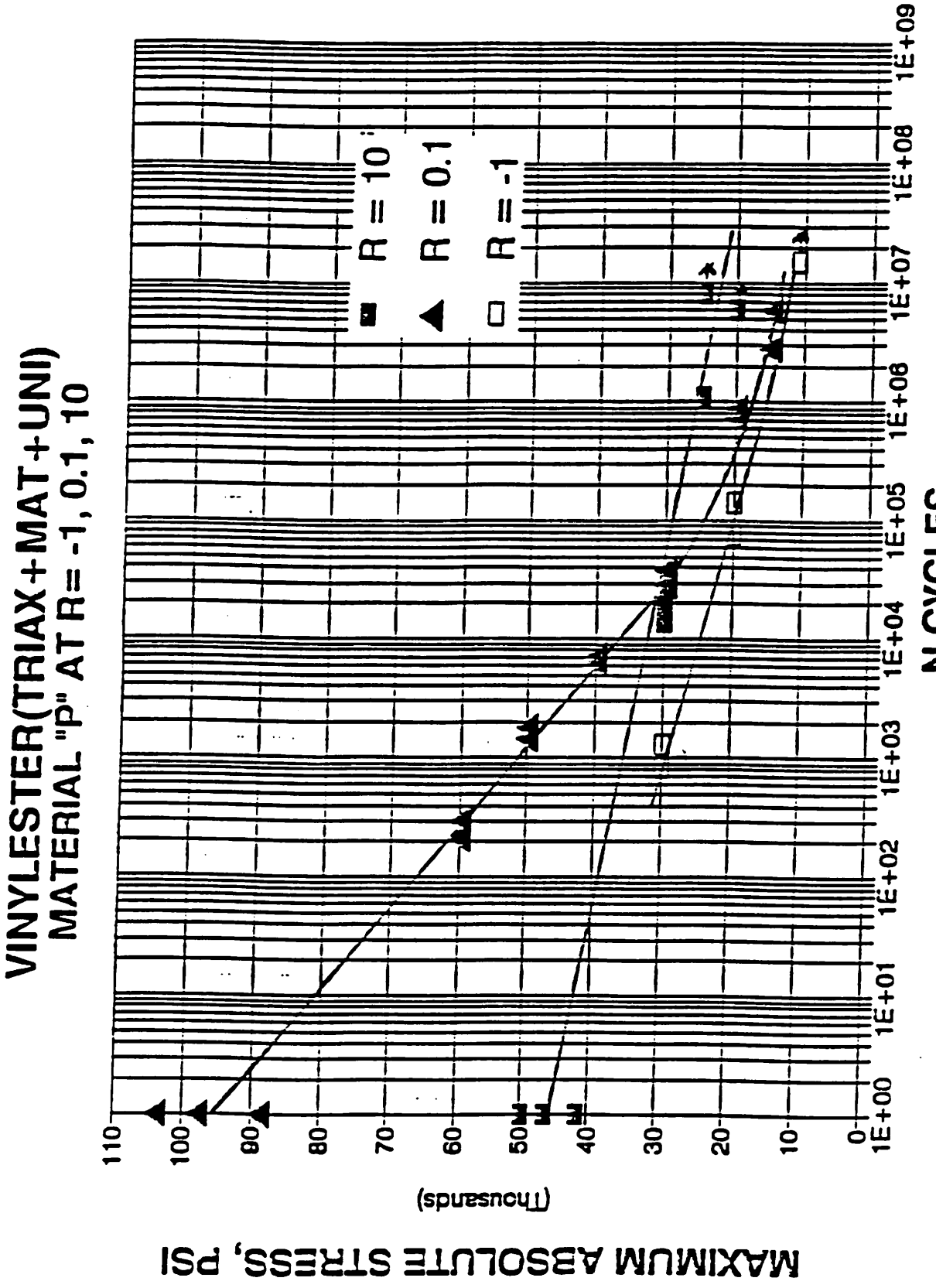
VINYLESTER(TRIAX+MAT+UNI)
MATERIAL "P" AT R= -1, 0.1, 10
R = 10
R = 0.1
R = -1
MAXIMUM ABSOLUTE STRESS, PSI
(Thousands)
N CYCLES
110
100
90
80
70
60
50
40
30
20
10
0
1E+00
1E+01
1E+02
1E+03
1E+04
1E+05
1E+06
1E+07
1E+08
1E+09

FIGURE 10

REVIEW OF DUTCH FATIGUE PROGRAM ON GLASS/POLYESTER

P.A. Joosse
Stork Product Engineering B.V.
Amsterdam
The Netherlands

SUMMARY

The fatigue research on glass reinforced polyester in the Netherlands is aimed at achieving a fatigue formulation to be used in design and certification of wind turbine rotor blades. For this purpose fatigue tests are carried out on laminates as delivered by blade manufacturers, for a number of laminate lay-ups and joint types. The main part of the material tests is done on small specimens.
Coupon data for several laminates and bolted specimen data give identical fatigue curves when normalized for the static strength. The effect of moisture on variable loaded bolted specimens seems to be smaller than constant amplitude tested specimens.
Test results are compared to two fatigue formulations. The formulation based on stress ranges gives the best approximation of the test results.

INTRODUCTION

In 1984 the design started of a 1 Megawatt wind turbine: the NEWECS 45. The rotor blades of the turbine were to be made of glass fiber reinforced polyester. During the design process it became clear that a realistic formulation of the fatigue behaviour of this material was not available. As a consequence a conservative design approach was followed, while at the same time steps were taken to start a fatigue research program.
The fatigue research program was and is aimed at achieving a realistic formulation of the fatigue behaviour of glass polyester as used by the industry for wind turbine rotors.
In this paper a global review will be given of the Dutch fatigue program. The program deals with basic material properties (coupon tests) and typical joints. The paper will focus on the fatigue formulations used during the program and compare these with the test results. Detail information on the test methods and data is given elsewhere ([2]-[5]).

STRUCTURE OF THE RESEARCH PROGRAM

The objective of the program is to give a master curve for the fatigue behaviour of glass reinforced polyester in laboratory conditions. The effect of parameters like humidity, temperature and clamping pressure (on bolted joints) will be given separately. As this curve will be used in design and certification, only materials and details as used by the manufacturers are tested.

The basic material data is found for laminates typical for rotor blades. A significant part of the research deals with joining glass/polyester with steel or other parts. Different joining types were used, e.g. bonding, bolts and the Hütter-type joint. To compare the small joint specimens with a real product a few full-scale blade root connections are tested.
Since the loading of a wind turbine rotor is variable in nature, both constant amplitude (c.a.) and variable amplitude (WISPER) tests are carried out. The WISPER spectrum gives an indication of the effect of the varying loads on the degradation compared to the combination of c.a. results and a damage accumulation method (e.g. Palmgren-Miner).
In the near future the available test data will be evaluated in a statistical manner to find a typical fatigue curve for glass fiber reinforced polyester.

The research is carried out by a working group made up by institutes and manufacturers. The institutes are ECN, NLR, Delft University of Technology and N.V. KEMA. The manufacturers/designers are Aerpac, Polymarin, NedWind and SPE.

FATIGUE FORMULATIONS

Mandell-type formulations

For design purposes a fatigue formulation is needed, to express the allowable number of cycles versus a loading. This S-N formulation is an interpretation from various test results, sometimes with a micro-theoretical backing.
At the start of the fatigue program very few formulations were available. Of these the formulation as proposed by Mandell [7] seemed the most promising.
Mandell's simple degradation model gives an adequate approximation for a variety of fiber textiles and matrix materials in tension-tension fatigue. A modification as proposed by Appel and Olthoff [1] takes into account the effect of the mean stress, this modification is called the Appel-Olthoff formulation.
The Mandell equation gives a relation between the maximum stress in the fatigue cycle and the lifetime: about 10% of the initial strength is lost every decade. By this it gives a model with which different types of glass/matrix materials and lay-ups can be described.
In fig. 1 the modified Mandell formulation is plotted in a Goodman diagram: lines of constant life in a stress amplitude versus mean stress diagram. The figure shows a draw back of the formulation: at 10^9 cycles the allowable stress amplitude is zero for a mean stress of 0% and 27% of the ultimate strength.

Range-type formulations

An alternative way to describe the fatigue behaviour is a range versus cycle formulation. In this formulation a linear relation is proposed between the (log of the) stress range in

the cycle and the (log of the) number of cycles. This formulation is common for steel and aluminum, but it was also proposed for glass/epoxy [6].
When using a range-type formulation it seems wise to take the effect of the mean stress into account.
In the present Dutch certification criteria [8] a range-cycle formulation is used. The mean stress is corrected for by a Goodman line: a straight line between the ultimate strength and the stress amplitude at R=-1 (R being the minimum divided by the maximum value in the stress cycle). The Goodman diagram is shown in fig. 2. Because of the log-log nature the allowable amplitude at high number of cycles is higher than in the Appel-Olthoff diagram.

SUMMARY OF THE TEST RESULTS

At present the majority of the tests are already carried out. The major exceptions are the 'ultra high cycle' tests (expected lifetime of at least $5*10^8$ cycles) and compression-compression fatigue.
Test results are presented in fig. 3 for glass-polyester laminates with a lay-up of 0° or $(\pm 45°)_s$, for R-values R=0.1 and R=-1. With the range on the vertical axes the scatter is rather low.

Most rotor blades have a lay-up using a combination of 0° or ±45° layers. It is expected that the fatigue behaviour of such a laminate can be calculated from the fatigue curves of the base materials, using some sort of rule-of-mixtures. To verify this expectation a symmetric laminate was tested with a lay-up using 50% 0° and 50% ±45° (as is used for bolted connections). Results of fatigue tests show this expectation to be true. When normalized with the static tensile strength the fatigue data fit the master curve of the 'base' materials (fig 4).
When the results of the 0/±45 laminate are presented in a Goodman diagram, the Goodman-line shows to be an adequate approximation (fig. 5). At the same time the weakness is shown: no data are available in the compression-compression part of the diagram.

WISPER results of the 0/±45 laminate show a different story: the curve of the 0° laminates is higher and steeper (fig. 6). One WISPER sequence being roughly the equivalent of 2 months, we are interested in the region from 100 to 200 WISPER passes. In this region the 0° laminate has a higher allowable stress, which seems to contradict the constant amplitude results.
For bolted specimens there is another peculiarity when comparing c.a. results with WISPER results. Specimens were preconditioned to find the effect of moisture. Lifetimes for c.a. loading are typically one decade shorter than "dry" specimens. At present only 3 specimens are tested with WISPER, but the lifetimes are similar to the dry specimens. Additional tests will be carried out in the future. The fatigue curve of bolted specimens coincides with the fatigue curve of coupons.

COMPARISON OF FORMULATIONS WITH TEST RESULTS

Several fatigue formulations have been discussed within the research program. Since we are looking for a general formulation it is necessary to normalize the data or to present the data on a strain-basis. At present we focus at normalization (by the static strength) because strain-life curves do not coincide very well.
The formulations as discussed in this paper are normalized by the tension strength. They are compared with the test results for R=.1 and R=-1 in figure 8. The results are presented in a log-log graph. For both R-values the results fall within a narrow band, except for a NLR-tested laminate at R=-1. This laminate gives a lower curve with a flat slope. The reason for this is not quite clear, it might be caused by the anti-buckling device.

For the tension-tension situation both curves represent the test data well up to 10^8 cycles.
For the tension-compression situation (R=-1) the Appel-Olthoff formulation is too optimistic for the lower cycle region and too conservative for the high cycle region. The 'hinge' lies near 10^7 cycles. The certification curve gives a kind of lower bound to the results.
For the available test results the range-Goodman formulation seems to give a better representation than the Appel-Olthoff formulation.

ACKNOWLEDGEMENT

The Dutch national program is sponsored by NOVEM, the Dutch agency for energy and environment, and works in close cooperation with a European program, sponsored by the European Community, DG XII.

LITERATURE

[1] N. Appel, J. Olthoff
Pre-design study NEWECS-45 (in dutch)
Polymarin, Medemblik, 28 June 1984

[2] P.W. Bach
Fatigue testing of glass fibre reinforced polyester coupon specimens, bolted and bonded joints of wind turbine blades. Report on phase III (in dutch)
Report ECN-88-78, November 1988

[3] P.W. Bach
Fatigue properties of glass- and glass/carbon-polyester composites for wind turbines
Report ECN-C-92-072, November 1992

[4] W.J.A. Bonnee
Constant amplitude and spectrum fatigue loading of glass fibre reinforced polyester coupon specimens
NLR, report NLR CR 90316 L, 1991

[5] W.J.A. Bonnee
Fatigue testing of pre-stressed bolted joints in glass fibre reinforced polyester
Sub-report on phase III (in dutch)
Report NLR TR 99181 L, December 1988 (2 volumes)

[6] E. Jarosch, A. Stepan
Fatigue properties and test procedures of glass reinforced plastic rotor blades
J. of American Helicopter Society, Jan. 1970

[7] J.F. Mandell, D.D. Huang, F.J. McGarry
Tensile fatigue performance of glass fiber dominated composites
M.I.T. research report R80-4, Nov. 1980

[8] L.W.M.M. Rademakers e.a.
Proposal to change the technical criteria with respect to the fatigue properties of fiber reinforced composites (in dutch)
ECN, DE-Memo-91-58, 10 december 1991

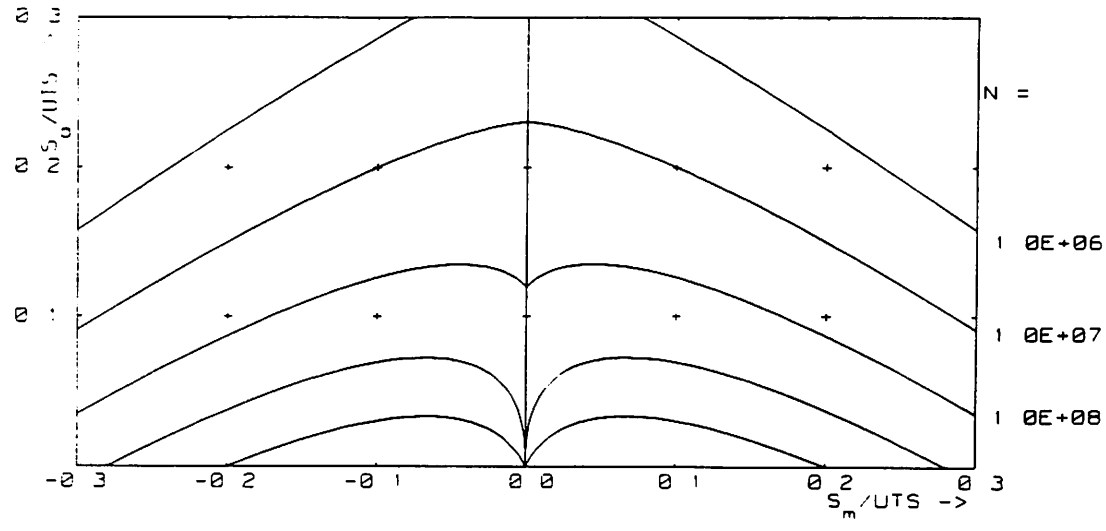

Figure 1: Goodman diagram of fatigue curves according to Appel-Olthoff, from 10^6 to 10^{10} cycles.

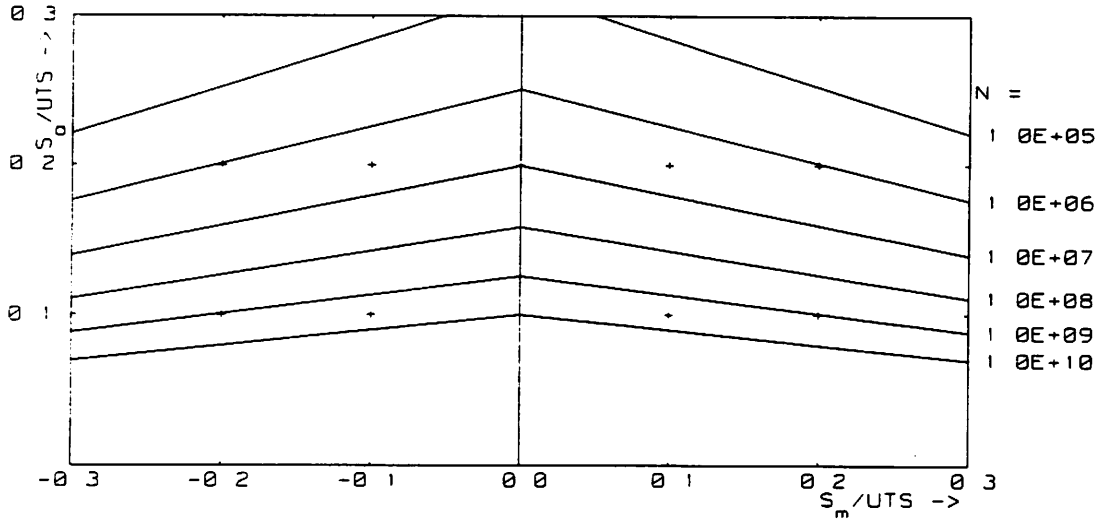

Figure 2: Goodman diagram according to present Dutch certification curve, from 10^5 to 10^{10} cycles.

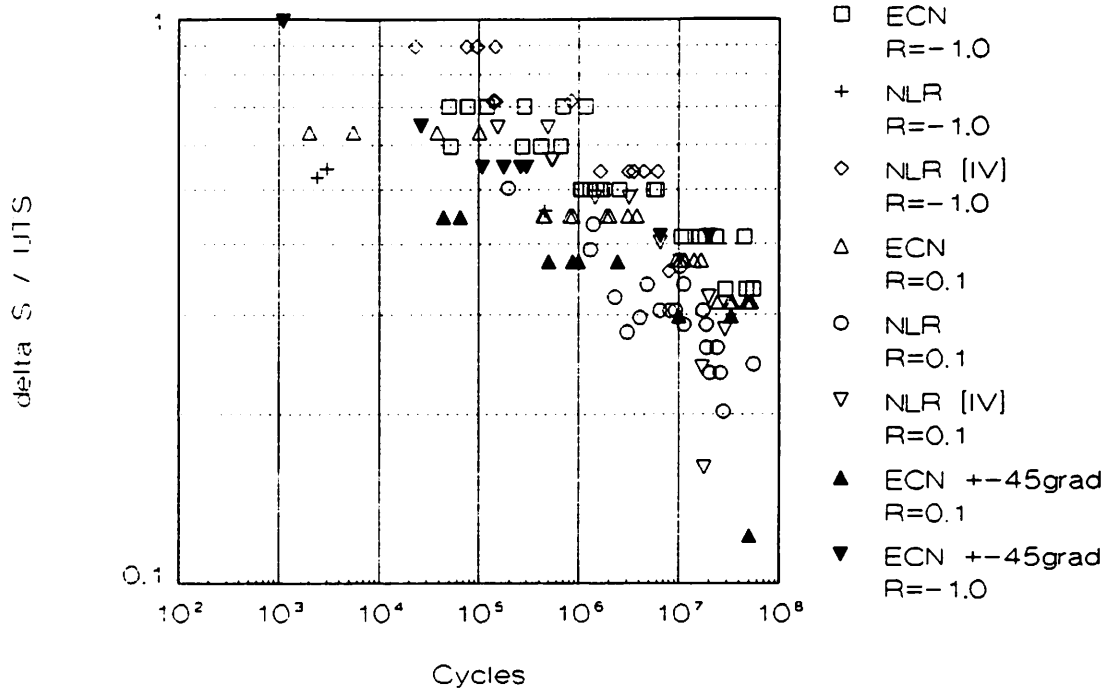

Figure 3: Normalized stress range plotted against the number of cycles to failure.

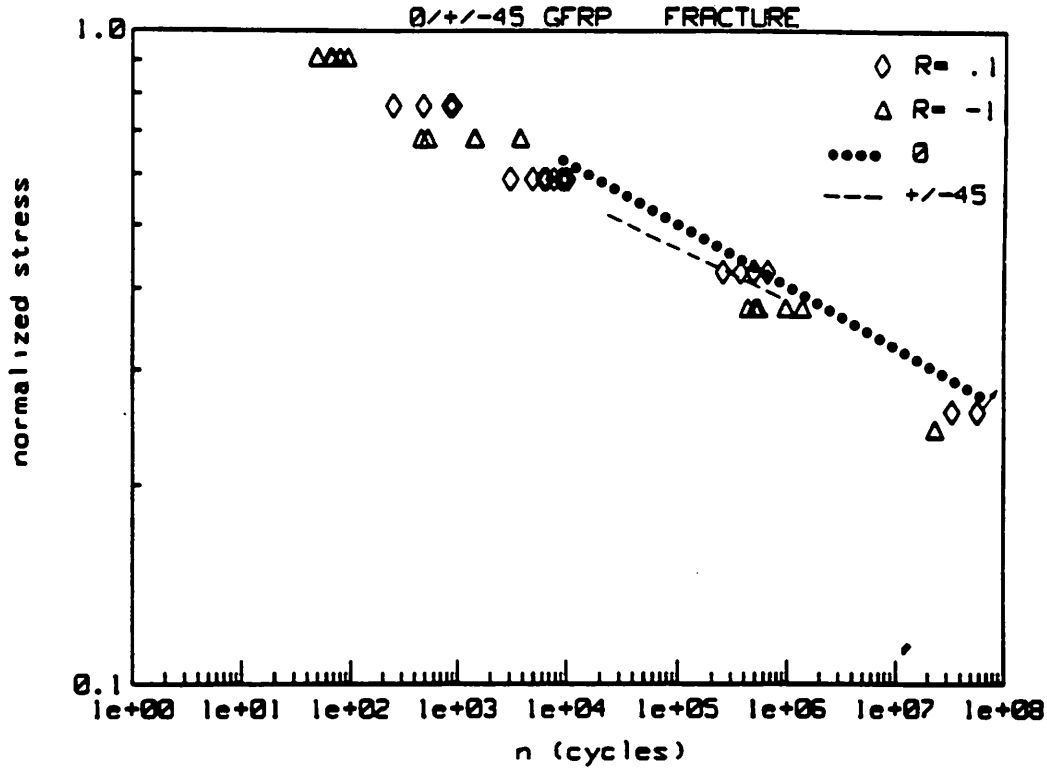

Figure 4: Comparison of c.a. results for three glass/polyester laminates: 0°, 45° and 0°/±45° lay-ups [3].

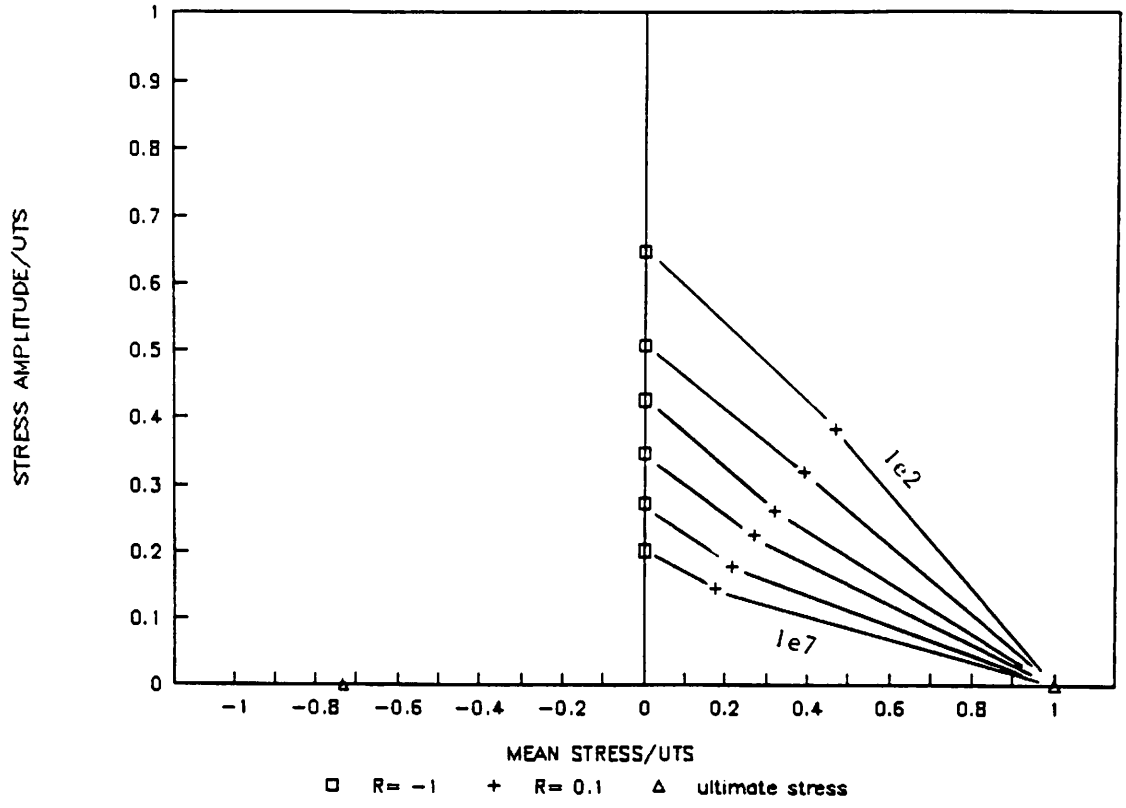

Figure 5: Goodman diagram for the 0°/±45° laminate [3].

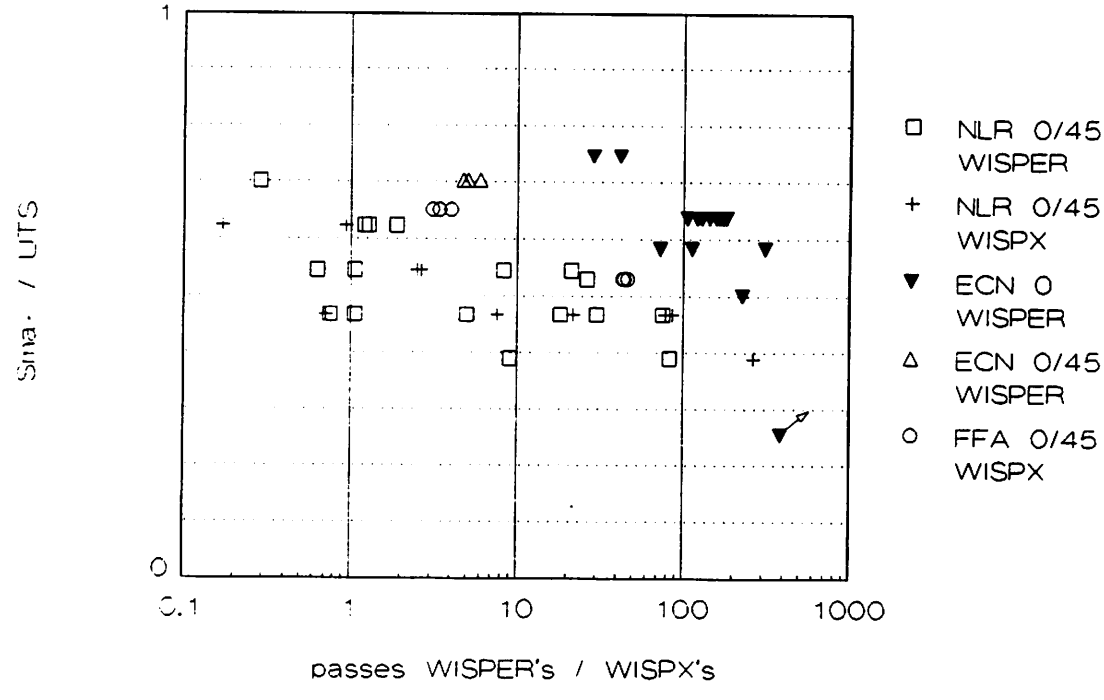

Figure 6: Comparison of WISPER results for 0° and 0°/±45° laminates.

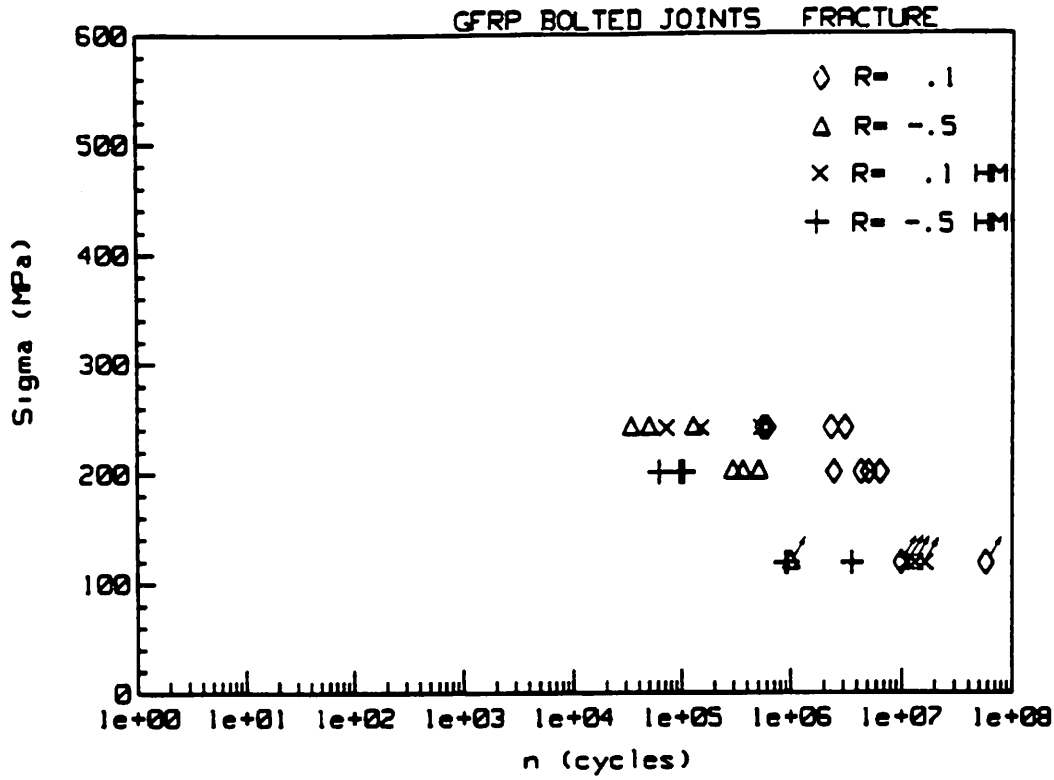

a) constant amplitude results

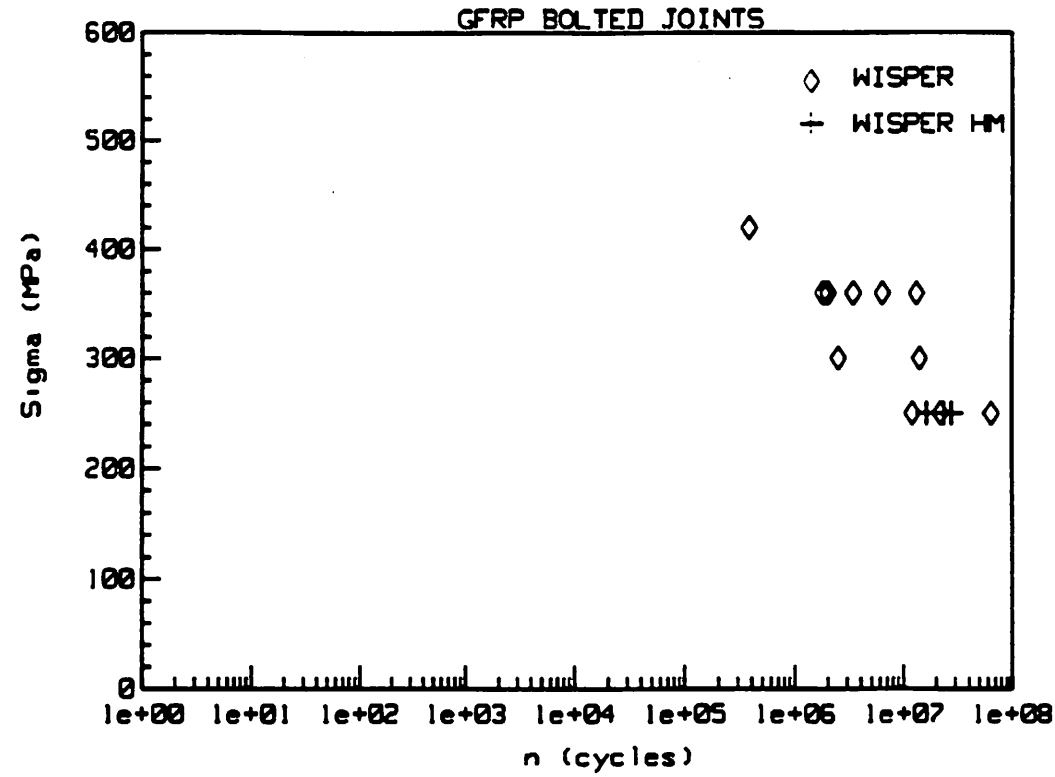

b) variable amplitude results (WISPER)

Figure 7: Influence of moisture on the fatigue results of bolted joints with lateral constraint (failure) [3].

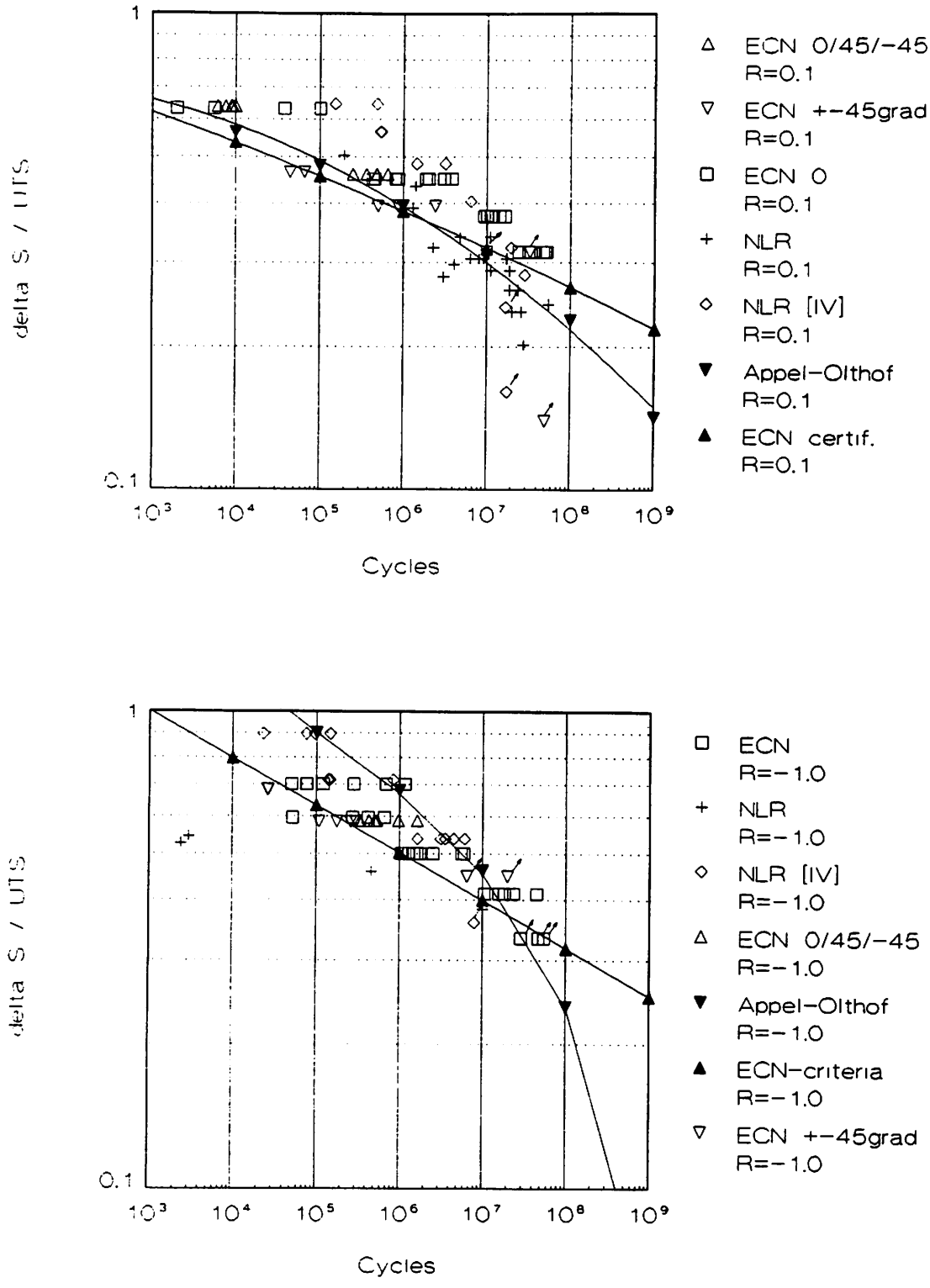

Figure 8: Comparison of test results with two fatigue formulations: Appel-Olthoff (Mandell-type) and the present Dutch certification (range-type).

IEA - Workshop on Fatigue of Wind Turbines
NREL, Golden, Colorado, USA. 15-16th October 1992

MATERIAL FATIGUE TESTING TECHNIQUES AND RESULTS

Fatigue testing of wood composites for aerogenerator blades. - Alternative wood species and joints.

P W BONFIELD, I P BOND, C L HACKER, M P ANSELL
University of Bath, UK

1.) Alternative Species

In the last ten years wood composite blades produced by the major British manufacturers, Composite Technology Ltd., James Howden and Co. Ltd. and Wind Energy Group Ltd., have been constructed from *Khaya ivorensis* (African Mahogany) veneers. *Khaya* is still considered an excellent material for blade fabrication but commercial and environmental pressures have led to the investigation of the potential that other wood species may offer.

The wood species considered to be suitable as alternatives to *Khaya* have been identified as birch, Baltic pine, poplar and beech. All were readily available at low cost and had good basic mechanical properties. Samples of each were laid up by WEG Ltd. and incorporated factory standard joints and a glass/epoxy skin reinforcement.

Reversed load (R=-1) fatigue testing and some static tensile testing was carried out in order to evaluate the various species' performance. Figure 1 is a S-N plot of all wood types tested with outer veneer scarf joints and inner veneer butt joints. The static data shows a great deal of scatter with birch marginally stronger than Baltic pine. The fatigue data also shows a large degree of scatter. Beech gives a marginally better performance than Baltic pine, Khaya and birch whilst poplar gives the poorest relative performance.

The effect of scarf jointing alone is shown in figure 2, where Khaya, beech and poplar are compared at R=-1. Again, poplar lives are generally the lowest but the difference in performance between Khaya and beech is more difficult to ascertain due to testing at different peak stress levels.

The choice of an alternative species to Khaya for the construction of wind turbine blades is difficult as mechanical property advantages must be weighed against raw material costs, manufacturing costs and availability and security of supply.
The fatigue performance of the wood species tested demonstrates that there is little

difference between the wood species examined, although the performance of poplar is slightly inferior. Baltic pine and birch, although low cost are only available in 2.5mm veneer which results in a larger quantity of expensive epoxy resin being required for blade manufacture. The viable alternatives to Khaya are beech (- good fatigue performance, higher density, lower cost, available in 6mm veneer) and poplar (- inferior fatigue performance, lower density, lower cost, available in 5mm veneer).

2). Joints

Another important consideration in blade manufacture and design is the way in which the individual veneers are end jointed during fabrication. The performance of these joints in service is crucial as they are likely to be the points from which failure may initiate.

Butt joints have traditionally been used in laminated wood construction for wind turbine blades. However, this type of joint is weak compared to scarf or finger joints. An investigation was made into the effect on performance of replacing some or all of the butt joints with scarf joints. It was felt the potential increase in performance could justify the more complex manufacture. Samples were also tested which contained the type of scarf joint faults that may occur in practice. If, for example, veneers are not joined accurately, the joint faces may not be in full contact (underscarf), or will ride up over each other (overscarf). Both of these faults may contain voids either empty or full of resin. These may act as stress concentrators or areas of weakness, causing premature failure.

All samples incorporated factory standard joints and GRP facings. In the case of Khaya, all butt, scarf/butt, 4 scarf, overscarf and underscarf samples were prepared, for poplar, scarf/butt, 4 scarf, overscarf and underscarf samples were prepared, and for beech, scarf/butt, 4 scarf and 5 scarf samples were prepared. The scarf joint geometry was 6:1 (length to height) and joint spacing in the samples was 55mm. Fatigue testing was all carried out at R=-1 (reversed loading).

Figure 3 shows S-N data for jointed Khaya samples. Of the jointed samples, those containing overscarf joints gave the best fatigue performance. The 4 scarf and underscarf Khaya were marginally poorer in performance to the overscarf but the number of data points is insufficient to be conclusive. The scarf/butt and all butt samplese were the poorest performers of all.

Figure 4 is an S-N plot of jointed poplar data. The fatigue performance of poplar at similar stress levels is far more susceptible to joint geometry. This is probably a result of poplar's lower static strength values. The 4 scarf samples consisently gave the best performance. Interestingly, in contradiction to the Khaya data, scarf/butt

poplar gave a better performance than either of the imperfect scarf joint samples, both of which performed similarly. Figure 5 is a comparison of 4 scarf poplar and scarf/butt Khaya. Scarf/butt jointed Khaya has previously been used, with success, in blade construction. This overlay plot implies that scarf jointed poplar may indeed have the required fatigue performance for use in turbine blades.

Figure 6 is the plot of jointed beech data. The samples containing scarf/butt joints are consistently out performed by the 4 and 5 scarf jointed samples. Their respective performances showed little discernible difference.

All scarf jointing, although technically more difficult and expensive from a manufacturing point of view, provides the best fatigue performance from any of the wood laminate systems (Khaya, poplar and beech) considered here.

References

Fatigue Testing of Wood Composites for Aerogenerator Blades.
Part VII. Alternative Wood Species and Joints;
Bonfield, P.W.; Bond, I.P.; Hacker, C.L.; Ansell, M.P. (1992). *Proc. of the 14th BWEA Wind Energy Conference - Wind Energy Conversion-1992.*, Ed. Clayton, B., Mechanical Engineering Publications., pp. 243-249.

Timber, its structure, properties and utilisation.;
H.E.Desch (revised by J.M.Dinwoodie). 6th Ed.;
McMillan Press Ltd., London, 1981.

Strength properties of timber.;
G.M.Lavers; Department of the Environment, London, 1983.

Wood Handbook: Wood as an Engineering Material.;
USFPL, (U.S. Forestry Products Laboratory);
U.S. Department of Agriculture Handbook 72, 1974.

Timbers of the World. Volumes I and II;
TRADA; Construction Press, 1980.

Figure 1 - S-N plot of scarf/butt jointed species at R=-1

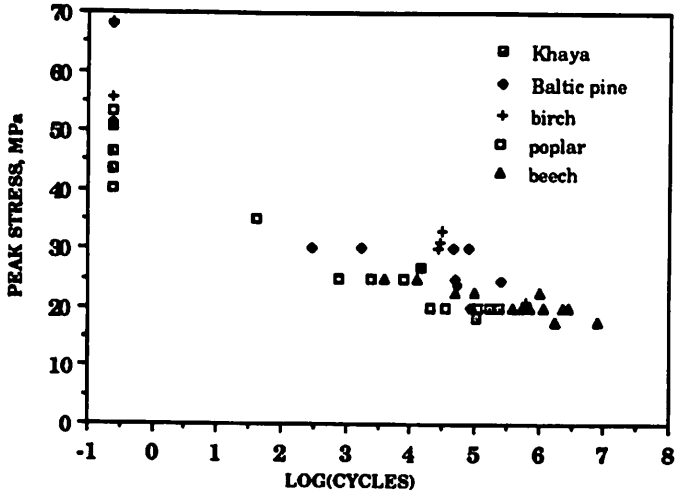

Figure 2 - S-N plot of all scarf jointed samples tested at R=-1

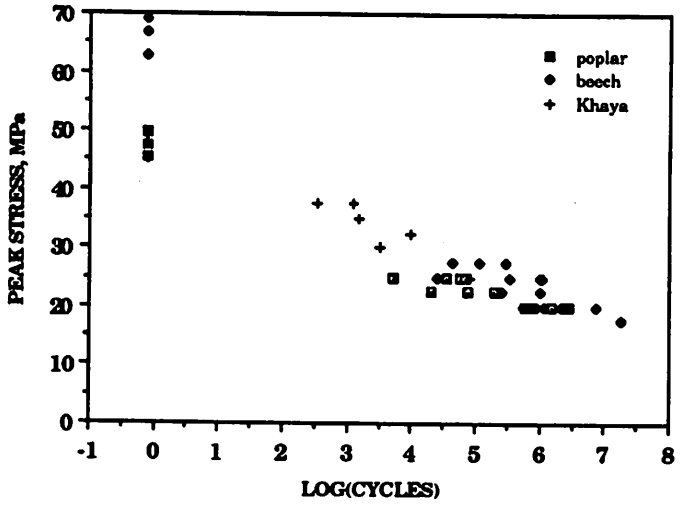

Figure 3 - Khaya joints data at R=-1.

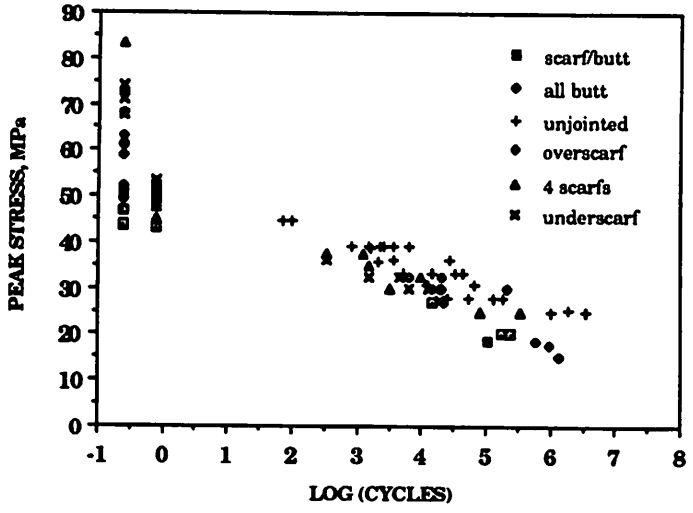

Figure 4 - S-N plot of jointed poplar

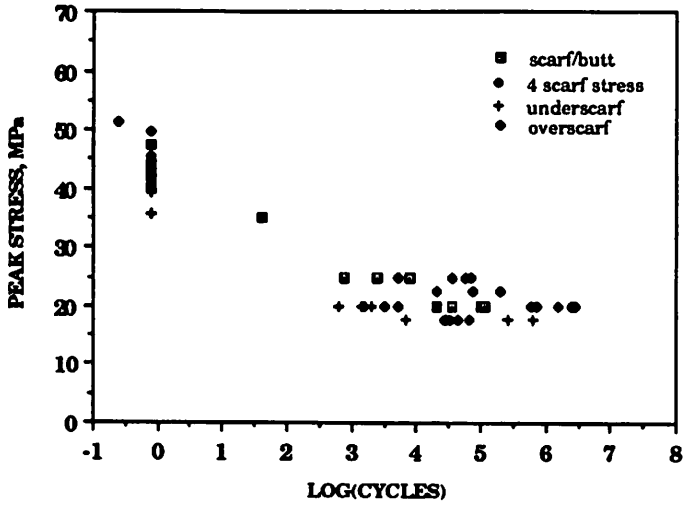

Figure 5 - S-N plot comparing scarf poplar and scarf/butt Khaya

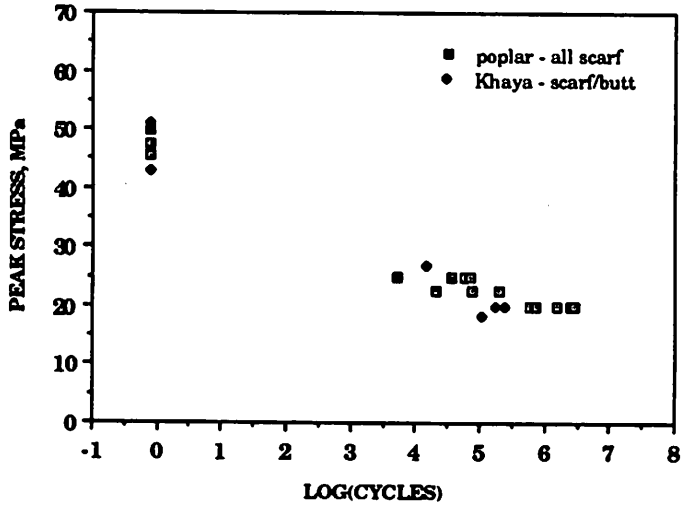

Figure 6 - S-N plot of jointed beech at R=-1

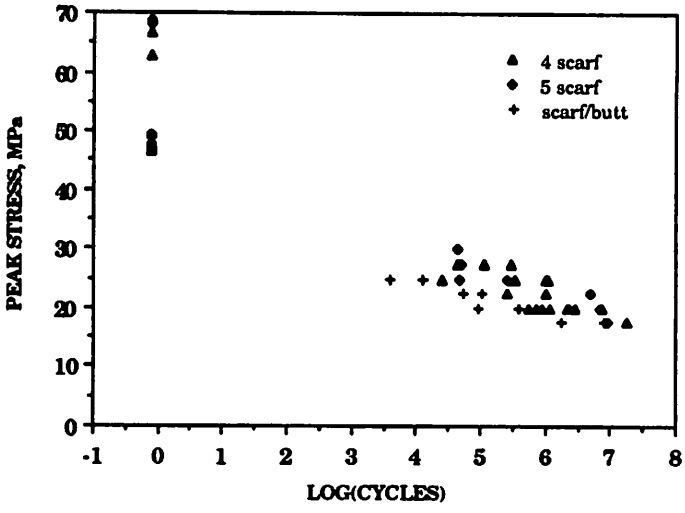

NATIONAL RENEWABLE ENERGY LABORATORY
IEA - FATIGUE EXPERTS MEETING, OCTOBER 15-16, 1992

U.S. WINDPOWER BLADE DEVELOPMENT

BY

BENJAMIN BELL
U.S. WINDPOWER, INC.
6952 PRESTON AVENUE
LIVERMORE, CALIFORNIA 94550

U.S. WINDPOWER BLADE DEVELOPMENT

PRESENTATION OUTLINE

- OVERVIEW
- STRUCTURAL REQUIREMENTS
- DESIGN PROCESS
- DESIGN CONSIDERATIONS
- TESTING PROGRAM

U.S. WINDPOWER BLADE DEVELOPMENT

OVERVIEW

- **MODEL 56-100:** 8.3 METER BLADE
  NACA 44 SERIES AND NASA LS(1) AIRFOILS
  OVER 15,000 BLADES IN SERVICE
  OVER 33,000 HOURS ON BLADE
  OVER 1.4 X 10^8 CYCLES ON BLADE
  OVER 231 MILLION CUM OPERATING HOURS

- **MODEL 33M-VS:** 16.1 METER BLADE
  66 BLADES IN SERVICE
  OVER 3,200 HOURS ON BLADE
  OVER 9.6 X 10^6 CYCLES ON BLADE
  OVER 210,000 CUM OPERATING HOURS

U.S. WINDPOWER BLADE DEVELOPMENT

STRUCTURAL REQUIREMENTS

- **STIFFNESS: TOWER CLEARANCE**
- **STRENGTH: 30 YEAR LIMIT LOAD**
- **LIFE: 30 YEARS**

U.S. WINDPOWER BLADE DEVELOPMENT

DESIGN PROCESS

- PROPOSE LAMINATE
- CALCULATE BLADE PROPERTIES
- CALCULATE BLADE STRESSES USING DESIGN LOADS
- MEET LIMIT AND FATIGUE LOAD REQUIREMENTS
- MEET STIFFNESS REQUIREMENTS
- ITERATE ON LAMINATE TO MINIMIZE WEIGHT

U.S. WINDPOWER BLADE DEVELOPMENT

DESIGN CONSIDERATIONS

- GEOMETRIC: AIRFOIL, BLADE TAPER AND TWIST, ROOT GEOMETRY
- STRUCTURAL: STATIC AND FATIGUE STRENGTH DRIVEN BY:
  - STEADY AND UNSTEADY AERODYNAMIC LOADS
  - CYCLIC GRAVITY LOADS
  - CENTRIFUGAL LOADS
  - LOAD COMBINATIONS AND TIME AT LOAD

  STIFFNESS REQUIREMENTS DRIVEN BY:
  - TOWER CLEARANCE
  - EFFECTS OF TURBULENCE AND BLADE DYNAMIC RESPONSE
- WEIGHT: GRAVITY AND CENTRIFUGAL LOADS OF THE BLADES

  EFFECT OF ROTOR WEIGHT ON THE REST OF THE WIND TURBINE STRUCTURE

  SPEED OF ROTOR RESPONSE AFFECTING CONTROL OF TORQUE TRANSIENTS AND OVERSPEED

U.S. WINDPOWER BLADE DEVELOPMENT

OTHER DESIGN CONSIDERATIONS

- SURFACE FINISH - HYDROPHOBIC AND ABRASION RESISTANCE
- LIGHTNING PROTECTION
- ANTI-ICING AND DE-ICING SYSTEMS
- EASE OF MANUFACTURE
- REPAIRABILITY
- COST

U.S. WINDPOWER BLADE DEVELOPMENT

BLADE TESTING PROGRAMS

- AIRFOIL TESTING
- LAMINATE STATIC MATERIAL TESTS
- BLADE ROOT BOND TESTS - DOUBLE LAP SHEAR TESTS
- BLADE ROOT BOND TESTS - 1/5 SCALE
- BLADE ROOT EPOXY RHEOLOGY TESTS OVER WIDE TEMP RANGE
- COMPOSITE MATERIAL FATIGUE TESTING
- FULL SCALE BLADE ROOT TESTING (SIAMESE TWIN)
- FULL SCALE BLADE LIMIT LOAD TESTING
- NREL - LIMIT LOAD, FATIGUE, AND MODAL TESTS

U.S. WINDPOWER BLADE DEVELOPMENT

AIRFOIL TESTING

- OHIO STATE UNIVERSITY / NREL
- NASA LS(1)-0417 MOD AIRFOIL
- 2-D AERO DATA AT OPERATING REYNOLD'S NUMBERS (1.5 - 3 x 10^6)
- EFFECTS OF REALISTIC ROUGHNESS BEING EVALUATED
- DYNAMIC STALL EFFECTS MEASURED
- FULL 360 DEGREE DATA

U.S. WINDPOWER BLADE DEVELOPMENT

FULL SCALE BLADE ROOT TESTING (SIAMESE TWIN)

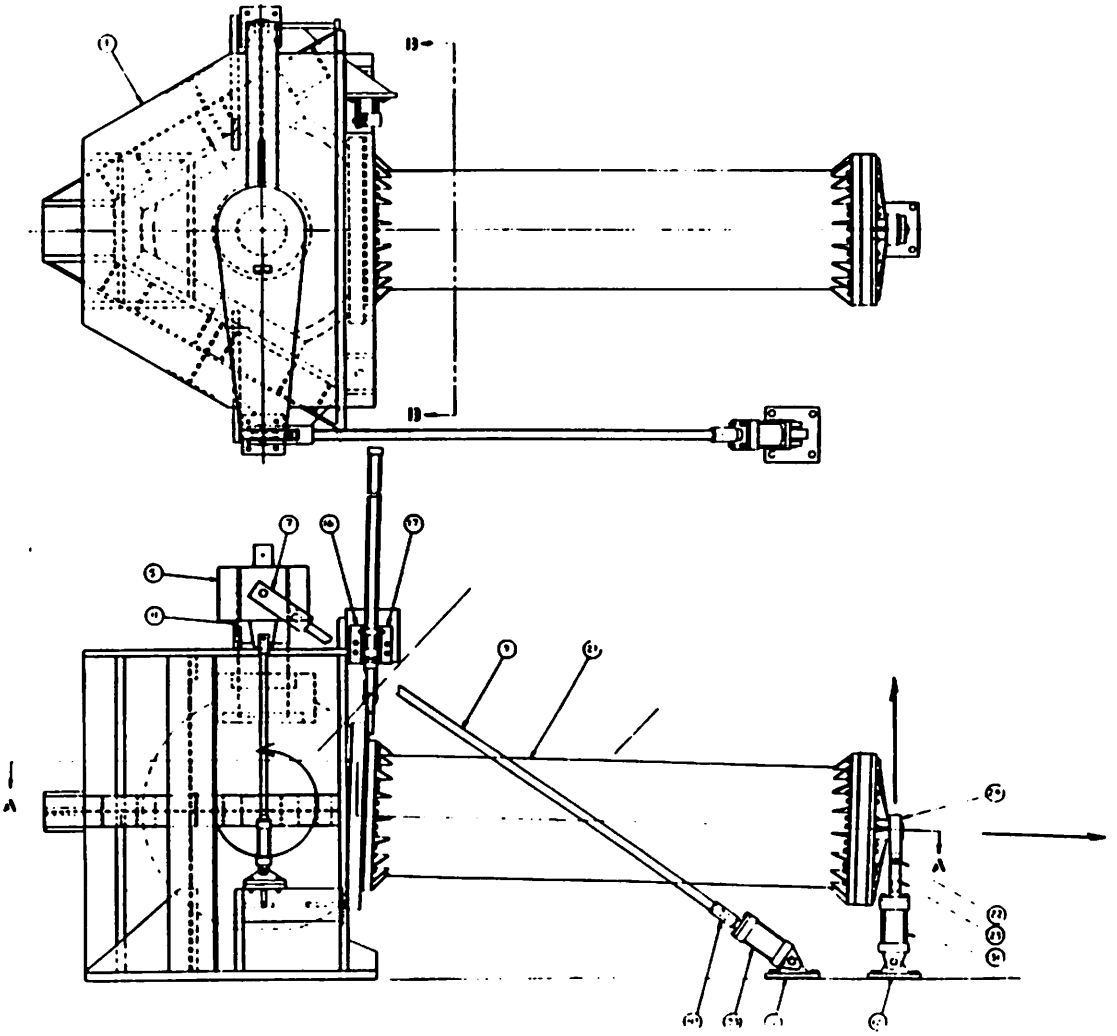

U.S. WINDPOWER BLADE DEVELOPMENT

FULL SCALE BLADE LIMIT LOAD TESTING

- DISTRIBUTED LOADING
- LOADS UP TO 10.5 x 10^6 IN-LBS
- BLADE STRAIN MEASUREMENT AND ANALYSIS
- DEFLECTED BLADE SHAPE MEASURED

U.S. WINDPOWER BLADE DEVELOPMENT

33M-VS WIND TURBINE BLADE BENDING DISTRIBUTION

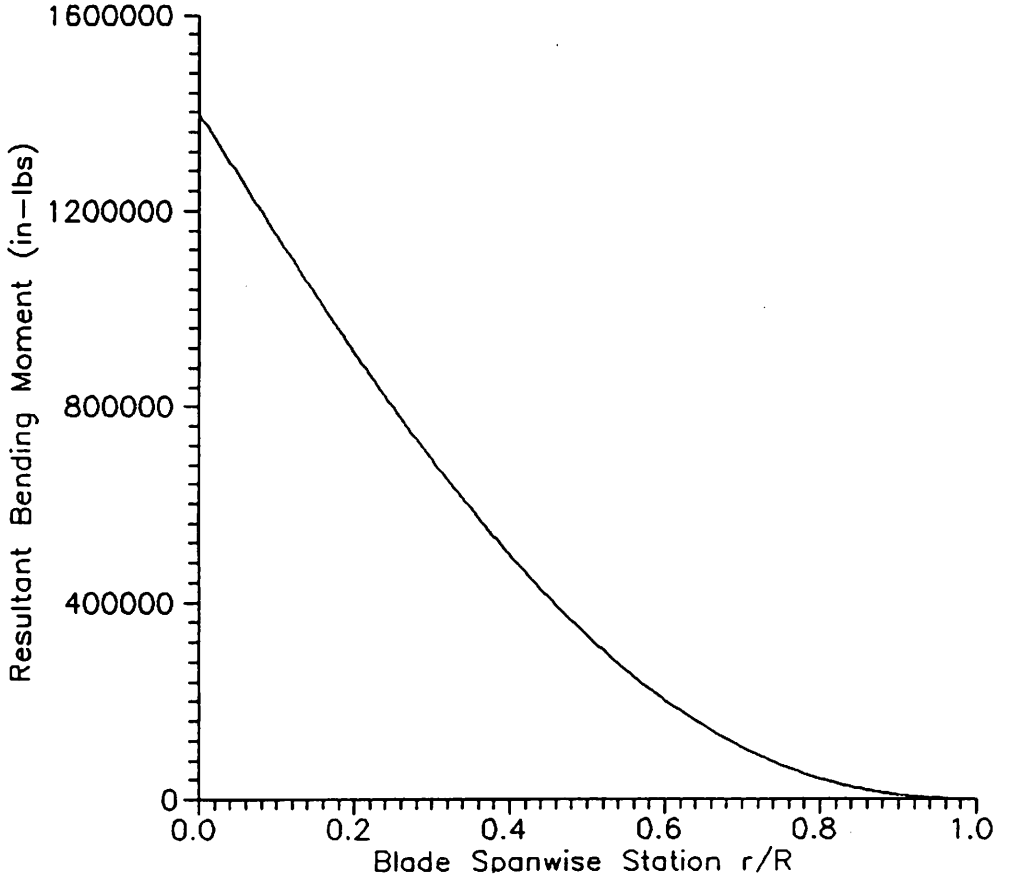

U.S. WINDPOWER BLADE DEVELOPMENT

33M-VS FULL SCALE LIMIT LOAD TEST STAND AND WHIFFLE TREE

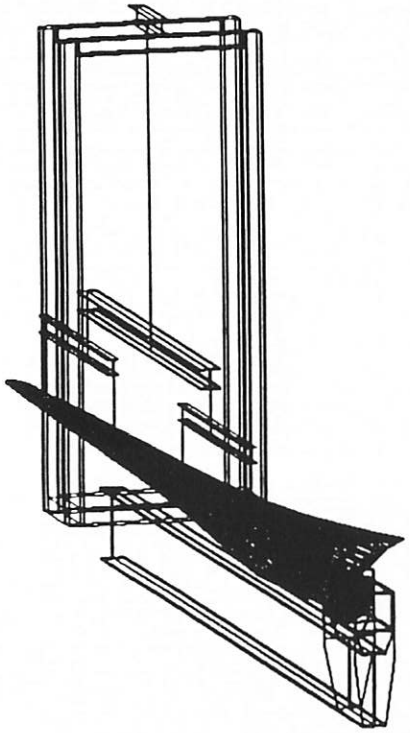

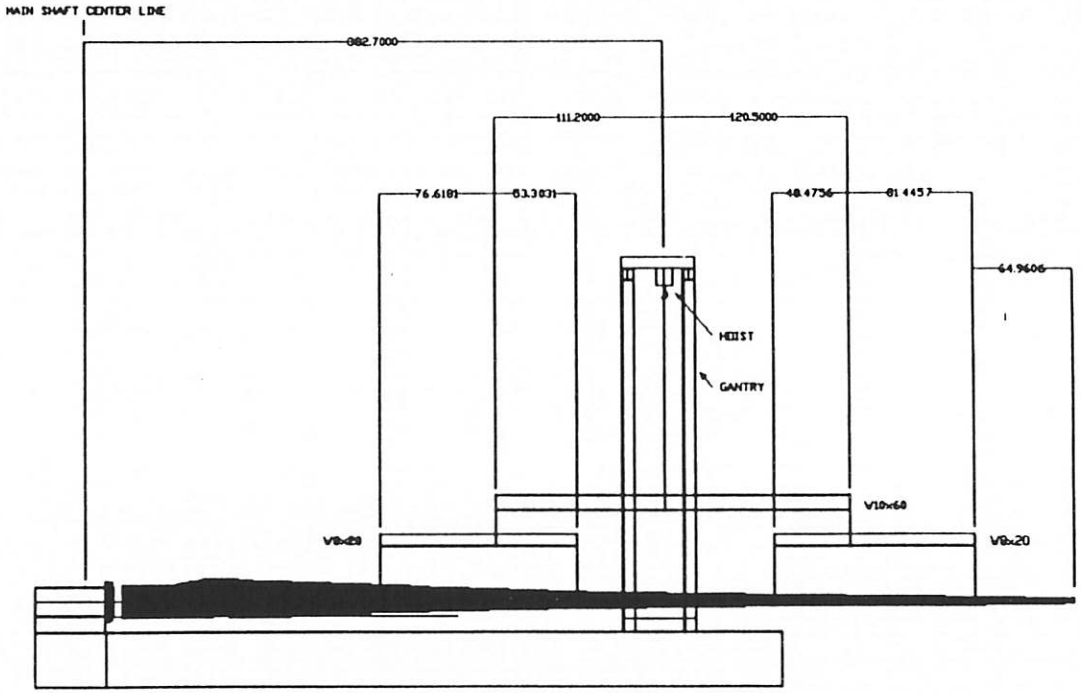

U.S. WINDPOWER BLADE DEVELOPMENT

33M-VS FULL SCALE LIMIT LOAD TEST BLADE SADDLE

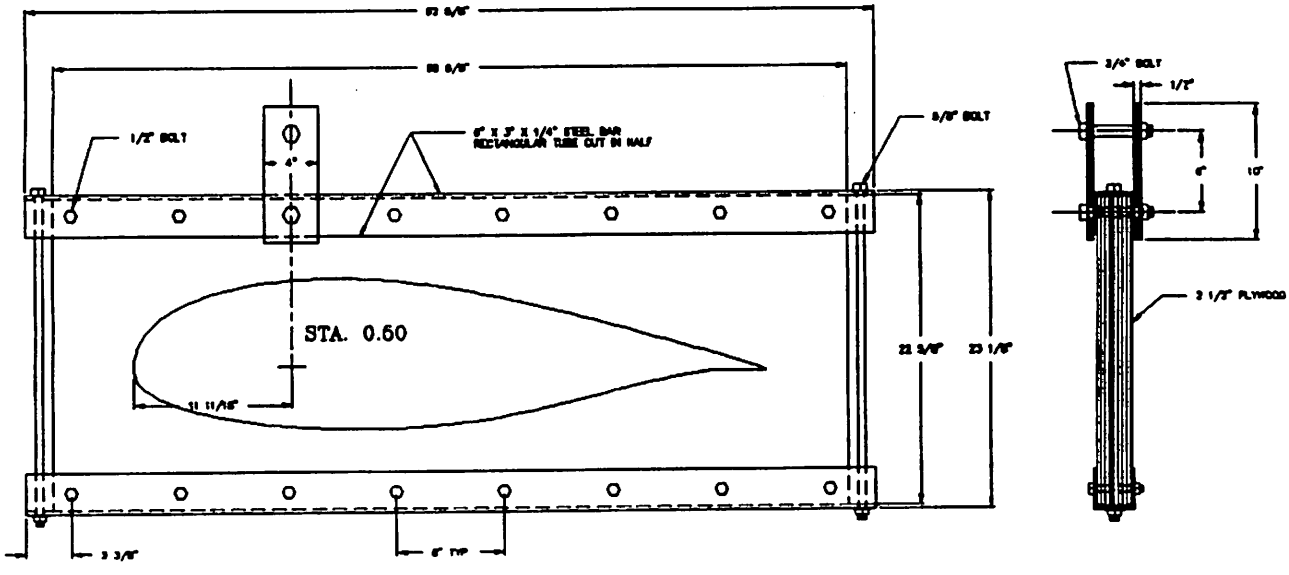

U.S. WINDPOWER BLADE DEVELOPMENT

33M-VS BLADE LIMIT LOAD TEST INSTRUMENTATION

- SIXTEEN (16) CHANNELS PER BLADE
- LOAD CELL
- FOUR (4) - RECTANGULAR ROSETTES (0, 45, AND 90 DEGREES)
- TWO (2) CALIBRATED BENDING MOMENT CHANNELS

TEST METHODOLOGY AND CONTROL OF FULL-SCALE FATIGUE TESTS ON WIND TURBINE BLADES

Walt Musial and Jack Allread
National Renewable Energy Laboratory
Golden, Colorado

ABSTRACT

Engineers at the National Renewable Energy Laboratory's (NREL) Structural Test Facility are conducting full-scale fatigue tests on wind turbine blades. The test system uses a closed-loop servo hydraulic system that applies repeated load cycles to a wind turbine blade. Two different blades have been tested to date: the U.S. Windpower, Inc. (USW) 56-100 blade with a new LS(1) airfoil design, and the first prototype Atlantic Orient Corporation (AOC) 15/50 blade being developed under the U.S. Department of Energy (DOE)/NREL Advanced Wind Turbine Program.

The USW 56-100 blade is constructed of fiberglass and was fatigue tested following multiple destructive tests using a quasi-static, eight-point load distribution. The fatigue tests used single-point loading to match the quasi-static bending moments along the inner 40% blade span. This blade test is still under way. The AOC 15/50 blade was fatigued to validate the design calculations and the manufacturing techniques used to build the first prototype. Both blade tests were performed using constant stroke-amplitude block loading.

During full-scale blade fatigue testing, it was necessary to consider several issues that are typically ignored during fatigue tests of material coupons. The issues include choosing the proper load introduction point, dynamic effects, test control, data collection, failure monitoring, and relating test results to material data. This paper describes how several of these issues were addressed during the test setup and execution. The experience we gained will be used to help establish better procedures and improve the quality of future tests.

INTRODUCTION

NREL has constructed a Structural Test Facility at its Wind Energy Test Center (WETC) in Golden, Colorado. The facility is designed to conduct composite blade research and assist the wind industry in developing more advanced blades. The capabilities of the facility range from static load testing to fatigue testing of blades up to 18.28 m (60 ft) long. Recently, we conducted tests on both the USW 56-100 and the AOC 15/50 blades. This paper overviews the test procedure used and discusses some of the fatigue testing issues that were encountered during these first blade tests.

TEST FACILITY DESCRIPTION

The test stand provides a rigid, flat surface to which a wind turbine blade can be mounted horizontally. Static and fatigue tests are performed on this stand. It is designed to carry a maximum overturning moment of 1,356 kN-m (1,000,000 ft-lb). The vertical mounting plate has an adjustable tilting feature of ±6° that allows the blade tip to be raised or lowered for the optimum placement of test equipment. Fatigue loads are applied by a hydraulic actuator mounted to the floor.

The NREL fatigue test facility uses a closed-loop servo-hydraulic system. Most of the equipment is supplied by MTS Systems Corporation, a company that specializes in simulating the testing of large structures. A schematic of the NREL fatigue test setup is shown in Figure 1.

The general configuration allows arbitrary load profiles and test parameters to be generated on a personal computer (PC) using the custom MTS software. The load profile and test parameters are downloaded from the PC to the MTS T/RAC controller. The T/RAC is a digital-to-analog controller/interface that can simultaneously control up to four separate tests. The analog control signal is sent from the T/RAC to the MTS Model 458.10 controller. This command signal is sent to a proportional servo-valve that allows hydraulic fluid to flow to and from the actuator. The first fatigue tests were run using a sinusoidal, constant stroke-amplitude control signal with a single hydraulic actuator. Single-point loading was used to avoid backlash and other problems caused by dynamic motion of the load apparatus.

On the hydraulic actuator are two sensors that provide feedback to the analog controller: a load cell transducer and a linear position transducer (LVDT). The transducers monitor actuator force and actuator displacement, and each is controlled by its own conditioning module, the Model 458.12 and the 458.14, respectively, which plug into the MTS 458.10 analog controller. Feedback from the transducers allows the hydraulic system to determine if the actual response is

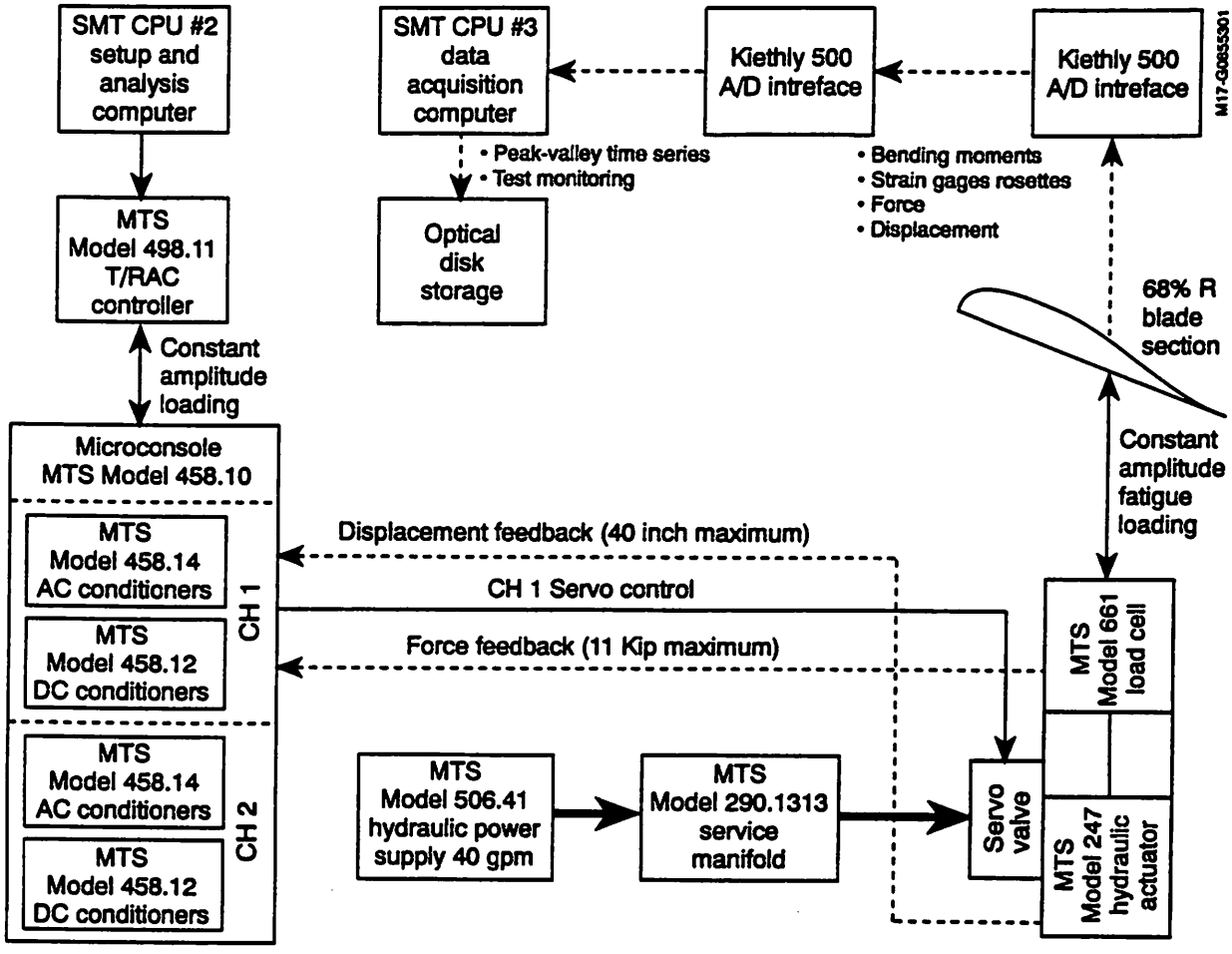

Figure 1. Schematic of NREL fatigue test system

consistent with the intended response. If it isn't, then a correction is made to the command signal at the controller.

Hydraulic fluid is supplied from the hydraulic power supply at pressures of 20,684 kPa (3000 psi) and flow rates up to 2.53 l/s (40 gpm). Pressure peaks are compensated for using hydraulic accumulators at several locations along the lines. An MTS hydraulic service manifold is located near the actuator. This device helps control pressure pluses, provides secondary filtration, and provides fast pressure unloading in the event of an emergency to isolate the test specimen from other tests operating off the same power supply.

Sixteen channels of data acquisition are available for each blade test. Strain-gages are used to measure the structural behavior of the blade during fatigue loading. Typically, twelve channels are dedicated to strain measurements using rectangular rosettes, two channels measure blade bending, and the final two record load and stroke. These two signals are used to control the test but are also recorded by the data-acquisition system. All strain-gage signals received bridge completion, bridge excitation, low-pass filtration at 10 Hz, and signal amplification from Honeywell 218 bridge amplifiers. All signals are passed to a Keithly Model 500 analog-to-digital interface and into a data-acquisition computer.

FATIGUE APPROACHES

Many techniques are used to perform fatigue testing on full-scale blades. A standardized approach is used by the European wind industry to certify blades for commercial operation in European markets. This approach provides standard values, based on rotor swept area, for load amplitude, peak load, allowable peak strain, and the number of cycles for a blade fatigue test that a blade must survive (Jensen et al., 1988). This method gives a good comparative evaluation of a blade and can uncover design flaws or weaknesses in a blade design. It may also guarantee a minimum blade fatigue life by applying conservative test criteria, but it does not predict the actual fatigue life. The conservative criteria may actually contribute to an excessive use of materials and, therefore, more costly designs. This can happen when loading characteristics, which vary among different wind turbine designs, are not accounted for.

To make the connection between the full-scale blade test and the operational fatigue life of the blade, more information must be known about the actual blade loading and the blade's material fatigue properties. A blade design must withstand between 10^8 and 10^9 cycles over a thirty-year lifetime. For a given blade, the content of the load spectrum is comprised of mostly small load cycles, which may be inconsequential to the fatigue life when compared to the less-frequent but larger-magnitude load transients. To conduct a representative full-scale blade fatigue test, the actual load spectrum must be compressed into a time history that can be applied in a reasonable amount of time. This is usually done by filtering the smaller, insignificant load cycles. This process is inexact, however; the properties of fiberglass under high-cycle fatigue are not yet understood, and damage accumulation models are inaccurate (Bach, 1991).

Generic load spectra have been developed (Ten Have, 1991) for composite blade and material testing. While variable-amplitude tests may more closely resemble the actual loading of the wind turbine blade and lead to more conservative results, it is not possible to extrapolate a blade life prediction from these tests. One reason is that turbine-specific loads alter the spectrum for a given wind turbine. Often, it is the high-amplitude but infrequent transient loads that are characteristic of a particular design and that contribute to much of the fatigue damage. In addition, most of the existing material properties data were generated from constant-amplitude sinusoidal block loading and are not easy to compare with spectrum-loaded coupon data. Some work is being done to try and correlate variable-amplitude data with constant-amplitude coupon data (Bonfield and Ansell, 1991). This is a necessary step toward understanding fatigue in composite wind turbine blades.

Because a good means for comparing spectral loading and constant-amplitude data is not yet available, we used constant-amplitude, sinusoidal block loading to perform the fatigue tests at NREL. This approach approximates the actual fatigue life of the blade by applying only the largest, most damaging load cycles to the blade. For a particular blade, the load levels and the load introduction point were selected to match the specific strength or loading distributions as best as possible. Although constant-amplitude tests may oversimplify the physics governing material fatigue, the results from this approach were easier to interpret and quickly provided the designers with important blade-specific information. A more sophisticated approach is still needed to be able to use the test results to predict the actual life of a blade operating on a wind turbine.

TEST CONTROL ISSUES

Frequency Effects:

During full-scale fatigue tests, it was important to run the cycle rate as fast as possible to obtain faster results. Unlike material testing, the effects of blade natural frequency must be considered. Prior to the beginning of the USW 56-100 blade tests, we conducted several tests at a lower load to investigate the effects of frequency on actuator load, stroke, and blade bending moment. Our objective was to determine an effective parameter that could be monitored and used to control blade motion while maintaining the proper blade stress.

As a specimen begins to fail in fatigue, the stress/strain relationship of the material changes. Most coupon tests are run under a constant load, so, as the elastic modulus decreases, the applied stress amplitude

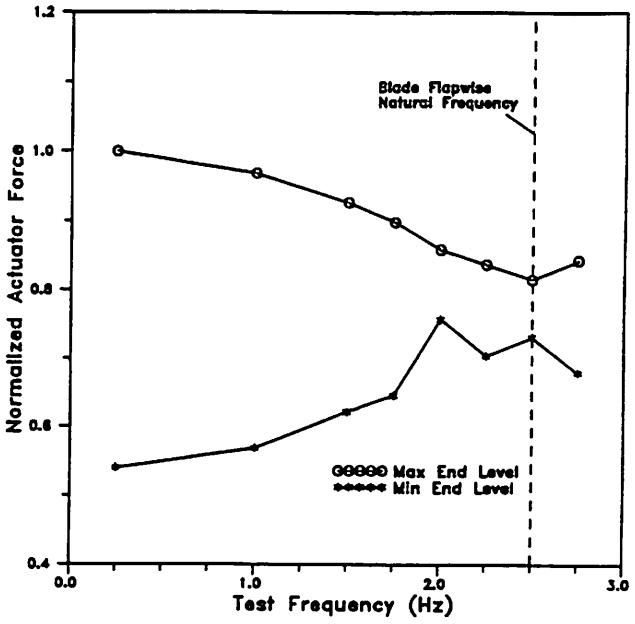

Figure 2. Frequency effects on actuator force for the USW 56-100 preliminary fatigue tests

remains constant. To make blade test results more comparable with coupon test data, tests should ideally be run at constant load. However, this is difficult because actuator force is very dependant on the frequency of the test and the natural frequency of the blade. Figure 2 shows how the range of actuator forces decreases for a constant stroke-amplitude of 19.05 cm (7.5 in.) as the test frequency was increased past the fundamental flap frequency. Note that at the natural frequency there is enough damping that a significant force is still required to maintain a constant stroke.

Bending moments measured on the blade can be used to approximate the actual blade stresses, but bending moments are poorly correlated with actuator forces near the blade's natural frequency. Figure 3 shows the relationship between bending moment and actuator force for three test frequencies. At very low frequencies, the bending moment and actuator force are linearly related. As the test frequency increases, the correlation becomes poorer. The phase angle between the actuator force and the bending moment also changes as the frequency increases. At low frequencies, load follows the bending moment and their extreme levels correlate well; however, at higher frequencies, extreme actuator loads do not correspond to extreme bending moments. Therefore, we cannot reliably infer blade stresses from actuator force.

A better correlation with bending moment is seen in Figure 4, where we show the relationship between bending moment and stroke, or actuator displacement, for three test frequencies. From this plot, we can see that peak stroke levels correspond to peak bending moments at all frequencies. The primary effect of going to higher frequencies is that the hysteresis increases. However, for the purpose of fatigue testing, the end levels are of primary importance. By controlling stroke amplitude, we could achieve the desired peak blade bending moment levels within a reasonable margin. Based on this, we used stroke as

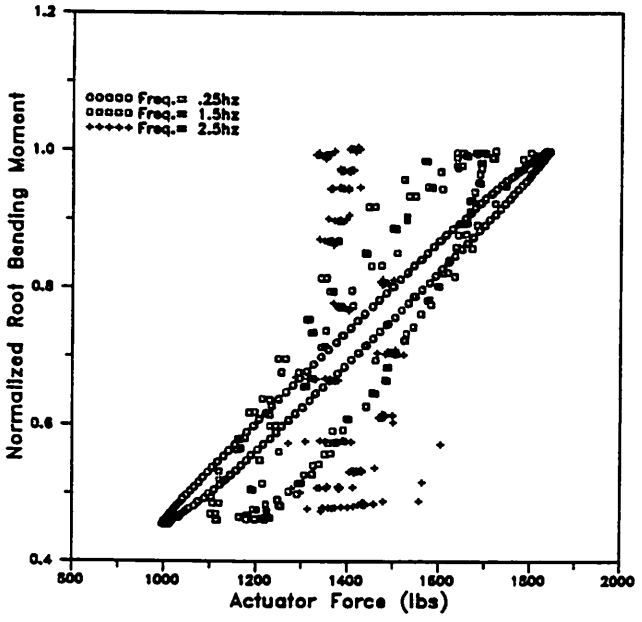

Figure 3. Frequency effects on bending moment and load for the USW 56-100 preliminary fatigue tests

the primary parameter for controlling the tests. We established the stroke envelope by setting the end levels of stroke, under static load conditions, to the actuator positions corresponding to the desired actuator force.

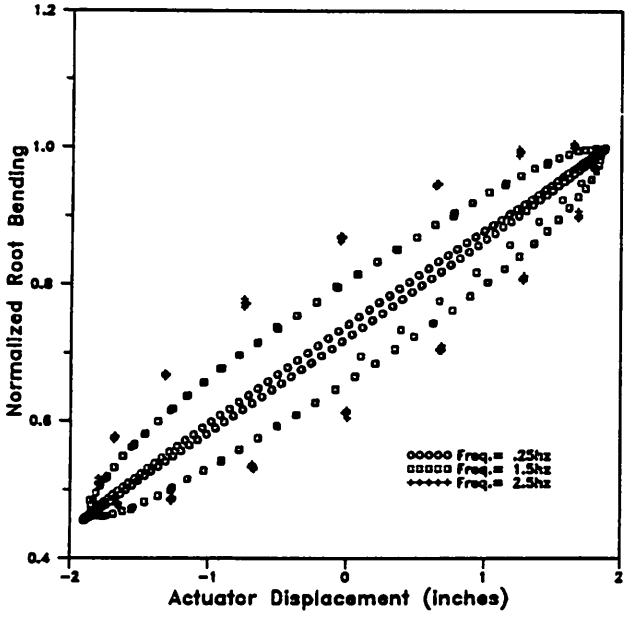

Figure 4. Frequency effects on bending moment and stroke for the USW 56-100 preliminary fatigue tests

The primary disadvantage of stroke control is that, as the blade softens, the stroke amplitude stays constant and the loads decrease. Thus, test results will show longer blade life than if load control were used to maintain a constant stress amplitude. However, by the time the blade has been significantly softened, the majority of the fatigue damage has been done. The best means for test control would probably be to use a signal such as bending moment or strain measured directly on the blade skin; these give a more direct measurement of the stresses. Unfortunately, the servo-hydraulic system at NREL is not yet equipped to use strain gages for control.

Another frequency problem that we were initially concerned about was the possibility that coalescence of the driving frequency and the fundamental blade flap frequency may cause test instabilities. This was not a problem, however. Blade motion in the flap direction was controlled by the actuator and the servo-hydraulic control system. There was no difficulty in maintaining control of blade flap motion up to and above the blade's natural frequency. When we increased the test frequency past the natural blade flap frequency, however, an unexpected dynamic instability developed in the edge direction. Motion in this direction is unrestrained and underdamped. Even though the blade was predominantly loaded in flap, small components of actuator force crossed into the edge bending plane. When the test frequency approached the blade edge natural frequency, at about 3.5 Hz, blade edge motion increased and the end of the blade began to move in an increasingly wide elliptical path. It was necessary to keep the test frequency below this limit to prevent these unwanted edgewise excursions. Note that blade natural frequencies must be recalculated or measured to account for the added weight of the load application hardware and the reduced tip weight.

Data Acquisition:

Data collection for this fatigue testing presented a unique problem. Sample rates had to be selected high enough to assure that peak loads would be captured, but we didn't want to collect every data point of all sixteen channels. A fatigue test to 10^6 cycles would require over 5000 megabytes of memory. The strategy was to collect only the end levels of each data signal and to store them as peak/valley sequences. We wrote a program in Microsoft Basic version 7.1 to count cycles and record peaks and valleys to a data file, significantly reducing the amount of data storage necessary. We performed data collection using one of three processors in the SMT 386/25 computer located at the Structural Test Facility. We monitored all signals at approximately 43 Hz. When the trigger channel reached a maximum or minimum level, the program would simultaneously write the values of all the channels to a hard disk.

The selection of a triggering channel was critical to ensure that only end levels were recorded. Initially, we used actuator load, but phase differences between the load and the other channels made the data meaningless. Root bending moment was the trigger channel used for both tests because we found it to correlate reasonably well with blade stress.

In addition to the data collection, it was necessary to monitor the test progress to detect changes in blade properties that were not be outwardly visible. We did this manually for these two tests by occasionally stopping the test and applying the load statically. The static load per unit deflection was recorded in a log book to detect changes in overall blade stiffness.

Further refinements are still necessary in this data-collection system. For high cycle frequencies, the sampling rates are marginal; it cannot be guaranteed that the end levels will be captured. Data throughput is limited by hardware constraints inherent in the Keithly A/D interface and the SMT 386 computer, so the sample rate cannot be increased much. For the tests described here, which use only constant-amplitude loading, the peak/valley data-acquisition strategy provided more data than was necessary. For this type of test, it may be adequate to intermittently collect data from all the channels and continuously monitor only a few. Test monitoring will be automated during future tests.

AOC 15/50 BLADE TESTS

The AOC 15/50 blade we tested was the first prototype manufactured at Gougeon Manufacturing Corporation (GMC). The purpose of this blade test was to validate the design calculations and the manufacturing techniques used, and to establish a preliminary benchmark to compare with European certification standards. We mounted the AOC 15/50 blades in flap bending with the chord-line at the load application point horizontal to the ground. The load amplitude and load introduction point were chosen to provide the best match to the predicted flatwise strength of the blade using a single-point load distribution, as shown in Figure 5. The objective was to match the bending moment from the root area out past station 118, approximately 3.0 m (118 inches) from the rotational axis. This portion of the span presented the greatest design uncertainty because it encompassed several geometry transitions that were the most difficult to analyze and fabricate. From Figure 5, the load introduction point was chosen to be at 5.18 m (17 ft). GMC prepared the AOC 15/50 blade load introduction point by cutting off the blade tip outboard from the load point and reenforcing the blade cavity to provide a mounting surface for the actuator head.

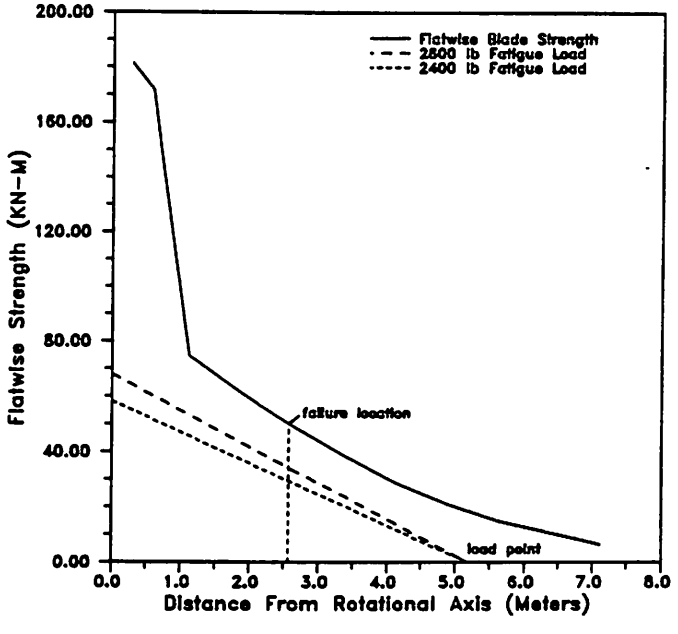

Figure 5. Flatwise strength for the AOC 15/50 blade.

Three-element rectangular (90°/45°/0°) strain-gage rosettes were bonded at four blade-skin locations, where the state of strain was measured. Rosettes were bonded at three blade stations to the compressive surface: 1.27, 1.82, and 2.89 m (50, 72, and 114 in.) from the axis of rotation. At the 1.82-m station, a rosette was also bonded to the tension surface and blade bending was monitored and recorded.

Block loading was applied to the blade using R = 0.1 stress amplitudes. (R is the ratio of the minimum stress to the maximum stress.) The load sequence began with a load block of 7.12 kN/0.712 kN (1600 lb/160 lb) applied for 100,000 cycles. The test was continued by increasing the peak load by increments of 1.78 kN (400 lbs) while maintaining the R = 0.1 stress amplitude. This resulted in a 8.90 kN/0.890 kN (2000 lb/200 lb) load block for 100,000 cycles and a 10.68 kN/1.068 kN (2400 lb/240 lb) load block for 250,000 cycles. The 10.68 kN (2400 lb) load sequence was continued to a quarter of a million cycles to provide a good basis for extrapolating the results to project the blade's ability to qualify under the European certification standard. To pass this standard, the blade would have to survive a 8.01 kN/0.801 kN (1800 lb/180 lb) load sequence at 10^7 cycles. Based on this test, preliminary calculations show that the blade probably would be able to survive this test. The final failure occurred during a 12.45 kN/1.245 kN (2800 lb/280 lb) loading sequence after 55,733 cycles. The failure was on the compressive side of the skin (upper surface) and occurred 2.6 m (102.5 in.) from the axis of rotation.

USW 56-100 BLADE TESTS

USW 56-100 blade fatigue tests are currently being conducted to test the new LS(1) airfoil design. Preliminary tests have been under way for several months, but no failures have occurred yet. Five blades of this type are scheduled to be fatigued, but NREL's hydraulic actuators do not currently have sufficient stroke or load to complete the testing. New actuators with 50.8-cm (20-in.) and 101.6-cm (40-in.) capacities have been purchased to permit R = 0.1 tests on most wind turbine blades. This section describes the methodology developed for the USW 56-100 tests, as well as some of the technical issues we encountered.

One of the primary objectives of the USW 56-100 fatigue tests was to determine the difference in failure mode between the quasi-static tests and the fatigue tests using similar loading conditions. Earlier in the project, ten USW 56-100 blades were destructively tested under quasi-static loading, and most of the blades failed at the 37% span station. Figure 6 shows the normalized static bending moment distribution that was used, along with the fatigue test loading. The load introduction point was chosen to match this static bending moment at the failure location. As shown, a single-point load applied at 68% blade span not only matches the bending moment at 37.5% span but also matches the quasi-static load distribution ranging from the root flange to 40% span. At the load introduction point, a 30.48-cm (12-in.)-wide saddle was built to provide a large contact area and a mounting surface for the actuator head. The tip of the blade was also cut off outboard from the load point to make it easier to install internal reenforcement at the introduction point, and to eliminate natural blade frequencies associated with the independent motion of the tip section.

For the USW 56-100 blade test, three-element rectangular (90°/45°/0°) strain-gage rosettes were also bonded at four blade-skin locations, where the state of strain was measured. These locations are

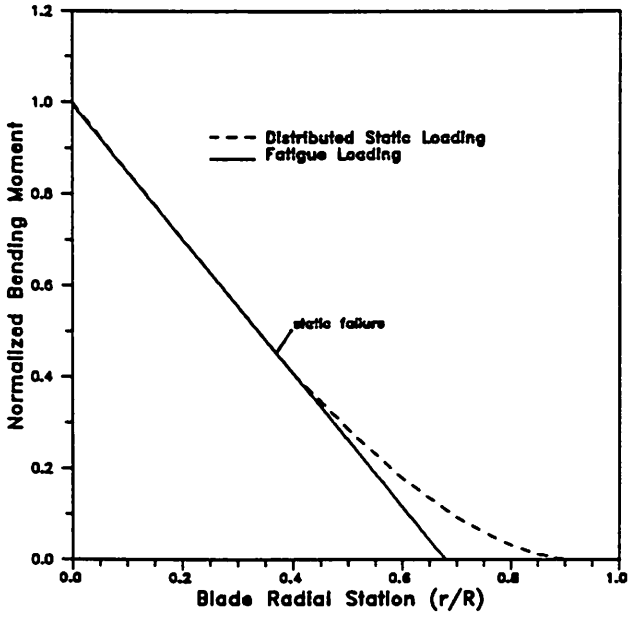

Figure 6. Bending moment distribution for the USW 56-100 static and fatigue load tests

shown in Figure 7. The placement was determined from the results of quasi-static tests conducted during an earlier phase of the project. Two rosettes were located at the 37.5% span, where most of the failures occurred during static load tests. Gages were bonded to the upper (compressive) and lower (tensile) surfaces, over the shear web located near the 1/3 chord line. Two additional rosettes were bonded on the root of the blade on the upper and lower surfaces 25.4 cm (10 in.) from the edge of the root flange. As shown in Figure 8, rosettes were oriented with one gage along the longitudinal axis (0°), one gage in the transverse or chordwise direction (90°), and one gage at 45°. Blade bending moments were measured by strain gages located at the root and the 37.5% span.

The peak load and amplitude for the USW 56-100 fatigue tests were determined semi-empirically from the quasi-static blade tests using a simple S-N curve model—an analogy of the stress level, S, versus logarithm of cycles, N. A large amount of material test data have already been generated on the fatigue properties of fiberglass in tensile-tensile loading using R = 0.1. From fatigue test data, S-N curves are constructed to characterize the material fatigue properties. For unidirectional E-glass in vinylester (VE) resin, from which the 56-100 blade is partially made, optimal performance on an S-N curve is considered to be approximately 10% strength reduction per decade (Mandell 1991).

Assuming that, under quasi-static loading, the blade behaves linearly, the applied load, F, and stress at the failure location will be proportional. This relationship is demonstrated in Figure 9, where strain is linearly related to load up until the blade fails during a quasi-static limit load test. Then, the ratio of the applied load to the static limit load should equal the ratio of applied stress to failure stress at the critical stress location:

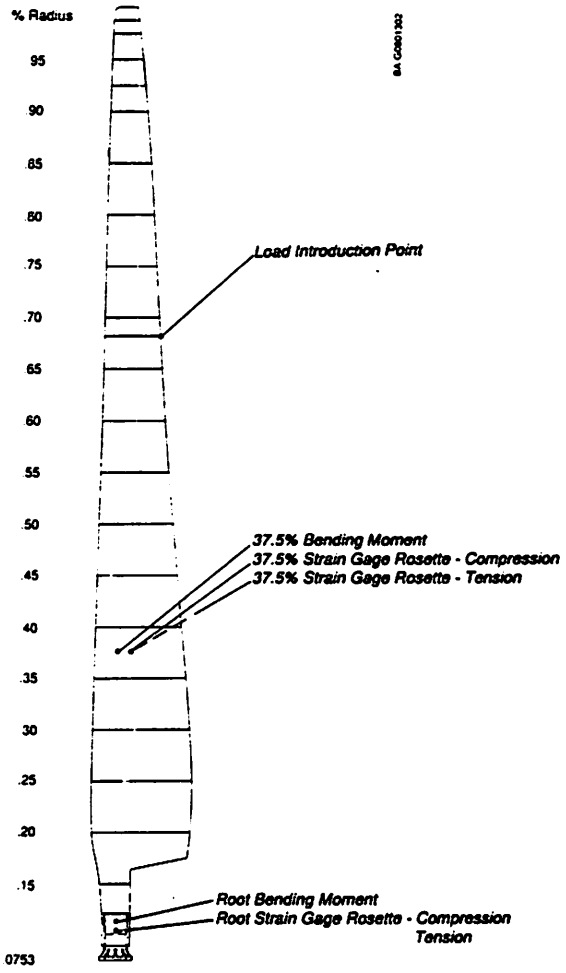

Figure 7. Location of strain gages for the USW 56-100 fatigue tests

$$F/F_0 = S/S_0$$

Using this assumption, a load magnitude equal to 50% of the failure strength of the blade should result in a failure at approximately 10^5 load cycles if 10% per decade strength reduction is valid. Unfortunately, the actuators available at NREL did not have a long enough stroke capacity to perform an R = 0.1 test at a peak load level that would cause the blade to fail. Therefore, the stress amplitude, S_a, and mean stress, S_m, were modified as shown in Figure 10. The stress ratio for this test was R = 0.5 with a peak actuator load of 50% of the static limit load, F_0.

As expected, the modified parameters of the current R = 0.5 test resulted in a longer fatigue life than the desired test of R = 0.1. To date, the USW 56-100 blade has exceeded the R = 0.1 predictions by over an order of magnitude with 2.5 x 10^6 cycles, as shown in Figure 11. Some of the higher life could be because of the smaller amplitudes of the R = 0.5 tests, but a significant part of this could be caused by nonlinearities, such as buckling, in the static tests. Measured strain levels in the blade skin under the current 50% loading

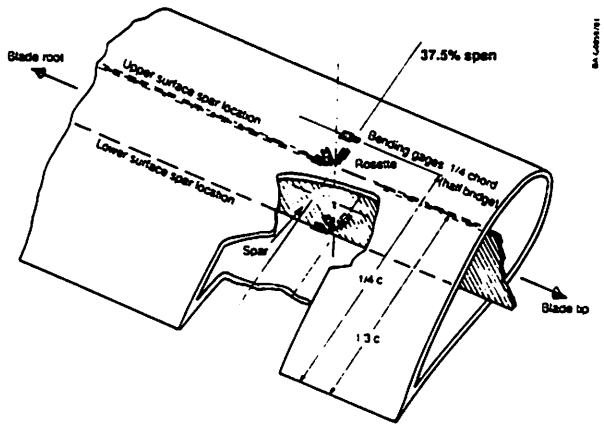

Figure 8. USW 56-100 blade cutaway showing the locations of the strain gages

scheme are approximately 0.26% and are still below any measured fatigue limit for the E-glass/VE material, as shown in Figure 11. The static test data shown in Figure 9 indicate that strain levels on the skin at the failure location did not typically exceed 0.6% strain, even at failure. This suggests that the failures induced under quasi-static loading were not caused by exceeding the ultimate strength of the blade material but more probably by a buckling instability in the blade structure. This makes it very difficult to predict anything about the fatigue life of the blade based on static strength, and it indicates that the S-N analogy described above is probably not valid for establishing

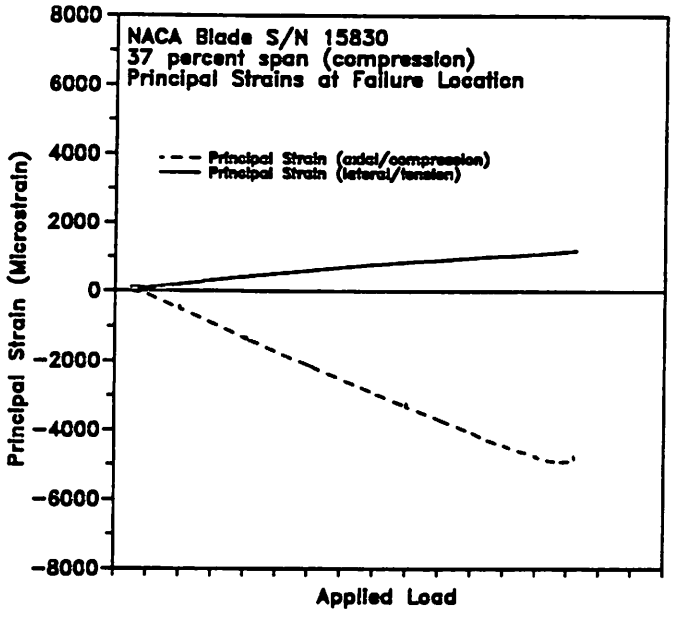

Figure 9. Principal Strain Versus Load for USW 56-100 destructive blade test.

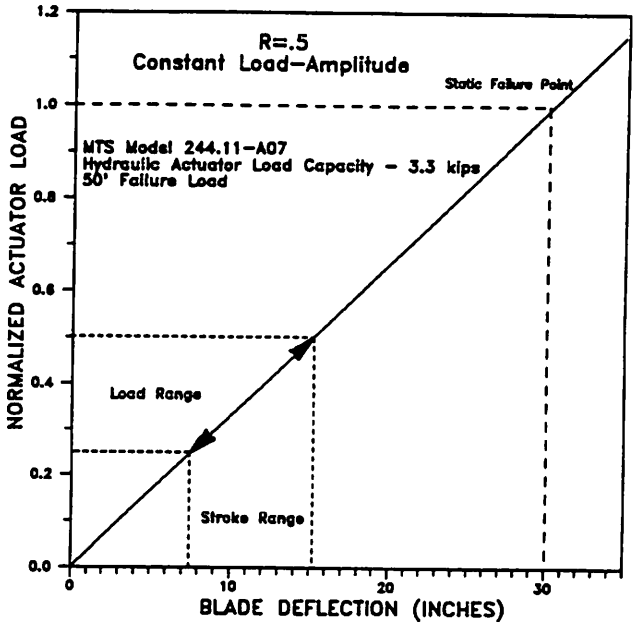

Figure 10. USW 56-100 fatigue test loading

fatigue loading. Based on this observation and fatigue test results to date, it is possible that the fatigue limit for these wind turbine blades may be closer to their ultimate strength than previously thought.

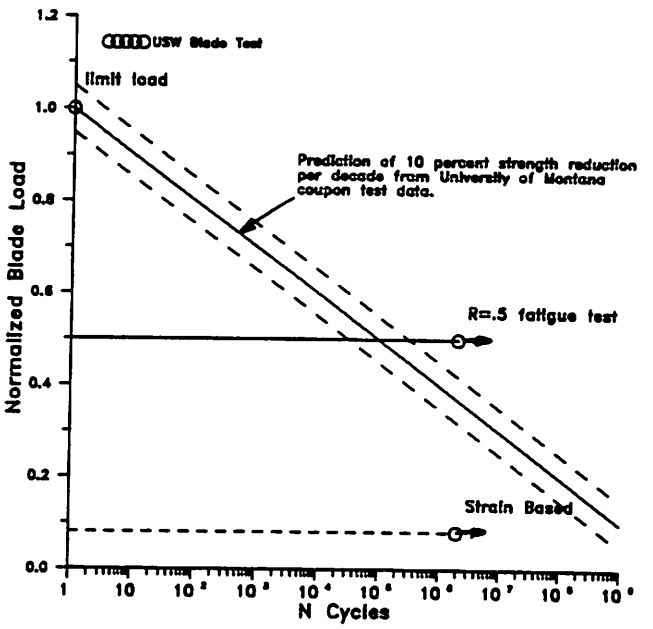

Figure 11. S-N curve for E-Glass/VE showing the USW 56-100 blade fatigue test parameters

CONCLUSIONS

We conducted USW 56-100 tests and AOC 15/50 blade fatigue tests at NREL's Structural Test Facility. USW 56-100 tests indicate that blade fatigue life may be longer than predicted using static test results. It may not be possible to model a complex structure, like a wind turbine blade, using an S-N curve analogy because the failure modes and failure locations may change as load increases. Fatigue testing of full-scale structures, such as the AOC 15/50 blade, was used to validate blade designs and help blade designers and manufacturers gain confidence before large-scale production begins. The AOC 15/50 blade met the manufacturer's expectations for structural load carrying capacity.

ACKNOWLEDGMENTS

The authors would like to thank the many people who contributed to this project. The efforts of Mike Jenks, Bob Keller, Bill Gage, Jim Johnson, and the other members of NREL's structural testing team were particularly valuable, and without their help this project would not have been possible. In addition, the cooperation and support of U.S. Windpower, Inc.; Atlantic Orient Corporation; Gougeon Manufacturing Company; and Mike Zuteck was critical to the development of NREL's test facility. Finally, the United States Department of Energy is acknowledged for their continuing support of this project.

REFERENCES

Bach, P.W., *High Cycle Fatigue Testing of Glass Fibre Reinforced Polyester and Welded Structural Details*, ECN report No. ECN-C--91-010, ECN, Petten, the Netherlands, March 1991.

Bonfield, P.W., and Ansell, M.P., "Fatigue Testing of Wood Composites for Aerogenerator Rotor Blades; Part VI. Spectrum Fatigue Loading , Life Prediction and Damage Rates," *Wind Energy Conversion: Proceedings of the 1991 Thirteenth BWEA Wind Energy Conference*, April 1991.

Jensen, P.H., Winther-Jensen, M., and Madsen, P.H., "Fatigue Aspects of The Danish Licensing of Wind Turbines," IEA R&D WECS Experts Meeting, *Proceeding of a Workshop on Fatigue in Wind Turbines*, Harwell Laboratory, Didcot, U.K., 21-22 March 1988.

Mandell, J. , "Fatigue of Fiberglass Wind Turbine Blade Materials," presented at the 10th ASME Wind Energy Symposium, Houston, Texas, January 20-24, 1991.

ten Have, A.A., *Whisper and Whisperx: Final Definition of Two Standardised Fatigue Loading Sequences for Wind Turbine Blades*, NLR Report No. NLR C 91476 L, Amsterdam, the Netherlands, December 1991.

FATIGUE TEST ON AN EIGHT METER CARBON-EPOXY ROTOR BLADE

by
Ton van der Wekken
and
Ben Hendriks

NETHERLANDS ENERGY RESEARCH FOUNDATION
ECN

This paper is prepared for the IEA R&D WIND expert meeting, on the subject Fatigue of Wind Turbines, full scale blade testing and non-destructive test methods, at NREL, Golden, Colorado October 15, 16 1992.

1. Introduction

At ECN, Business Unit Renewable Energies, starting from the first half of 1991 preparations are going on for setting up a laboratory for testing full scale wind turbine rotor blades both with respect to static strength and demonstration of sufficient fatigue life. The electronic and hydraulic test equipment has been delivered at ECN in September and October 1992. In the laboratory it is possible to test rotor blades or parts of rotor blades up to a length of 25 meter. The test control equipment, called Aero-90, is supplied by MTS in Minneapolis, USA.

The first test that will be performed by ECN is the fatigue test of an eight meter rotor blade. The aim of the test is twofold. Of course the fatigue test is meant to verify sufficient fatigue life of the blade and on the other hand it is meant to build up experience in performing such tests on rotor blades.

As a result the work is financed only partly by the wind turbine manufacturer and the remaining part by ECN.

After some experiments on a steel beam with rectangular cross section, having about the same stiffness properties as the blade specimen, the test will start the second half of November and be finished in June 1993.

2. Test specimen

The test specimen is an eight meter carbon-epoxy rotorblade. The blade weight is about 75 kg, including an iron bar in the blade nose of 16 kg. The blades are manufactured by the French firm Atout Vent. The blades are part of the two bladed wind turbine type Lagerwey LW18/80, which is designed and manufactured by the Dutch company Lagerwey B.V. The rotor diameter is 18 meter, the nominal generator power is 80 kW and the rotor speed is variabel between 60 and 125 rpm. The wind turbine Lagerwey LW 18/80 has been in production starting from the end of 1991.

At this moment already a large number of this wind turbine type has been built and installed. Lagerwey is the only manufacturer in the Netherlands making use of carbon-epoxy rotor blades. Also the forerunner of the Lagerwey LW18/80, the Lagerwey LW 15/75, has no carbon-epoxy blades but is equipped with glass fibre reinforced polyester blades. The advantages of carbon-epoxy with regard to glass fibre reinforced polyester are: higher stiffness (E-modulus), higher tensile and compression strength and better fatigue properties. So as a result this may lead to lighter blades. A lighter blade leads to less heavy blade and hub loading, especially this is true for the lag load.

The blade root is attached by means of six bolts to two steel plates, see figure 1, and the two steel plates are attached by two large bolts to the blade pitch shaft. The steel plates will be part of the test specimen in the fatigue test, but the two large bolts will be attached to the test frame instead of the pitch shaft.

The hub structure of the Lagerwey wind turbine has been designed in such manner that the blades, within limits, are free to rotate in flap direction. As a result of the flap hinges, in the blade root section the flap bending moment is near to zero during normal energy production. The blade

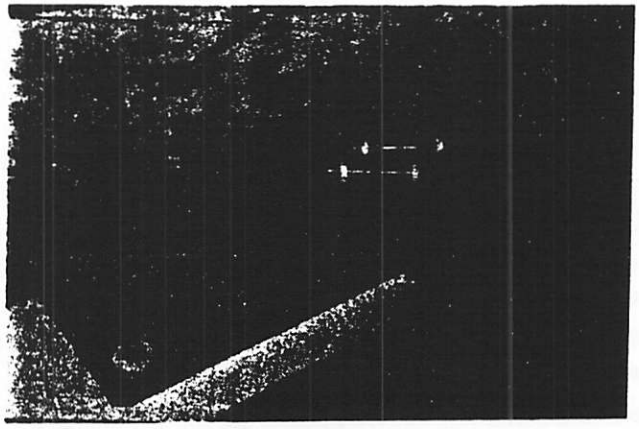

Figure 1 - blade root structure of the wind turbine Lagerwey LW 18/80

hits elastic blocks, which limitate the flap freedom, only due to severe wind gusts, high wind shear, start up and stop procedures and during parking. In the fatigue test the blade is clamped in such a way the blade is not free to rotate in flatwise direction.

The laminate lay-up is built up in such a manner that the carbon fibres are mainly in zero-direction, which implies in spanwise direction for the blade. In the root more ±45° laminates are added to make the load transfer possible from blade root to steel plates. The blade cross section, figure 2, is built up from three closed cells. This is the load transferring part of the blade. The only function of the trailing edge is to keep the aerodynamic profile in shape. The blade is filled with rigid foam.

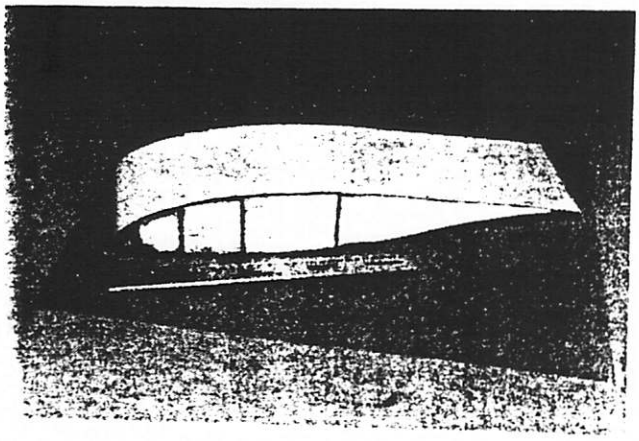

Figure 2 - View of the blade cross section (blade tip)

3. Experimental setup

In the laboratory the blade root will be clamped by means of the steel plates in a test frame. The blade will be loaded by two hydraulic cilinders at a cross section which corresponds to 65 per cent of the rotor radius. Only the flatwise and edgewise loads will be applied in the test. The torsional moment is relatively small and, although the rotor speed is rather high, the centrifugal force is also negligible. During normal wind turbine operation the stress in the blade root due to the centrifugal force is approximately 8 MPa (or 100 μ-strain), which is very low compared to strains caused by edgewise (500 to 1000 μ-strain) and flatwise (1000 to 3500 μ-strain) loads.

The MTS Aero 90 control system has the facility to perform the test in load or position control. The natural frequencies of the blade however, clamped in the test frame, are 2.5 Hz and 5.6 Hz in flatwise and lagwise direction respectively. So in load control, to avoid dynamic amplication of the moments in the blade the maximum test frequency would be 0.3 Hz. In position control the test can be carried out faster. The fatigue test will be carried out in position control and the number of test cycles will be about 15 million.

4. Material coupon tests

Before the project started, at Atout Vent, Lagerwey B.V and ECN not very much was known on the static strength and fatigue properties of the applied carbon-epoxy blade laminate.

For that reason at the materials department of ECN, on coupon material, the material properties have been determined of the laminate that is used in the root section of the blade. The coupon material is built up as follows: ±45°,4x(±45°,0°). On a large number of coupons the following tests are performed:

- Ultimate Tensile Strength (UTS);
- Ultimate Compression Strength (UCS);
- Fatigue tests with the stress ratios R= -1 (compression- tension), R= 0.1 (pure tension),

R= 10 (pure compression) and some tests with the variable amplitude sequence WisperX. For each R value and WisperX tests have been carried out at three load levels.

The results show the following:

- UTS value is 10.000 μ-strain;
- UCS value is 5500 μ-strain;
- On a linear-log scale the slope of the measured S-N curves is 5 to 6 per cent of the UTS or UCS value per decade on logarithmic scale. The slope [a] is defined as follows:

  $a = \{\sigma 1-\sigma 2\}/\{\log(N1)-\log(N2)\}/UTS$ or

  $a = \{\sigma 1-\sigma 2\}/\{\log(N1)-\log(N2)\}/UCS$
- The fatigue strength, defined as the level below which no damage appears, is 2000 to 2500 μ-strain.

The results of the test are used for the composition of the test sequence. From the coupon tests can be derived which load variations do not contribute to the fatigue damage. It gives also an indication what the reduction in test cycles may be in case of increasing all loads in the test

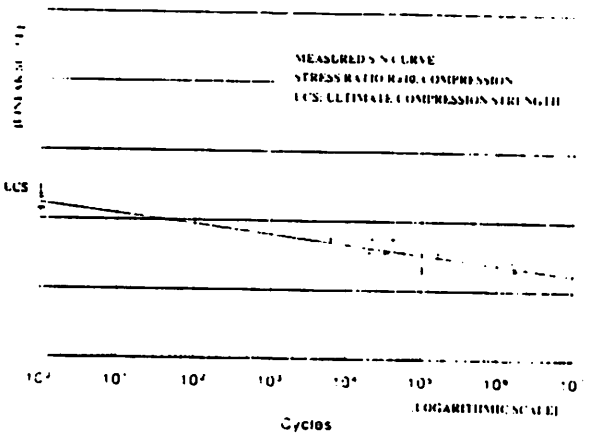

Figure 3- Carbon epoxy S-N curve derived from the measurements

sequence with a fixed percentage. Of course it is meant that the fatigue damage will remain the same.

Figure 3 shows a measured S-N curve. The figure shows, due to the smooth slope, the carbon epoxy material is not very sensitive for fatigue. At a certain stress or strain level the fatigue life may be almost infinite and after increasing the load level with ten to twenty per cent the fatigue life may become very short.

5. Test spectrum and test sequence

The load or displacement sequences that are applied in the fatigue test have to be based on the design load spectra of the wind turbine Lagerwey LW18/80. The wind turbine has been designed for an operational life of 20 years. The design loads have been calcultated by the technical con-

sultancy office STENTEC BV by means of a program which makes use of stochastic wind field generation program. To obtain the required load sequences, at ECN time response calculations have been performed by means of the aeroelastic time simulation program PHATAS, reference [1. The wind data for the calculations is according to the wind climate of the Netherlands, laid down in reference [2]. The calculations have been carried out for 18 load cases. The corresponding average wind speed varies from 8 to 20 m/s and coherent wind gusts with amplitudes from 2.4 to 17.6 m/s. The duration of the wind gusts is 15 seconds. Figures 4 and 5 show the relevant flatwise and edgewise load spectra of the blade root section. The obtained spectra are similar to the by STENTEC BV calculated design spectra. Fatigue calculations, based on the derived spectra, are carried out to determine critical blade locations.

From the load sequences at a number of relevant locations of one blade cross section the stress sequences are determined. These stress sequences are searched for peaks and valleys. By using a range filter small cycles are omitted. Next, from the obtained stress turning points the corresponding flatwise and edgewise bending moments are sought for and the cilinder loads determined. As a result of this method the flatwise and edgewise bending moments do not have to be in phase with regard to each other.

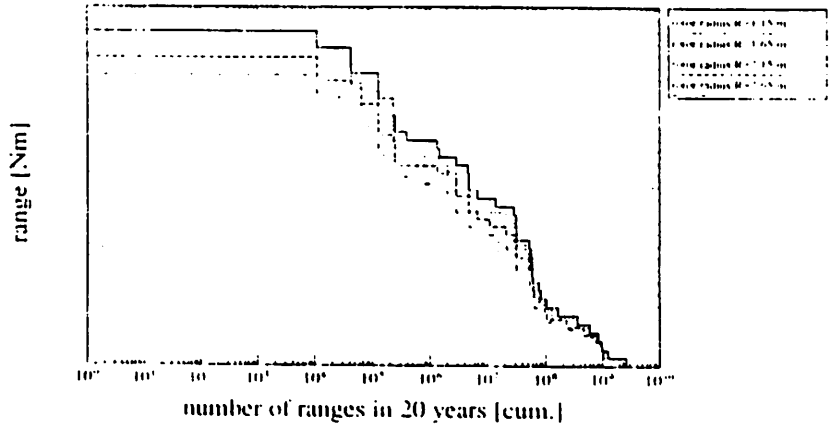

Figure 4- rainflow spectrum flatwise bending moment

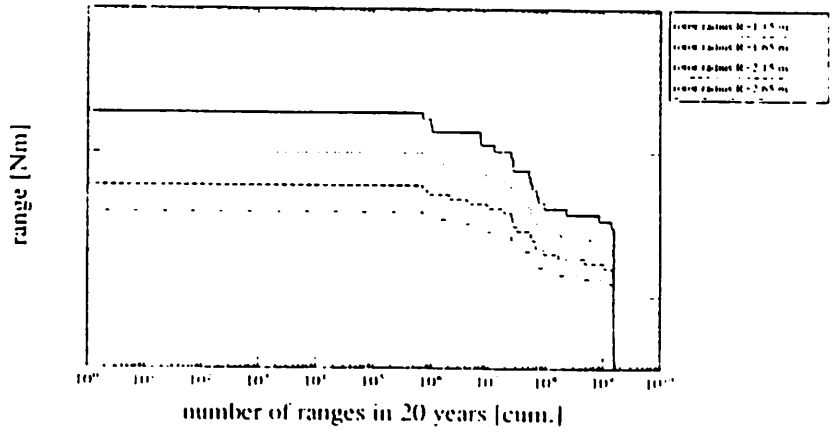

Figure 5- rainflow spectrum edgewise bending moment

The calculated loads are nominal loads. According to the Dutch technical criteria for wind turbines [3] a load factor of 1.35 and a material factor for composites of 1.50 has to be taken into account. These safety factors are applied in the analysis to take into account uncertainties in blade loading and material properties. Because the test is meant to study the material behaviour, only the load factor of 1.35 will be applied.

Further a small test factor will be used, about 1.05 times the load level, with as result that the number of cycles may be reduced leading to the same fatigue damage.

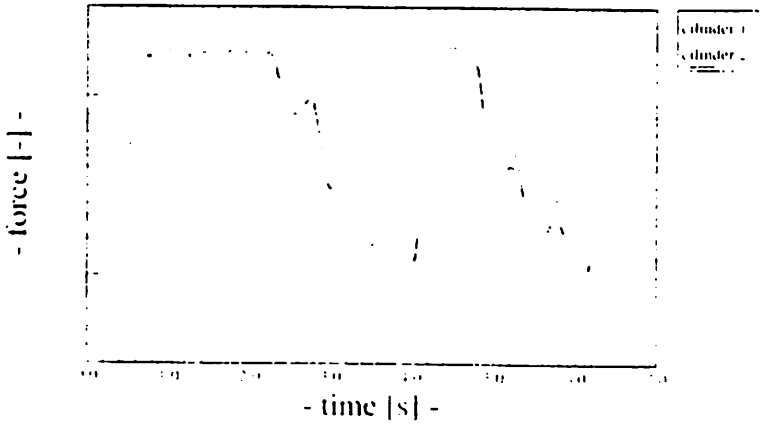

Figure 6- cilinder forces corresponding to load case 18

6. Measurement program

Besides the fatigue test on the blade a number of signals will be measured during the test. The measurements will be performed by a measurement device and a workstation, for running the program and data storage, which are controlled by the MTS Aero 90 control system.

The aim of the measurements is to check if the fatigue test is carried out properly, to determine blade stiffness reduction and to obtain the load and strain spectra at relevant blade locations. The blade bending moments during the test can be measured most accurately on the blade itself. In this manner, no corrections have to be performed due to stiffness reduction and effects of dynamic amplification. The measurements are not suited to determine local blade damage as small cracks and delaminations.

The blade root will be instrumented with strain gauges at two cross sections. At each cross section the instrumentation is built up from [4]:

- A Wheatstone bridge measuring the flatwise bending moment;
- A Wheatstone bridge measuring the edgewise bending moment;
- Two strain gauge rosettes -three signals per rosette - at high loaded spots.

Besides the above mentioned 16 strain signals, eight at each cross section, also the two load and two displacement signals from the hydraulic cilinders will be measured.

Before the fatigue test starts the cilinder displacements will be measured for all occurring load conditions in the test. The obtained displacements will be send to the MTS control system and

subsequently be used as drive signal.

During the fatigue test only the 2 displacement signals, the 4 Wheatstone bridge signals and 4 signals from single strain gauges will be measured continuously. In total 10 signals will be recorded during the fatigue test. The fatigue test sequence is built up from 'profiles', which corresponds to a load case, and a number of 'profiles' which is called a 'sub-sequence'. The fatigue test sequence is built up from a number of 'sub-sequences' that will be repeated in a fixed order. The test duration of a 'sub-sequence' will be about 24 hours.

The ten signals will be on-line reduced to peak/valley histories. Of each 'sub-sequence', and of each signal separately, from-to Markov matrices will be created. For checking purposes the Markov matrices corresponding to the same 'sub-sequences' may be compared to each other. The summation of all matrices of a signal leads to the overall applied spectrum.

At regular time intervals, the fatigue test will be interrupted for reference and calibration runs. These measurement runs will be carried out automatically. The reference runs will be carried out twice a 'sub-sequence' and are meant to check the condition of the instrumentation, quantification of zero-drift of the strain gauges and to recognize appearing stiffness reduction of the blade or problems with the blade - test frame attachment. The frequency of the calibration runs is low, two times a week, compared to the reference runs. The aim of the calibration runs is to determine the relation between Wheatstone bridge output in μ-strain and bending moments. During reference and calibration tests the test will have a quasi-static character.

7. Results

In case, during the fatigue test, no problems arise with the blade or blade attachment the blade has proven sufficient fatigue life for 20 years wind turbine operation. Subsequently the test will be continued on a higher load level, to determine the remaining fatigue life and to find out the critical blade locations with regard to fatigue.

On the other hand, if the blade fails before the test has been finished, the real fatigue life has been shown and the critical blade locations will be known.

The results of the fatigue test should be analysed and interpretted with great care. For the results of the coupon tests have shown that , due to the smooth slope of the S-N curve, a small variation in overall load level may have large consequences on the blade fatigue life.

8. References

[1] - PHATAS II, Program for Horizontal Axis wind Turbine Analysis and Simulation, version II. AEROELASTIC MODELLING.
H. Snel, C. Lindenburg
ECN-C--92-027, May 1992.

[2] - Handbook of design wind-data for wind turbines, version 3.
INTRON, TNO, ECN, Februari 1991.

[3] - Regulations for the type certification of wind turbines: technical criteria.
W.J. Stam (ed.)
ECN--91--001, Februari 1991.

[4] - Measurement programme of fatigue test eight meter Atout Vent rotor blade.
Ton van der Wekken
DE-Memo-92-28, Renewable Energies ECN, May 1992.

FATIGUE AND RELIABILITY ANALYSES FOR WIND TURBINES*

Herbert J. Sutherland
Wind Energy Technology
Sandia National Laboratories
Albuquerque, NM 87185

ABSTRACT

This paper presents a summary of two areas of research into the fatigue of wind turbine components at Sandia National Laboratories. The first area is the fatigue analysis of turbine components and the second is reliability analysis. For the former, current work is addressing the examination of experimental data in the time and frequency domain. Emphasis in this paper is directed at the determination of the "high-stress" tail of the cycle count distribution. For the reliability analysis, research is quantifying the uncertainties and the inherent randomness associated with turbine performance and the prediction of service lifetimes. Both research areas are highlighted with typical results.

INTRODUCTION

Sandia National Laboratories is conducting a comprehensive program into the fatigue of wind turbine components for the U.S. Department of Energy. Two of the research areas in this program are the analysis of the fatigue life of turbine components and a reliability analysis of the predicted service lifetimes. This paper summarizes the current activities in these two research areas.

Fatigue Life Predictions

The analysis of the fatigue life for turbine components has been developed along two paths. The first led to the development of the LIFE code and the second led to the LIFE2 code. The former was developed by Veers[1] for the analysis of Vertical Axis Wind Turbine (VAWT) blades. Industrial critiques of the code were evaluated by Sandia and appropriate modifications were included in an updated version of the code that was released by Sutherland et al.[2]

The second path has led to the development of the LIFE2 code.[3] This generalized analysis framework was developed because fatigue problems in California illustrated that analysis techniques for fatigue were required for all wind energy conversion systems (WECS) and because the rather severe set of simplifying assumptions and limited scope of the LIFE code precluded the use of advance fatigue models. This code was designed with a top-down, modular format and with a "user friendly," interactive interface.

Recently, this code has been modified to examine experimental stress data in the form of time series and frequency spectra.[4,5&6] This paper presents typical results for these analyses.

Reliability Analysis

The analysis of the fatigue life of the Sandia 34-m VAWT[7] by Ashwill et al.[8] has shown that the predicted service lifetime of a turbine is very sensitive to small differences in the input parameters, such as operating stress levels or wind speed statistics. Structural reliability methods are being used in the Sandia program to evaluate the effects of these uncertainties and the inherent randomness on turbine performance (especially fatigue life). Additional information on the relative importance of each source of uncertainty, as well as the sensitivity of the reliability to each input, is obtained from the analysis.

The analysis of a wind turbine blade by Veers et al.[9] is used here to illustrate the typical results from this class of analyses.

* This work is supported by the U.S. Department of Energy under contract DE-AC04-76DP00789.

CYCLE COUNTING EXPERIMENTAL DATA

The LIFE2 code is a fatigue/fracture mechanics code that is specialized to the analysis of wind turbine components.[3] This code permits the analysis of both time series[4] and frequency domain data.[5&6] In the case of the former, a "rainflow counting" algorithm is used to convert time series data into a cycle count matrix suitable for fatigue analysis. For the latter, a Fast Fourier Transform (FFT) is used to synthesize time series data that are suitable for cycle counting using the rainflow counter in the LIFE2 code.

Typical Data

Both the rainflow counting and the frequency spectrum techniques have been used by Sutherland and Osgood[6] and Sutherland[10] to analyze the behavior of the Northern Power Systems (NPS) 100-kW turbine, see Figure 1. A large data set was collected for this turbine by Coleman and McNiff[11] under the auspices of the NREL* Cooperative Research Program. The turbine is a two-bladed, upwind, teetering hub design utilizing full-span hydraulic passive pitch control. The fiberglass rotor blades, including the elastomeric teetering hub, span 17.8 meters (rotor diameter). The rotor's low-speed shaft turns a two-stage, two-speed gearbox. The high-speed shaft of the gearbox is connected to one of two fully enclosed induction generators. The present paper discusses data collected during operation of the turbine's 100-kW generator, which is rated at full power when rotating at 71.8 rpm in a 14 m/s wind.

Several turbine configurations were used during the collection of the NREL data set. Here, we have selected a data set for the turbine in a "locked yaw" (stiff spring) and "free teeter" with damping and stiffness. For this configuration, a 1.14-hour data segment was extracted from the main data set. During this period, the turbine was operated continuously at approximately 71.6 rpm. The average wind speed for this data set was 11.00 m/s with a turbulence factor (RMS) of 3.62 m/s. The first 400 seconds of the wind speed data are shown in Figure 2.

Time Histories

Data from two strain gauge channels are discussed here. The channels employ full-bridge bending configurations located on the fiberglass blade's hollow circular root shank. The first channel measures the root flap bending moment; i.e., the blade's out-of-plane bending moment. The second channel measures the root edgewise bending moment; i.e., the blade's in-plane bending moment. These two channels were reduced using the NREL data reduction package[12] to the stress level at the outer fibers of the blade's root. Typical stress histograms (time series data) from the selected data set are shown in Figures 3 and 4.

* Formerly the Solor Energy Research Institute (SERI).

Frequency Spectra

The frequency-domain amplitude spectra for the two principal bending stresses are shown in Figures 5 and 6. These spectra were obtained by applying a forward FFT[5] to the 1.14 hours of time series data. The data were divided into 71 segments, each 56.9-seconds long. The sample rate was 36 samples per second; i.e., 0.028 seconds between data scans. Thus, the Nyquist Frequency for these calculations is 18 Hz, and the frequency interval is 0.018 Hz. The average spectra were obtained using an ensemble average at each frequency in the 71 individual spectra up to 10 Hz. Above 10 Hz, the spectrum is set equal to zero (the time series data were filtered with a low-pass 10 Hz filter, see Reference 11). The peak near 1 Hz in Figure 6 has a magnitude of 3.2 MPa.

Coherence Function

As discussed below, the coherence, or lack thereof, of the two bending stress histograms are important in the determination of the off-axis stresses. The coherence of the two was determined using the computer program developed by Akins.[13] The result for the cross-spectral density analysis is shown in Figure 7.

Akins[13] notes that the coherence is a dimensionless quantity that is a measure of the correlation of the two signals as a function of frequency. A coherence of 1.0 indicates perfect correlation, less than 0.5 indicates weak correlation, and less than 0.1 indicates no correlation.

As shown in Figure 7, the coherence is large (near unity) for the first and second "per-rev" responses (harmonics), near 1 and 2 Hz, respectively. The amplitudes of these two harmonics are relatively large. Most of the remaining components of the spectrum have a coherence in the range of 0.2, with three exceptions that approach the 0.6 range. The amplitudes of these three are relatively low. Thus, the relatively high-amplitude harmonic components of the spectra are highly correlated and the relatively low-amplitude random components are weakly or not correlated.

Analyses Along the Primary Bending Axes

The current efforts in the analysis of experimental data have centered on the use of frequency domain data to predict the stress cycles imposed on a turbine component. The first set of analyses will examine the stress states along the primary bending axes of a turbine blade, the edgewise and the flapwise bending axes. The second set will examine off-axis stress states.

Rainflow Count

Data from the two channels analyzed here were rainflow counted using the algorithm in the LIFE2 code.[4] Results of the analyses are shown in three-dimensional (3D) plots in Figures 8

and 9 for the root flapwise and root edgewise bending stresses, respectively. In these and subsequent cycle count plots, the number of cycle counts has been normalized to 100 seconds. This normalization permits the direct comparisons of cycle counts for time series of different lengths.

As shown in these figures, the cycle count matrices have a significantly different structure. The difference in the shape of these two distributions is a direct result of the strong deterministic signal (azimuth average signal) contained in the edgewise bending data. The action of gravity on the blades imposes these deterministic loads on the blade. The deterministic component is shown in Figure 4 as a dashed line. These cycle counts are similar to those obtained by Thresher, Hock and Osgood.[14]

The distribution of the cycle counts in the high-stress tail of the time series data is expected to achieve a stable, relatively smooth, and monotonically decreasing distribution of cycle counts, if the time series is sufficiently long for the process(es) being sampled. As seen in Figures 8 through 14, such a distribution is not achieved with the time series analyzed here, even though over 4000 seconds of data are analyzed. Thus, the distribution of cycle counts in the high-stress tail appears to be based on insufficient data.

Spectral Analysis

As noted by Sutherland,[5] the spectrum for a turbine component may be analyzed by the LIFE2 code using one of two different techniques. Both techniques yield synthesized time series data suitable for rainflow counting. In the first technique, the complete spectrum is used in the synthesis process with fixed phase angles on selected components of the spectrum and random phase angles on the remainder. In the second technique, the component's spectrum, with the azimuth average signal (deterministic signal) removed, is used for the synthesis of time series data. The azimuth average signal is added to the synthesized time series to complete the synthesis process.

In the following discussion, the root flap bending stress will be used to illustrate the first technique and the root edgewise bending stress will be used to illustrate the second.

Root Flap Bending Stress: The root flap bending stress spectrum, see Figure 5, is used in its entirety for this analysis. The phase angles for the two peaks at approximately 1.2 and 2.4 Hz were retained, and random phase angles were used for the other components of the spectrum. The results for approximately 4000 sets of synthesized time series data are summarized in Figure 10. Each synthesized time series was 56.9 seconds in length. Thus, the total time synthesized for this figure is approximately 240,000 seconds (66 hours). In this figure, the cycle counts are plotted as a function of the alternating stress range. Namely, the alternating-stress cycle counts have been summed over all mean stresses. This format was chosen for the presentation of these data because it permits a clear, detailed comparison of the respective distributions of alternating stress cycle counts.

As illustrated in this figure, the synthesized data fit the body of the cycle count distribution very well. However, the high-stress tail of the distribution is not fit very well. As discussed by Sutherland[5] and Malcolm,[15] the population of cycle counts in the high-stress tail of the cycle count distribution is very important in the determination of the service lifetime of a turbine component. And, the frequency-domain technique should be able to duplicate the time series data if the spectrum contains sufficient information.

The average frequency-domain stress spectrum, Figure 5, was used in this analysis. The RMS of this spectrum is 2.45 MPa. Sixty-nine (69) percent of the individual spectra had an RMS within 50 percent of this average value. However, large excursions from the mean occurred in many of the individual spectra. The RMS ranged as high as 6.51 MPa in the individual spectra. Sixteen (16) percent had an RMS 100 percent greater than the average, and 4 percent had an RMS 150 percent greater than the average RMS. Rather than trying to duplicate this distribution of the RMS values, we have taken a relatively simplistic and empirical approach to the synthesis of time series data from these spectra. On the basis of our previous experience with synthesis of time series data, we have chosen to vary the RMS of the average spectrum uniformly about its mean value for 95 percent of synthesized time series. For this 95 percent, the spectral amplitude was varied by ± 50 percent. The remaining 5 percent of the synthesized time series was used to add "large-excursion" cycle counts to "average" cycle counts. The large excursions were synthesized using a 110 percent increase in the RMS of the average spectrum. As discussed below, this simplified distribution of RMS values produces excellent agreement with the rainflow counted time series data.

The cycle count distribution for the synthesized time series containing the large-excursion data is shown in Figure 11. A similar plot for the mean stress cycle count distribution is shown in Figure 12. As shown in these two figures, the distribution of cycle counts is predicted very well using the frequency-domain technique. Moreover, the distribution in the high-stress tail is also predicted. As discussed in Sutherland,[5] the ability of the frequency synthesis algorithm to generate relatively long time series permits the high-stress tail to be defined. Over 240,000 seconds (66 hours) of synthesized time series data were required to achieve a stable and relatively smooth distribution of cycle counts in the high-stress tail.

When the counts in the high-stress tail of the synthesized time series data are compared to the counts obtained directly from the 4400 seconds of time series data, the spectral technique predicts more cycles in the high-stress tail of the distribution. The relatively smooth distribution of cycle counts in this high-stress tail is indicative of the relatively long time series, over 240,000 seconds, synthesized for this analysis. As discussed in Sutherland,[5] Thresher et al.[14] and Malcolm,[15] the cycle counts from time series data should converge to a relatively smooth distribution as time lengths are increased. The relatively disjoint distribution for the time series data,

shown in Figures 8, 10 and 11, is a direct result of the relatively short duration (4004 seconds compared with 240,000 seconds) of the time series data. Thus, the distribution and magnitudes of the cycle counts obtained over the alternating stress range using the frequency-domain technique are in excellent agreement with the cycle counts obtained directly from the time series data.

As anticipated, the distribution of mean-stress cycle counts, see Figure 12, is a relatively symmetric distribution, unlike that obtained directly from the time series data. The frequency synthesized data do contain cycles with higher mean stresses. As discussed above, the distribution for the time series data will smooth as the duration of the time series increases. The smoothing of the time series distribution may fill out its distribution. Moreover, a close examination of these high mean-stress cycles shows that they are associated with small alternating-stress cycle ranges. Since determination of service lifetimes is a weak function of mean stress and a strong function of alternating stress, these cycles do not contribute significantly to the accumulation of damage in the blades.

Thus, the distribution and magnitude of cycle counts for the flapwise bending stresses that were obtained from the spectral analysis technique are in excellent agreement with the distribution obtained from the time series data.

Root Edgewise Bending Stress: The cycle count distribution for root edgewise bending stress is significantly different from the distribution for root flap bending stress. As shown in Figures 4 and 9, the root edgewise bending contains a strong, one-per-revolution deterministic (azimuth average) signal (due to the gravity component of the blade loads). These data will be used to illustrate the synthesis of time series data from frequency data containing a strong deterministic signal. For the LIFE2 analysis, the frequency spectrum for the non-deterministic ("random") load is transformed to time series data and then the deterministic signal is added directly to that time series.[5] The total time series is then cycle counted using the rainflow algorithm.

Using the assumed ± 50 percent variation in the spectral amplitude and the inclusion of the 5 percent large-excursion data, the synthesized time series data for approximately 240,000 seconds (66 hours) yield the cycle count distribution shown in Figures 13 and 14. Again, a comparatively long synthesis procedure was required to achieve a relatively smooth and stable distribution of cycle counts in the high-stress tail. As shown in Figure 13 and discussed above, the distribution and magnitudes of the cycle counts obtained using the frequency-domain techniques are in excellent agreement with the cycle count distribution obtained directly from the time series data. The distribution and magnitude of in-plane mean stress cycle counts, Figure 14, are in good agreement with the distribution and magnitude obtained directly from the in-plane time series data. The frequency-domain technique does produce more high mean-stress cycles. However, as discussed above, these high mean-stress cycles are associated with small alternating-stress ranges. Thus, these cycles do not contribute significantly to the accumulation of damage in the blades.

Off-Axis Analyses

The second set of analyses that use frequency domain data to predict the stress cycles imposed on a turbine component examines off-axis stress states. In this analysis, the off-axis stresses are obtained by adding the flapwise and edgewise bending signals vectorially.[10]

Rainflow Count

As analyzed by Sutherland,[10] the flapwise and edgewise time histories may be added vectorially to one another at the outside fibers of the root section over a range of angles that varied from 0 to 360 degrees about the root. The resulting time series was then counted using the LIFE2 rainflow counting algorithm. Figures 15 and 16 illustrate typical plots of the cycle counts. The figures are for +45°; i.e., halfway between the tension side of the flapwise bending moment and the tension side of the edgewise bending moment. In Figure 16, the cycle counts at 45° are compared to the cycle counts at 0° and 90°; i.e., the cycle counts are counts along the principal flatwise and edgewise bending axes, respectively. As seen in both figures, the typical "two hump" characteristic of the edgewise bending stress is still strong at 45°.

As discussed above, the distribution of the cycle counts in the high-stress tail is expected to achieve a stable, relatively smooth, and monotonically decreasing distribution of cycle counts. As seen in Figure 16, such a distribution is not achieved for the off-axis bending data analyzed here, even though over 4000 seconds of data are analyzed. Thus, the conclusion that the distribution of cycle counts in the high-stress tail appears to be based on insufficient data is also valid for both the primary axes and the off-axis time-series data.

Spectral Analysis

Two techniques for determining the off-axis bending moment stresses from frequency domain data have been investigated.[10] The first technique assumes that the two principal bending stresses are perfectly correlated to one another, and the second technique assumes that the bending stresses are partially correlated. Both techniques assume that the two principal bending stresses have been divided into their deterministic (azimuth average or harmonic) and non-deterministic (random) components. For the first analysis, the harmonic components (deterministic) of the two bending stresses and random components (non-deterministic) are assumed to be correlated and in-phase with one another; i.e., a correlated harmonics and correlated random, CHCR, analysis. In the second analysis, the harmonic components are assumed to be correlated and in-phase, and the random components are assumed to be

uncorrelated; i.e., correlated harmonics and uncorrelated random, CHUR.

Using the CHCR and the CHUR analysis techniques, the frequency domain data for the edgewise and flapwise bending stresses were analyzed for angles from 0 to 360 degrees. The CHCR analysis over predicts the distribution of cycle count matrix in the high-stress trail of the distribution, while the CHUR analysis predicts the distribution very well. Figures 17 and 18 illustrate the CHUR analysis at angles of +45°, -30°, -45° and -60°.

Remarks

As illustrated in Figures 8 through 18, the frequency-domain analyses permit the synthesis of comparatively long time-series data; over 240,000 seconds of data were synthesized for each of these cycle-count figures. The ability of the analysis to achieve a stable, relatively smooth and monotonically decreasing distribution is significant. However, the ability to fill out the tail of the distribution should not be confused with the actual distribution of stress cycles imposed upon the turbine. The frequency spectra used in the analysis are still based upon a rather limited set of data, and those spectra may not contain sufficient information to define the high-stress tail of the distribution of cycle counts, either.

RELIABILITY ANALYSIS

In their recent analysis of the Sandia National Laboratories 34-meter VAWT, Ashwill et al.,[8] analyzed the highest stressed region of the blade using the LIFE2 code. Several parameters are varied, including the characterization of the site's wind regime, the S-n curve for the extruded aluminum blades, and estimates of the blade stress. The influence of these parameters on the estimated service lifetime is illustrated in Table I using three wind speed distributions: a Rayleigh distribution with a 6.2 m/s (14 mph) average (R); the Amarillo Airport (located 20 miles across flat terrain from Bushland) distribution with a 6.6 m/s (15 mph) average (A); and the Bushland site distribution with a 5.8 m/s (13 mph) average (B). Table I also lists the estimated fatigue lives using both the analytically predicted (Ana) and measured (Mea) operating stresses for each of the three wind regimes. In the analytical case a published "reference" S-n curve (Ref) is used. A least squares curve fit (LSC) to newly generated S-n data is used for the measured case. Predicted lifetimes vary by a factor of 50, depending on the input parameters. Thus, this parametric study of fatigue life indicates that the predicted service lifetime is extremely sensitive to input parameters that are, at best, uncertain. The usefulness of a fatigue analysis tool is suspect when the designer realizes the magnitude of this sensitivity. Veers et al.[9] have examined this variability using reliability analysis techniques to obtain a probabilistic measure of meeting a target lifetime for economic decision-making purposes.

Table I. Effect of the Wind Regime on Lifetime (in years)

Wind	S-n Curve	Operating Stresses	Fatigue Life
R	Ref	Ana	11.9
A	Ref	Ana	7.86
B	Ref	Ana	29.4
R	LSC	Mea	150.
A	LSC	Mea	100.
B	LSC	Mea	391.

Reliability Estimate

Using a specialized solution for the estimate of fatigue life as the failure state function and the software developed by Rackwitz,[16] Veers et al.[9] have performed a FORM/SORM reliability analysis of the Sandia 34-m turbine. Relatively low levels of uncertainty were assumed to fit the situation in which substantial test data have already been obtained. The distributions for the random variables are shown in Table II. The resulting median lifetime is 370 years; however, the estimated probability of less than a 20-year target lifetime is about 2% (1.8% with FORM and 2.2% using SORM with reliability indices of 2.1 and 2.0, respectively). Importance factors are also calculated, see Figure 19. The high variability of the S-n data dominates the uncertainty, while the stress concentration factor and wind speed distribution shape make up the bulk of the remainder.

TABLE II. Definition of Variables in the Closed Form Solution.

Definition	Mean	COV	Distribution
S-n Coefficient	5×10^{21}	0.613	Weibull
Avg. Frequency	2.0 Hz	0.2	Normal
RMS Slope	0.45 MPa/(m/s)	0.05	Normal
Stress Con. Factor	3.5	0.10	Normal
Mean Stress	25 MPa	0.20	Normal
Mean Wind Speed	6.3 m/s	0.05	Normal
Dist. Shape	2.0	0.10	Normal
S-n Exponent	7.3	-	Constant
Ultimate Strength	285 MPa	-	Constant

Remarks

The calculation of fatigue lifetimes indicates the sobering variability in predictions with relatively small changes in inputs. A fatigue reliability calculation shows that even with a median lifetime of hundreds of years, the probability of premature

failure is still over 2% at 20 years. A log-normal check on the reliability calculation shows that the FORM/SORM solution[9] matches these analytical results well. However, the log-normal model is highly non-conservative.

CONCLUDING REMARKS

Two of the current activities in the fatigue research program at Sandia have been summarized here. In the analysis section, the analyses of experimental data are discussed. Particular emphasis is placed on the analysis of frequency spectral data for cycle counting and the ability to predict the high stress tail of the cycle count distribution where the major portion of the blade damage occurs. Both primary and off-axis blade bending loads are used to illustrate the results of this research.

In the reliability section, the probability of failure is quantified based on the uncertainties and the inherent randomness associated with turbine performance and the prediction service lifetimes. The results illustrate that even for a comparatively well understood and tested turbine with a long median lifetime, the probability of failure is relatively high, even for less than 10 percent of its median life.

ACKNOWLEDGMENTS

As noted in the Bibliography, this paper is a compilation of the work of many researchers. Of particular note are the research activities of Tom Ashwill, Larry Schluter and Paul Veers. All of these researchers have had significant inputs into the Sandia Wind Turbine Fatigue Program. Paul is currently leading the research into structural reliability and I am leading the research into the analysis of fatigue.

BIBLIOGRAPHY

1. P. S. Veers, *A General Method for Fatigue Analysis of Vertical Axis Wind Turbine Blades*, SAND82-2543, Sandia National Laboratories, Albuquerque, NM, September 1983.

2. H. J. Sutherland, T. D. Ashwill and N. Slack, *The LIFE Computer Code: Fatigue Life Prediction for Vertical Axis Wind Turbine Components*, SAND87-0792, Sandia National Laboratories, Albuquerque, NM, August 1987, 57 p.

3. H. J. Sutherland, "Damage Predictions for Wind Turbine Components Using the LIFE2 Computer Code," *Proceedings of EWEC '89*, Peter Peregrinus Ltd, July 1989, pp. 384-388.

4. L. L. Schluter and H. J. Sutherland, "Rainflow Counting Algorithm for the LIFE2 Fatigue Analysis Code," *Proceedings of the Ninth ASME Wind Energy Symposium*, D. E. Berg (ed), SED-Vol. 9, ASME, January , pp. 121-123.

5. H. J. Sutherland, "Frequency-Domain Stress Prediction Algorithm for the LIFE2 Fatigue Analysis Code," *Proceedings of the Eleventh ASME Wind Energy Symposium*, P. S Veers and S. Hock (eds), SED-Vol. 11, ASME, January 1992, pp. 107-113.

6. H. J. Sutherland and R . M . Osgood, "Frequency-Domain Synthesis of the Fatigue Load Spectrum for the NPS 100-kW Wind Turbine," *Proceedings of WindPower '92* (in publication).

7. T. D. Ashwill, D. E. Berg, L. R. Gallo, R. D. Grover, P. C. Klimas, M. E. Ralph, M. A. Rumsey, W. A. Stephenson, and H. J. Sutherland, "The Sandia 34-Meter VAWT Test Bed," *Proceedings of Wind Power '87, American Wind Energy Association*, SERI/CP-217-3315, October 1987, pp. 298-308.

8. T. D. Ashwill, H. J. Sutherland and P. S. Veers, "Fatigue Analysis of the Sandia 34-Meter Vertical Axis Wind Turbine," *Proceedings of the Ninth ASME Wind Energy Symposium*, D. E. Berg (ed), SED-Vol. 9, ASME, January 1990, pp. 145-151.

9. P. S. Veers, H. J. Sutherland and T. D. Ashwill, "Fatigue Life Variability and Reliability Analysis of a Wind Turbine Blade," *Probabilistic Mechanics and Structural and Geotechnical Reliability*, Y. K. Lin (ed), ASCE, July 1992, pp. 424-427.

10. H. J. Sutherland, "Effect of the Flap and Edgewise Bending Moment Phase Relationships on the Fatigue Loads of a Typical HAWT Blade," *Proceedings of the Twelfth ASME Wind Energy Symposium*, ASME, January-February 1992 (in publication).

11. C. Coleman and B. McNiff, *Final Report: Dynamic Response Testing of the Northwind 100 Wind Turbine*, Subcontractor Report, SERI Cooperative Research Agreement #DE-FC02-86CH10311, Solar Energy Research Institute, Golden, CO, December 1989, 40 pp.

12. T. Olsen, *WINDATDS, Wind Data Analysis Tool Set: User's Manual*, Solar Energy Research Institute, Golden, CO, September 1990, 148 pp.

13. Akins, R. E., 1990, "Cross-Spectral Measurements in the Testing of Wind Turbines," *Proceedings of the Ninth ASME Wind Energy Symposium*, D. E. Berg (ed), SED-Vol. 9, ASME, January 1990, pp. 155-161.

14. R. W. Thresher, S. M. Hock and R. M. Osgood, "Data Record Length Effects on Rainflow Analysis," *Proceedings of the Eleventh ASME Wind Energy Symposium*, P. S Veers and S. Hock (eds), SED-Vol. 11, ASME, January 1992, p. 117.

15. D. J. Malcolm, "Predictions of Peak Fatigue Stresses in a Darrieus Rotor Wind Turbine Under Turbulent Winds," *Proceedings of the Ninth ASME Wind Energy Symposium*, D. E. Berg (ed), SED-Vol. 9, ASME, January 1990, pp. 125-135.

16. R. Rackwitz, *User's Manual for Structural Reliability Programs CUTALG-FORM-SORM-SYSREL*, Bericht zur Zuverlassigkeitstheorie der Bauwerke, SFB 96, LKI, Technische Universitat Munchen, 1985.

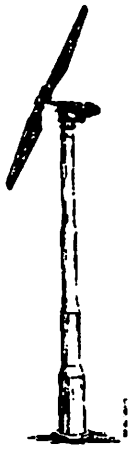

Figure 1. The Northern Power Systems 100-kW Turbine.

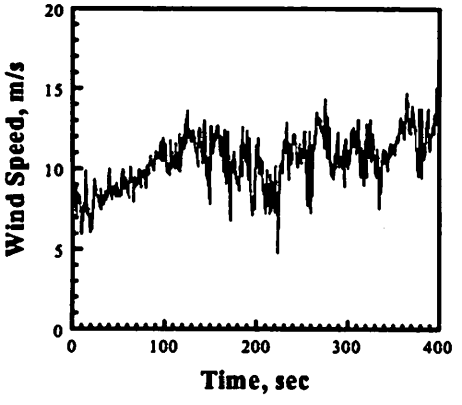

Figure 2. The First 400 Seconds of the Wind Speed Record.

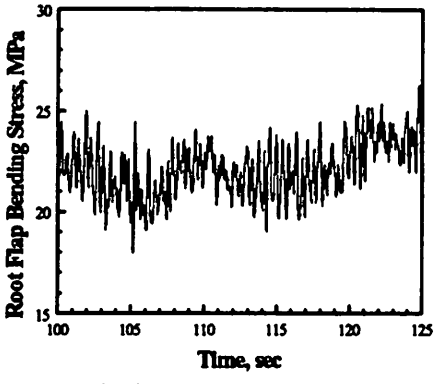

Figure 3. Typical Root Flap Bending Moment Stress Histogram.

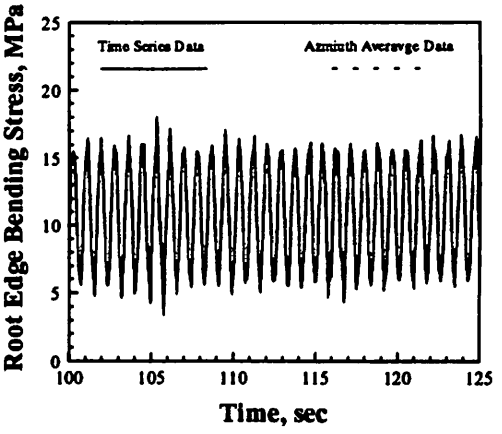

Figure 4. Typical Root Edgewise Bending Moment Stress Histogram. The solid and dashed lines overlay one another almost everywhere.

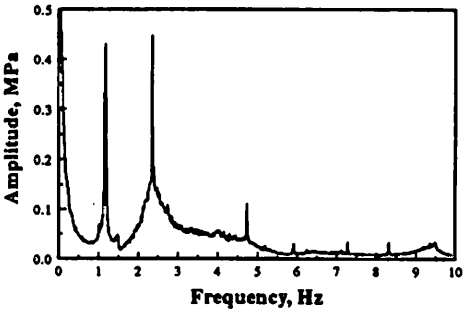

Figure 5. Amplitude Spectrum for the Root Flap Bending Stress.

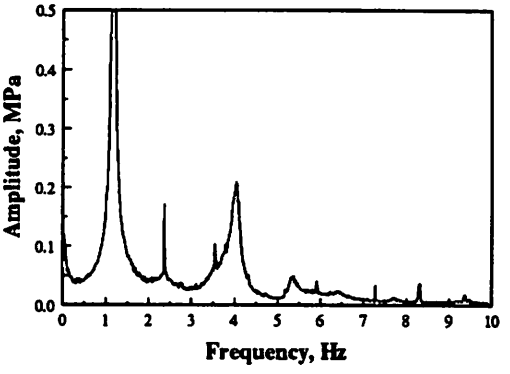

Figure 6. Amplitude Spectrum for the Root Edgewise Bending Stress.

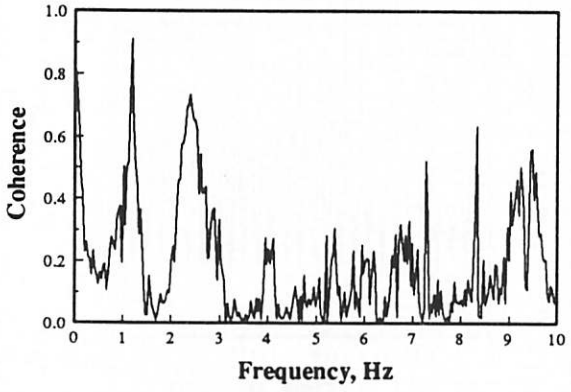

Figure 7. The Coherence Between the Root Flapwise and Edgewise Bending Moments.

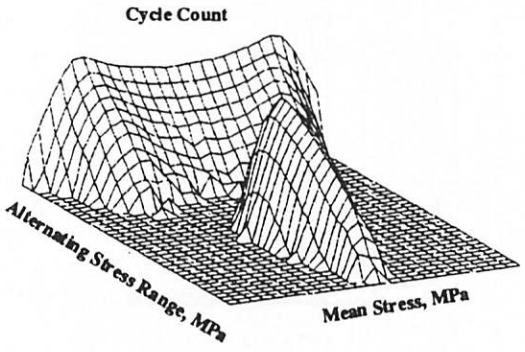

Figure 8. Semi-Log Plots of the Cycle Counts for the Root Flap Bending Stress.

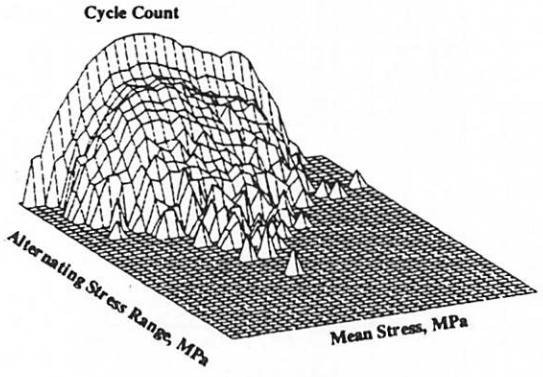

Figure 9. Semi-Log Plots of the Cycle Counts for the Root Edgewise Bending Stress.

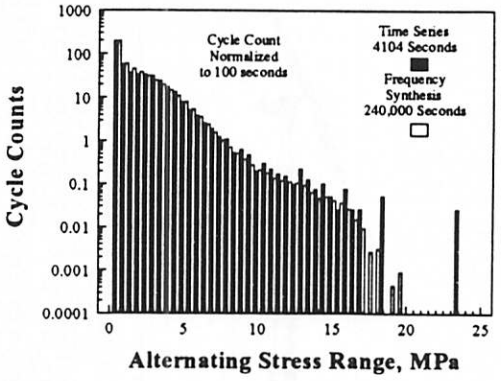

Figure 10. Alternating Stress Cycle Count Distribution for Measured Data and Synthesized Time Series Data from Average Spectra, Root Flap Bending Stress.

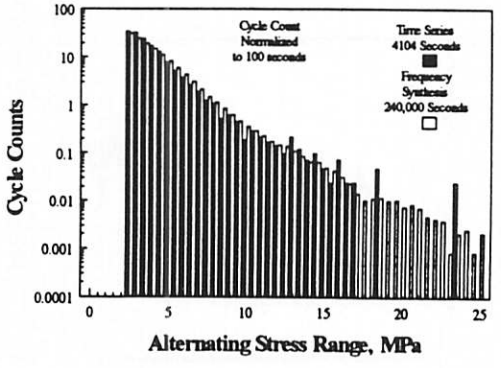

Figure 11. Alternating Stress Cycle Count Distribution for Measured Data and Synthesized Time Series Data with "Large-Excursions," Root Flap Bending Stress.

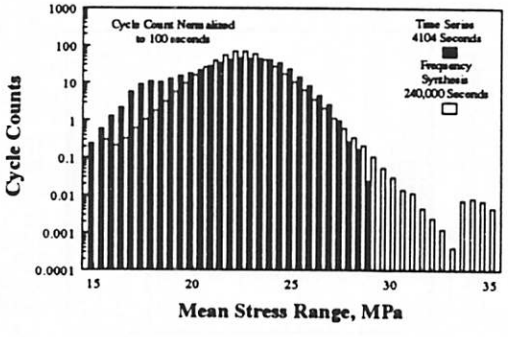

Figure 12. Mean Stress Cycle Count Distribution for Measured Data and Synthesized Time Series Data with "Large Excursions," Root Flap Bending Stress.

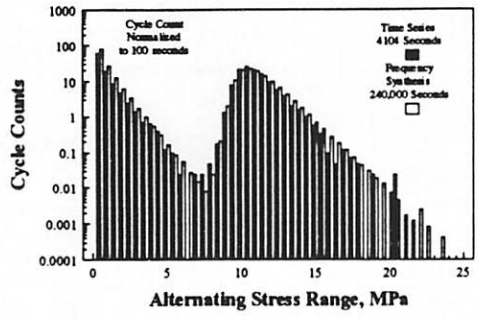

Figure 13. Alternating Stress Cycle Count Distribution for Measured Data and Synthesized Time Series Data with "Large Excursions," Root Edge Bending Stress.

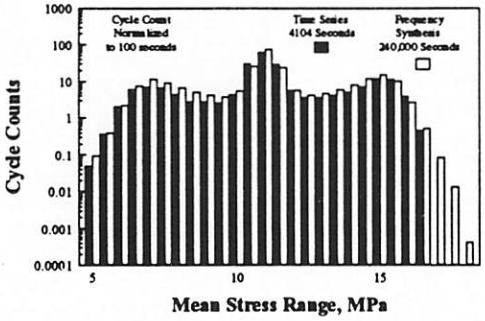

Figure 14. Mean Stress Cycle Count Distribution for Measured Data and Synthesized Time Series Data with "Large Excursions," Root Edge Bending Stress.

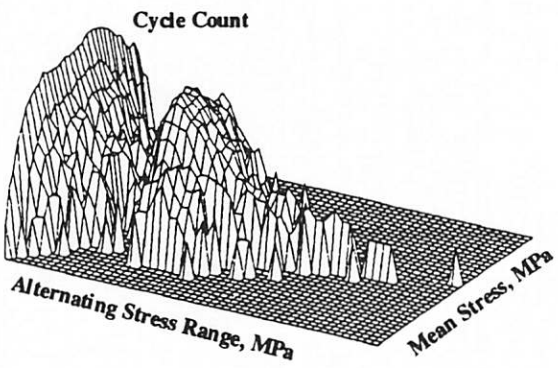

Figure 15. Cycle Count Matrix for the Bending Stress at 45°; Obtained by Cycle Counting Time-Domain Data.

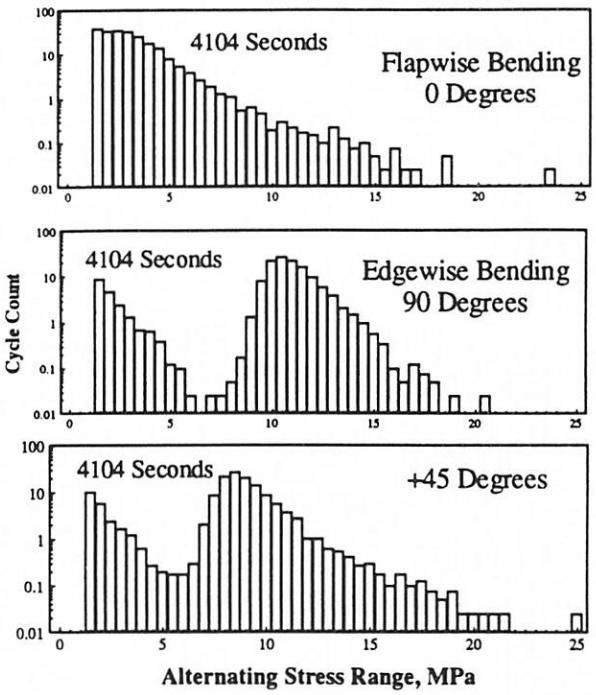

Figure 16. Cycle Count Matrix for the Principal Bending Stress Ranges at 0°, 45° and 90°; Obtained by Cycle Counting Time-Domain Data.

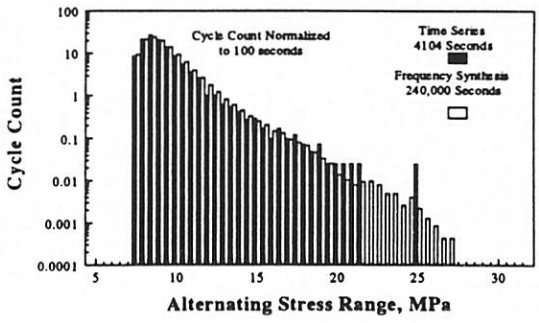

Figure 17. Cycle Count Matrix for the Bending Stress Ranges at 45°, Obtained Using the CHUR (Partially Correlated) Analysis.

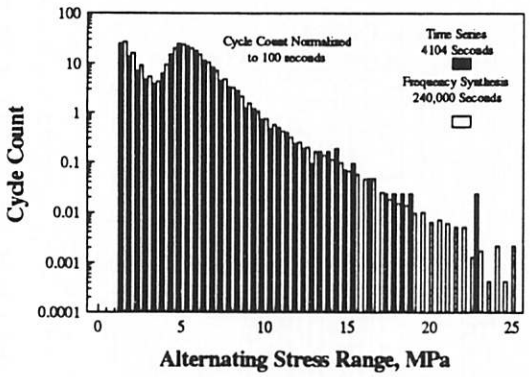

Figure 18a. Bending Stress Ranges at -30°.

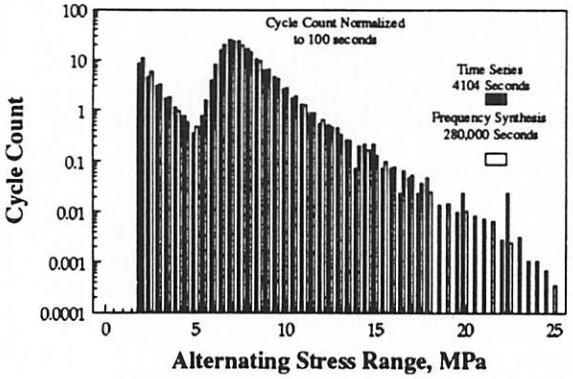

Figure 18b. Bending Stress Ranges at -45°.

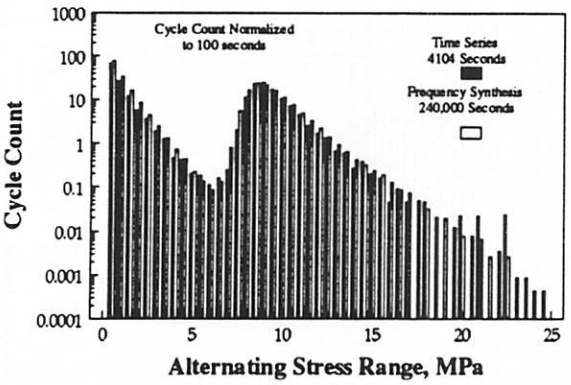

Figure 18c. Bending Stress Ranges at -60°.

Figure 18. Cycle Count Matrix for the Bending Stress Ranges, Obtained Using the CHUR (Partially Correlated) Analysis.

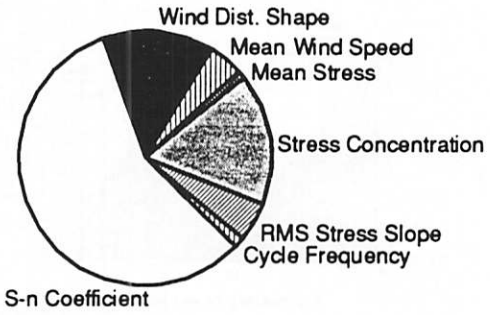

Figure 19. Importance Factors For A Log-Normal Formulation: Closed Form Solution

USING FREQUENCY DOMAIN METHODS TO PREDICT STRUCTURAL FATIGUE OF WIND TURBINE BLADES

N W M BISHOP Department of Mechanical Engineering, University College London (from 1.1.93), Department of Civil and Structural Engineering, University of Sheffield (until then).

A number of projects are being undertaken by the Random Loading and Fatigue Group at Sheffield University to improve fatigue life prediction techniques in the frequency domain. Specific areas of work are being undertaken to develop the current theories to deal with;

(1) non-Gaussian data,

(2) non-stationary data,

(3) data containing large periodic components,

(4) fatigue analysis of materials for which mean stress effects are important.

The frequency domain approach to fatigue analysis is a particularly useful tool for the design of wind turbine blades because of its computational simplicity and speed. However, acceptance of the theories will require solutions for most, if not all of the above tasks. This paper represents an enhancement and extension of earlier work presented at the British Wind Energy Conference in March 1992.

NOTATION

PSD, Power Spectral Density function
m_n, n_{th} moment of PSD function
$E[0]$, expected number of +ve zero crossings per unit time
$E[P]$, expected number of peaks per unit time
γ, irregularity factor
pdf, probability density function
b, material parameter from S-N (fatigue life) curve
$p(S)_{TD}$ and $p(S)_{FD}$, the pdf of rainflow ranges produced from time signal or using Theoretical Solution.
$p(S,ms)_{TD}$ and $p(S,ms)_{FD}$, the joint pdf of rflow. rgs. and means produced from time signal or using Theor. Soln.
I_p, II_p, probabilities of event as defined in Section 4.
I_t, II_t, as I_p and II_p after inverting Fig 6.
k, a function of relative mean stress defined by S_{ult}/S_{max}

1. INTRODUCTION AND BASIC THEORY

The use of frequency domain based techniques for the analysis of structural systems is now widely accepted in many engineering fields. The offshore industry, for instance, relies very heavily on the use of PSD (Power Spectral density) techniques for the dynamic analysis of deepwater platforms [1]. Dynamically sensitive structures are efficiently analysed in this way. Statically responsive structures can also be more efficiently analysed this way if the loading conditions are complex.

It is very important to note, however, that application of PSD based analysis techniques assumes that the system is linear, stationary and Gaussian (normal). However, structural reliability engineers have two main practical requirements which must be met before the techniques can be applied. Firstly, an accurate and robust method of predicting fatigue damage from the PSD must be available, and secondly it must be possible to deal with structural systems which do not conform rigidly to the inherent requirements of linearity, normality and stationarity. The purpose of this paper is to deal with these two topics for the particular case of wind turbine blade loadings.

The whole of this paper relies on the assumption that a standard S-N approach can be adopted and so a traditional S-N curve as shown in Fig 1 is used to model the material properties of the components being analysed. This simply shows that under constant amplitude cyclic loading, a linear relationship exists between cycles to failure N and applied stress range S when plotted on log-log paper.

Because 'real' signals rarely conform to this ideal constant amplitude situation, an empirical approach is used for calculating the damage caused by stress signals of variable amplitude. Despite its limitations, Miner's rule is generally used for this purpose. The rule states that at failure;

$$\sum \frac{n}{N} = 1.0$$

This linear relationship assumes that the damage caused by parts of a stress signal with a particular range can be calculated and accumulated to the total damage separately from that caused by other amplitudes. A ratio is calculated for each stress range, equal to the number of actual cycles at a particular stress range n divided by the allowable number of cycles to failure at that stress N (obtained from the S–N curve). Failure is assumed to occur when the sum of these ratios, for all stress ranges, equals 1.0.

If n is obtained from a time history of stress then the most convenient way of storing the information is in the form of a probability density function (pdf) of stress ranges. Since 'rainflow ranges' of stress are generally regarded to give the best indication of the fatigue damaging potential of a random signal it is the pdf of rainflow ranges which is the desired result. An example of the way rainflow ranges are extracted from a time signal is given in Fig 2.

Since we are concerned with structural systems analysed in the frequency domain we require a method for extracting the pdf of rainflow ranges directly from the PSD of stress. The characteristics of the PSD which are used to obtain this information are the nth moments of the PSD function:

$$m_n = \int_0^\infty f^n G(f) df$$

A method for computing these moments is highlighted in Fig 3. Some very important statistical parameters can be computed from these moments, such as the expected number of zeros and peaks per second;

$$E[0] = \left[\frac{m_2}{m_0}\right]^{1/2} \qquad E[P] = \left[\frac{m_4}{m_2}\right]^{1/2}$$

from which the irregularity factor factor γ can be computed, which gives an indication of the spread of frequencies present in the signal;

$$\gamma = \frac{E[0]}{E[P]}$$

γ varies between 1.0 and 0.0. A value of 1.0 corresponds to a narrow band signal which, as the term implies, means that the signal contains only one predominant frequency. A value of 0.0 implies that the signal contains an equal amount of energy at all frequencies.

2. ORIGINAL THEORETICAL SOLUTION FOR ESTIMATING RAINFLOW RANGES FROM PSD'S

Rainflow ranges have been widely used for estimating fatigue damage from random signals since Matsuishi and Endo first introduced the concept to the scientific community over twenty years ago [2]. When the loading sequence is specified as a time history the procedure for calculating rainflow ranges is relatively simple. However, the analysis of structural systems subjected to random loadings is often most efficiently carried out in the frequency domain using PSD's. There was therefore a need to be able to predict fatigue, based on rainflow ranges, directly from these PSD's. Many researchers have since tried to develop such solutions mostly for application in the offshore industry. Until 1985, these solutions consisted entirely of correction factors which produced a damage value directly using a modified 'narrow band' solution [3]. Dirlik then produced an empirical formula for the pdf of rainflow ranges [4]. This solution has been shown to be far superior, in terms of accuracy, than the previously available correction factors.

The need for certification of the technique before its use meant that theoretical verification was required. This was achieved in 1988 [5] when a theoretical solution for predicting rainflow ranges from the moments of the PSD was produced.

All the solutions mentioned above make assumptions about the characteristics of the signal. In particular, it is assumed that the signal is Gaussian (or normal), stationary and random. The consequences of these assumptions and methods for dealing with 'real' signals are discussed later in this paper. Mean stress effects, which are important for some materials are also ignored by these methods. The consequences of this are also considered later in this paper and an extension of the original Theoretical Solution to include mean stress effects is given.

Before these topics can be properly addressed it is important to identify the main elements of the original Theoretical Solution. The summary given below can be fully enhanced by referring to a more rigorous derivation given elsewhere [6].

An essential requirement of any Theoretical Solution was a statistical rather than spatial description of rainflow ranges. This was initiated in [7] and further extended later [6] to the form given in Fig 4.

In practical terms this definition asserts that the probability of three events Y_1, Y_2 and Y_3 can be used to define the probability of a rainflow range S occurring with a peak at the level corresponding to point 1 and a trough at a level corresponding to point 2. Obviously there are a number of configurations that can occur with the same distance or range between point 1 and point 2 as given in Fig 5. The total probability of a particular rainflow range is therefore the summation of these individual probabilities. The definition is expressed in terms of peak and trough values and the relationships between these. This is not surprising since fatigue damage is determined by ranges of stress, which are themselves determined by peak and trough values.

The problem then reduces to one of finding the individual probabilities of Y_1, Y_2 and Y_3. For this a Markov chain model was used as shown in Fig 6.

In order to reduce the computational effort required to obtain a solution, the assumptions of normality and stationarity were used. By assuming that the signal is stationary, one can assume that the signal is statistically equivalent after reflection about a vertical axis. Events Y_1 and Y_2 can then be treated in the same way. By assuming the signal is Gaussian, one can assume that the signal is statistically equivalent after reflection about a horizontal axis. Event Y_3 can then be treated in the same way as events Y_1 and Y_2. This is shown in Fig 7 where this equivalence is highlighted by identifying the four identical elements which exist in a stationary and Gaussian turning point matrix. The task of obtaining these three events then reduces into that of obtaining the 'long run' absorbtion probabilities of transitions into states 1 and 2 depicted in Fig 6. These are;

(I_p) Given the assumption that a signal starts from some peak at level ip, what is the probability that it will move (via any number of peaks and troughs) to some other level kp directly, without going

back to (or above) the level of ip (the first peak) or to a level below kp.

(II_p) Given the assumption that a signal starts from some peak at level ip, what is the probability that it will move (via any number of peaks and troughs) to some other level below kp, without going back to (or above) the level of ip or into the level of kp.

Of course this information must be evaluated for every configuration of peak and trough in the signal.

If the Markov assumption is valid, that the probability of going to any adjacent peak (or trough) in the signal is dependent only on the position of the current trough (or peak), then the probabilities of the above two multi transition events can be obtained from the one step peak to trough and trough to peak probabilities using Markov Chain theory. This assumption is generally true for typical engineering situations.

The one step transition probabilities are obtained using the (approximate) solution of Kowalewski [8] for the pdf of adjacent peaks and troughs in a Gaussian signal. The reader is referred to [6] for a detailed description of the method of evaluating the Markov Chain model. The complete procedure can therefore be described by four distinct stages;

(1) evaluation of the 2 dimensional (one step) pdf of adjacent peaks and troughs using the approximate formula of Kowalewski,

(2) evaluation of the 2 dimensional matrix of multi-step probabilities (f_j^i) defined by I_p and II_p above using an appropriate Markov Chain model, where f_j^i is defined as the long run (multi-step) probability of absorbtion into level i from level j.

(3) evaluation of Y_1, Y_2 and Y_3 using the following equations,

$$\begin{aligned} Y_2 &= f_{ip}^{1}, \quad \text{and by symmetry about the vertical axis} \\ Y_1 &= f_{ip}^{1} + f_{ip}^{2}, \quad \text{and by symmetry about a horizontal axis,} \\ Y_3 &= f_{tp+S-ip}^{1*} + f_{tp+S-ip}^{2*} \end{aligned}$$

where tp is twice the mean signal value, state 1* is level $tp-ip$, state 2* is all levels below $tp-ip$ and levels ip, kp and states 1 and 2 are defined by Fig 6.

(4) evaluation of the pdf of rainflow ranges using the expression,

$$p(S)_{FD} = \frac{2}{dS} \cdot \sum_{ip=S+1}^{ip=nts} (f_{ip}^{1} + f_{ip}^{2}) \times (f_{ip}^{1}) \times (f_{tp+S-ip}^{1*} + f_{tp+S-ip}^{2*}) \times p(ip)$$

for $S=1$ to $ip-1$ (nts=no of intervals in the discretised time signal).

3. INCLUSION OF MEAN STRESS EFFECTS

Most S-N curves apply to constant amplitude cycles with zero mean stress. In order to use stress cycles with a non zero mean stress it is usual to convert the stress range into an equivalent stress cycle range at zero mean stress using, for instance, the Goodman formula;

$$\frac{S_a}{S_{a0}} + \frac{S_m}{S_{ult}} = 1.0$$

Or alternatively;

$$S_{a0} = \frac{S_a}{(1 - \frac{S_m}{S_{ult}})}$$

Since it is only random time signals in which we are interested we have to make the additional assumption that mean stresses can be used with rainflow cycles which, by their very definition, are made up of sections of signal which may be separated by a large time interval. The concept of mean stress

then becomes rather abstract. However, as with many engineering situations the use of mean stress in conjunction with rainflow ranges would appear to be the best option available and one which has some experimental backing.

Previous work [3] has shown that both the Dirlik and Theoretical Solutions produce very good results for data that is reasonably Gaussian and stationary as long as mean stress effects are ignored. However, wood epoxy and grp wind turbine blades have been shown to be very fatigue sensitive to mean stress [9] and so it is important that this parameter is included in any design tool. However, only the Theoretical Solution is capable of being adapted in this way since the Dirlik solution is a closed form empirical expression which is impossible to separate and rework.

In order to extend the Theoretical Solution stage 4 above needs to be redefined as follows;

$$p(S,ms)_{FD} = \frac{2}{dS}.(f_{ip}^{1} + f_{ip}^{2})\times(f_{ip}^{1})\times(f_{ip+S-ip}^{1*} + f_{ip+S-ip}^{2*})\times p(ip)$$

where ms is the mean stress value defined by $(ip+kp)/2$

In order to evaluate the effect of mean stress on some typical wind turbine loading signals the 24 WEG MS1 data files used in an earlier paper [10] were investigated using both the revised Theoretical Solution ($p(S,ms)_{FD}$) and by analysing the time histories directly to obtain $p(S,ms)_{TD}$, the joint pdf of means and ranges obtained directly from the time signal. Fig 8 shows an example of these joint pdf's for data sample y27a. The plot of $p(S,ms)_{TD}$ highlights the important fact that the distribution of ranges and means is very irregular because of the relatively short sample length which was analysed. The general form of the distribution is, however, broadly in line with that for $p(S,ms)_{FD}$.

In order to estimate the effect on fatigue damage of including mean stress effects using the Goodman diagram a value for S_{ult}, the ultimate tensile strength, is required. The 24 MS1 load cases were analysed by assuming that S_{ult} was equal to $k\times S_{max}$, the maximum stress present in each data sample multiplied by some factor k. Fig 9 gives an example (for y27a) of fatigue damage ratios computed both from $p(S,ms)_{TD}$ and $p(S,ms)_{FD}$. Damage ratios are defined as the computed damage, after normalisation by the damage computed directly from the whole time sample ignoring mean stress effects. Damage ratios have been shown in Table 1 for all 24 load cases at k values of 5, 10, 20 and 30. This data shows that there is a certain amount of scatter at all values of k. This scatter is broadly in line with that found when the load cases were analysed whilst ignoring mean stress effects (see [11] Table 3). The data presented in Figs 8 and 9 is for an S-N slope of 8.

4. TREATMENT OF NON-GAUSSIAN DATA

The Theoretical Solution described in section 2 makes a number of assumptions about the data being analysed. Perhaps the most important of these is that of normality. In its original form all the stages of the solution either depend on, or make use of, this assumption. However, stages 2 to 4 can be generalised to cover non-Gaussian data. In order to do this the events Y_1, Y_2 and Y_3 must be readdressed. In particular, it is not sufficient to compute the probabilities I_p and II_p alone. Instead, a second pair of probability sets I_t and II_t must be computed, which are obtained using a Markov Chain model similar to the one shown in Fig 6, after reflection about the horizontal axis. Events Y_1, Y_2 and Y_3 can then be evaluated in full without assuming the signal is Gaussian.

In order to obtain a complete solution for the non-Gaussian situation, a suitable replacement for the Kowalewski solution (stage 1) must be obtained. Work on this is in progress.

5. TREATMENT OF NON-STATIONARY DATA

Inspection of the PSD's obtained from the 24 MS1 load cases shows that there is often a large very low frequency spike near to DC. It is also true that the choice of window size (the FFT length) used to compute each spectral estimate has an effect on this spike. It is therefore useful to investigate this

phenomenon for different window sizes, or number of blocks used to carry out damage estimates.

In order to do this the whole signal was divided into a number of segments or blocks. This defined the window size for each block. For each window, an FFT was computed on the whole window, without any spectral averaging. From this FFT the PSD was obtained, and then the fatigue damage calculated using the Theoretical Solution. This damage was then averaged over all the blocks and the mean and scatter calculated.

Table 2 presents the results from this procedure for 4, and 8 blocks. Two very important observations can be made from this data. Firstly, the scatter of the averaged damage values for the 24 load cases reduces with increasing number of blocks used, and secondly, the mean of the averages appears to decrease with increasing number of blocks (reducing window size). A similar observation was made about this effect elsewhere [12].

A more detailed examination of this has been carried out for load case y27a. The average damage (in both the time and frequency domain) normalised by that from the whole time signal has been plotted and, as expected, it shows a reduction as the number of blocks is increased.

Fig 10(a) shows the reduction in normalised damage in the time domain, with decreasing block size. Figs 10(b) and 10(c) show a similar effect in the frequency domain. In this case the damage was estimated from one PSD which was computed using spectral averaging. The number of FFT's used for the PSD was approximately equal to the total signal length divided by the window size. Fig 10(b) highlights the effect for y27a. This is broadly in line with the time domain estimate in Fig 10(a). Fig 10(c) shows, however, that that for a regenerated 'stationary', 'Gaussian' signal there appears to be no significant trend. This implies that it is a characteristic of the wind signal which is causing the change in damage. It would appear that it is a reduction of m_0 which is the primary cause of this reduction in fatigue damage. This is perhaps because of the loss of the spike at the low frequency end of the PSD.

6. STATISTICAL ANALYSIS

An important requirement of any further work in this area is a thorough understanding of the statistical characteristics of all signals which may be encountered. Up to now, too little data has been obtained to be able to carry out a thorough study of the topic. Only the MS1 data was available at the time of writing this report. The analysis of this data is presented in Table 3.

The mean, root mean square (rms) and irregularity factor (γ) were computed directly from each time signal as a complete block. Stationarity or trend tests were carried out using the Reverse Arrangement Test (rat) [13] applied to separate segments taken from each load case. For this, each load case was broken up into a number of segments which were then analysed as independent records. Each segment had a length of 2048 points. The rat test was applied to the means and rms's of each segment of a load case by considering them as sequences of N (number of segments or blocks) observations (denoted by x_i, i=1,N) of a random variable x. Then the number of times (A) that $x_i > x_j$ for $i<j$ was counted and compared with an expected value for a truly random sequence.

The expected values are 76.5 for N=18, 45.5 for N=14 and 7.5 for N=6. The acceptance regions for a confidence level $\alpha = 0.05$ are

N=18, $50 \leq A \leq 102$
N=14, $27 \leq A \leq 63$

For N=6 the number of observations is too small for there to be any practical significance. Table 3 shows that, apart from y12a, y19a, y27a, and y35a all the signals have no significant non-stationarity or trend.

Tests for normality were carried out using both the χ^2 parameter and the Kurtosis Test. For $\chi^2(30)$ (with a significance level of 0.99), the upper bound on $\chi^2(30)$ is 50.9. Inspection of the results would suggest that all the data can be assumed to be Gaussian.

The Kurtosis (Coefficient of Excess) Test was applied to the data. Kurtosis can be used as a measure of the flattening of a distribution near its center. For a normally distributed signal a value of 0.0 would be expected. The minimum value of Kurtosis is -2 which corresponds to a symmetric binary random variable (|x| = constant). At the other extreme, a value of ∞ would be obtained for a distribution with slowly decaying tails. It is difficult to draw any conclusions from the values obtained for Kurtosis (or for the other parameters) but once a larger quantity of statistical data is available a relative assessment of the values will then be possible. However, if the χ^2 value for each load case is plotted against damage rate divergence a linear bound on the maximum divergence with increasing χ^2, or non-normality, would appear to be appropriate (see Fig 11). This requires further analysis but raises the question, can a frequency domain approach be used for non-Gaussian data if an error factor is applied in conjunction with the Theoretical Solution?

7. COMPUTATIONAL CONSIDERATIONS

This section is intended to draw together the various computational considerations which are important when carrying out a frequency domain analysis. It is not possible to make firm conclusions about most of these, at the present time, but further work is in progress which will hopefully make it easier to come up with design guidelines in the near future.

Previous work [11] demonstrated that the frequency cutoff point for the PSD has an important effect on the damage value produced. This is shown in Fig 12. A detailed inspection of the variation of this damage, and the moments which are used to compute it, highlights some interesting points. Firstly, there is energy in the PSD above the normally used 15Hz cutoff frequency. How much of this is real loading energy and how much is electrical noise is difficult to assess. However, since it has a pronounced effect on the fourth moment and hence on fatigue damage, it is important to fully understand the problem.

The choice of PSD cutoff point is a frequency domain problem. There is, however, a similar problem in the time domain in that the number of intervals used to discretise the time sample can have an effect on fatigue damage if the numbers of peaks per second is not carefully worked out. In general, the number of peaks per second, should correlate with the number of peaks in the signal (after discretisation) that was used to produce the pdf. In theory, the same argument should apply to the frequency domain PSD cutoff but this is a little harder to confirm. This raises the interesting question of the relationship (if any) between PSD cutoff point and time signal discretisation interval width. Previous work has also shown that damage estimates, both in the time and frequency domains, show considerable scatter if short sample lengths are used. This must be remembered if other statistical variations are being investigated at the same time. The effect is shown in Fig 13 where a progressively larger sample has been used to compute fatigue damage in both the time and frequency domains. It is very important to note that the damage value is apparently a random variable when viewed against sample length and the time and frequency domain variations seem to be independent.

If one is trying to compare the difference between two different pdf's it is important to be aware of the fact that there will be a difference in performance between solutions at different values of b, the S-N material parameter. Fig 14 shows this effect for load case y27a.

8. CONCLUSIONS

(1) A modified Theoretical Solution for computing the joint pdf of rainflow ranges and means of a signal specified in the frequency domain has been developed and verified against a limited amount of data.

(2) Non Gaussian load cases have been considered and some theoretical progress made towards extending the Theoretical Solution, but no data was available at the time of writing this paper which could be used to verify the technique.

(3) Non-stationary data has been considered and the specific problem of the low frequency element contained within the available data has been discussed. Further work in this area is planned.

(4) Some interesting tentative conclusions can be made from the statistical analysis of the MS1 data, although much more data is required before these can be verified. The χ^2 parameter appears to offer some hope as a means of defining a possible error bound on the error associated with application of the Theoretical Solution to non-Gaussian data.

(5) There are many complicated computational considerations when carrying out a frequency domain fatigue calculation and some of these have been discussed

(6) Some verification of the theories presented in this paper has been carried out on the MS1 data. Much more data is required before conclusive statements can be made about the applicability of the methods described within this report.

9. REFERENCES.

[1] N W M Bishop, Dynamic fatigue response of deepwater offshore structures subjected to random loading, Structural Engineering Review, SER 76/11, Aug 1991.

[2] M.Matsuishi and T.Endo, Fatigue of metals subject to varying stress, paper presented to Japan Soc Mech Engrs, Jukvoka, Japan, 1968.

[3] Fatigue life prediction from power spectral density data. Part 1, traditional approaches and Part 2, recent developments. Environmental Engineering, Vol.2, Nos. 1 and 2, 1989.

[4] T.Dirlik, Application of computers in Fatigue Analysis, University of Warwick Thesis, Jan 1985.

[5] N.W.M.Bishop, The use of frequency domain parameters to predict structural fatigue, PhD thesis, Warwick University, submitted December 1988.

[6] N.W.M.Bishop and F.Sherratt, A theoretical solution for the estimation of rainflow ranges from power spectral density data. Fat. Fract. Engng. Mater. Struct., 13 no.4, 1990.

[7] I.Rychlik, A new definition of the rainflow cycle counting method, Int J Fatigue, 9, pp 119-121, April 1987.

[8] J.Kowalewski, On the relationship Between Component Life Under Irregularly Fluctuating and Ordered Load sequences. Part 2, DVL Report 249, 1963.

[9] P Bonfield and MP Ansell, Fatigue testing of wood composites for aerogenerator rotor blades. Part V. Life Prediction and Hysteresis. Wind Energy Conversion 1990, eds TD Davies et al.

[10] N.W.M.Bishop , F Sherratt and Hu Zhihua, The Analysis of Non-Gaussian Loadings from Wind Turbine Blades Using Frequency Domain Techniques, British Wind Energy Conference 13, Swansea, April 1991.

[11] N.W.M.Bishop and Hu Zhihua, The Fatigue Analysis of Wind Turbine Blades Using Frequency Domain Techniques, EWEC '91, Amsterdam, Oct 1991.

[12] C A Morgan and A J Tindal, Further analysis of the Orkney MS1 data, Wind Energy Conversion 1990, eds TD Davies et al.

[13] J.S.Bendat and A.G.Piersol, Random data, analysis and measurement procedures (2nd edition), John Wiley & Sons, Inc., New York 1986.

10. ACKNOWLEDGEMENTS

The authors of this paper are most grateful to The Wind Energy Group for the provision of data from the MS1 wind turbine and to SERC for their financial assistance under grant number GR/G 53903.

Table 1. The effect on damage of different relative mean stress levels. Larger S_{ult}/S_{max} levels indicate a relatively lower mean stress level.

Damage rates at different S_{ult}								
data	S_{ult}/S_{max} (time signal)				S_{ult}/S_{max} (theoretical soln)			
	5	10	20	30	5	10	20	30
y12a	3.10	1.87	1.98	1.61	3.88	2.42	2.32	1.81
y19a	2.81	1.53	1.69	1.47	3.19	1.98	1.90	1.49
y27a	3.06	1.38	1.69	1.69	3.20	1.97	1.90	1.50
y35a	3.33	1.37	1.87	1.95	1.95	1.19	1.15	0.92
y12b	2.49	1.40	1.50	1.36	1.38	0.89	0.82	0.63
y19b	2.50	1.30	1.42	1.37	1.31	0.85	0.77	0.59
y27b	2.70	1.32	1.49	1.51	1.19	0.77	0.71	0.54
y35b	3.31	1.30	1.73	1.87	1.11	0.70	0.66	0.51
y12c	2.58	1.52	1.51	1.16	1.63	1.01	0.97	0.76
y19c	2.61	1.41	1.41	1.30	1.46	0.91	0.87	0.68
y27c	2.54	1.53	1.50	1.17	1.22	0.76	0.73	0.57
y35c	2.44	1.52	1.49	1.23	1.18	0.74	0.70	0.55
y12d	2.74	1.52	1.53	1.44	2.59	1.65	1.55	1.19
y19d	3.56	1.76	1.97	1.60	2.57	1.64	1.53	1.18
y27d	3.35	1.82	1.97	1.40	2.32	1.47	1.39	1.07
y35d	2.58	1.47	1.54	1.32	2.29	1.41	1.36	1.07
y12e	2.51	1.41	1.51	1.35	2.00	1.24	1.19	0.94
y19e	3.57	1.78	1.95	1.69	2.62	1.63	1.56	1.22
y27e	1.75	0.99	0.92	1.00	2.08	1.31	1.24	0.96
y35e	3.61	1.49	2.06	2.09	2.52	1.58	1.50	1.17
y12f	2.96	1.72	1.72	1.41	2.84	1.79	1.70	1.32
y19f	2.30	1.22	1.31	1.33	2.46	1.55	1.47	1.14
y27f	3.34	1.70	1.79	1.58	3.37	2.12	2.01	1.56
y35f	2.62	1.55	1.71	1.49	2.99	1.90	1.79	1.38

Table 2. The average damage values obtained over different numbers of blocks after normalising by the damage obtained directly from the time signal

Data	Lnth	blocks		
		1	4	8
y12a.	37500	1.07	0.864	0.650
y19a.	37500	1.09	0.921	0.740
y27a.	37500	1.23	0.890	0.691
y35a.	37500	1.37	0.958	0.754
y12b.	30028	0.79	0.997	0.564
y19b.	30028	0.86	1.052	0.576
y27b.	30028	0.91	1.157	0.564
y35b.	30028	1.30	0.903	0.557
y12c.	37500	0.61	0.555	0.504
y19c.	37500	0.61	0.579	0.509
y27c.	37500	0.51	0.506	0.462
y35c.	37500	0.46	0.440	0.381
y12d.	37500	0.81	0.707	0.655
y19d.	37500	0.83	0.719	0.679
y27d.	37500	0.81	0.710	0.626
y35d.	37500	0.87	0.595	0.686
y12f.	37500	1.01	0.940	0.800
y19f.	37500	1.13	1.043	0.873
y27f.	37500	1.11	1.086	0.924
y35f.	37500	1.17	1.078	0.938
mean		0.928	0.835	0.656
rms		0.252	0.212	0.147

Table 3. WEG MS1 statistical analysis

Data	Lnth	Blks	Mean	Rnm	RMS	Rnr	$\chi^2(30)$	γ	Kts
y12a.	37500	18	-132.77	35	25.85	90	33.47	0.24	-0.12
y19a.	37500	18	43.55	119	25.13	93	29.47	0.24	-0.04
y27a.	37500	18	44.74	116	25.67	89	36.85	0.25	0.00
y35a.	37500	18	68.78	115	31.28	80	50.10	0.26	-0.12
y12b.	30028	14	-67.82	30	27.55	50	29.99	0.31	0.00
y19b.	30028	14	-9.02	60	27.01	51	32.45	0.32	0.03
y27b.	30028	14	-50.87	60	26.50	48	37.29	0.32	-0.02
y35b.	30028	14	-93.32	59	30.04	37	45.80	0.29	-0.12
y12c.	37500	18	-90.30	70	20.67	71	49.77	0.15	-0.51
y19c.	37500	18	19.34	83	19.94	70	48.36	0.16	-0.41
y27c.	37500	18	6.78	83	18.50	69	48.22	0.18	-0.26
y35c.	37500	18	42.09	84	16.86	73	54.26	0.21	-0.25
y12d.	37500	18	-168.94	88	21.47	93	37.47	0.23	-0.11
y19d.	37500	18	77.04	64	20.81	94	36.82	0.24	-0.06
y27d.	37500	18	68.30	67	20.18	86	37.40	0.26	-0.03
y35d.	37500	18	114.85	69	20.80	69	45.17	0.27	-0.04
y12e.	12823	6	-184.20	14	15.99	12	58.04	0.27	-0.26
y19e.	12823	6	68.48	1	17.31	12	39.91	0.28	-0.29
y27e.	12823	6	50.85	2	17.99	11	32.26	0.33	-0.23
y35e.	12823	6	106.54	3	19.86	11	56.65	0.35	-0.24
y12f.	37500	18	-149.28	70	16.03	73	51.18	0.22	-0.21
y19f.	37500	18	66.92	83	14.87	74	47.16	0.24	-0.15
y27f.	37500	18	46.39	83	14.50	71	50.31	0.29	-0.14
y35f.	37500	18	90.43	83	14.75	84	54.76	0.32	-0.12

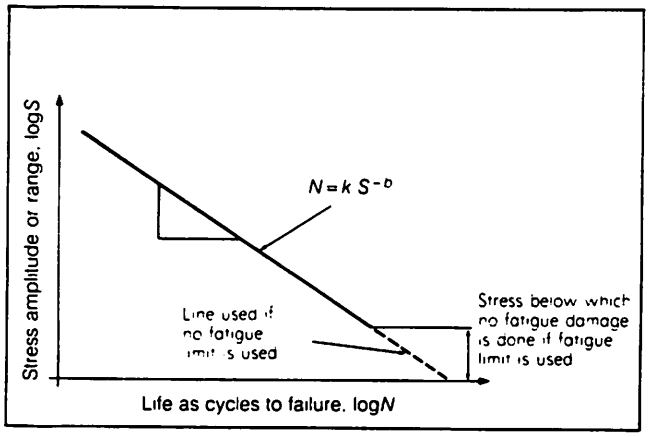

Fig 1. A typical stress-life diagram

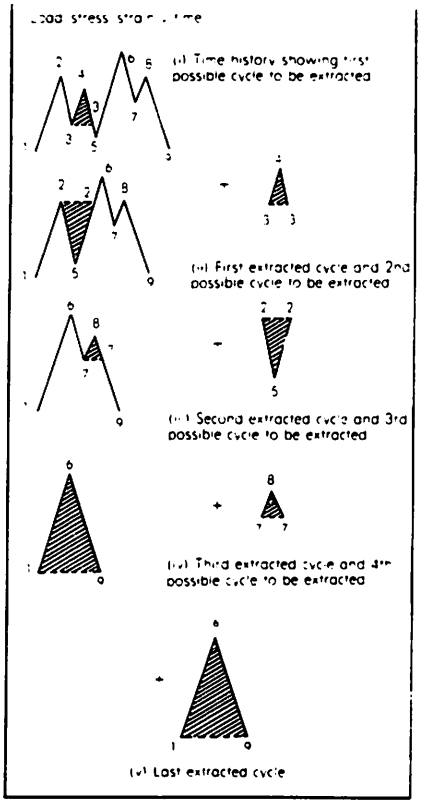

Fig 2. Stages in rainflow cycle counting a simple time record

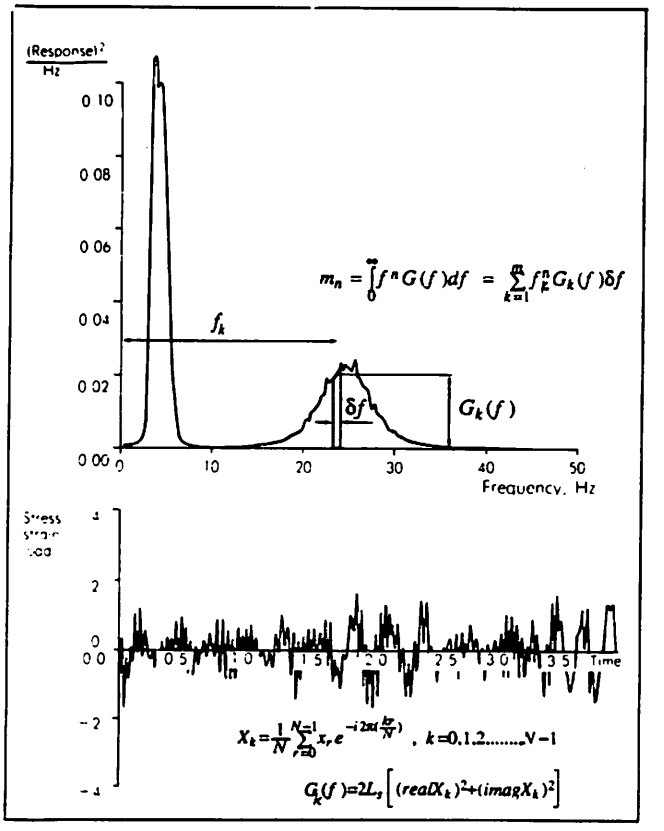

Fig 3. The method of calculating the moments of a typical PSD

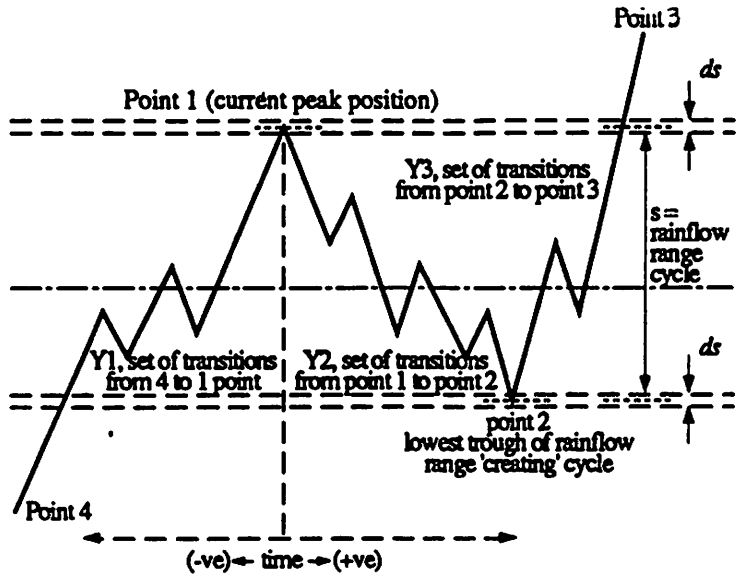

Fig 4. A new rainflow range definition using a statistical rather than spatial description

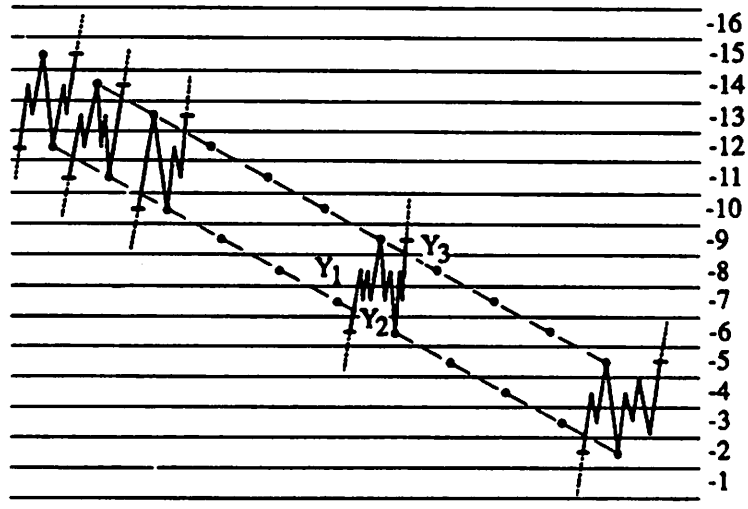

Fig 5. Different combinations of rainflow cycle with the same stress range

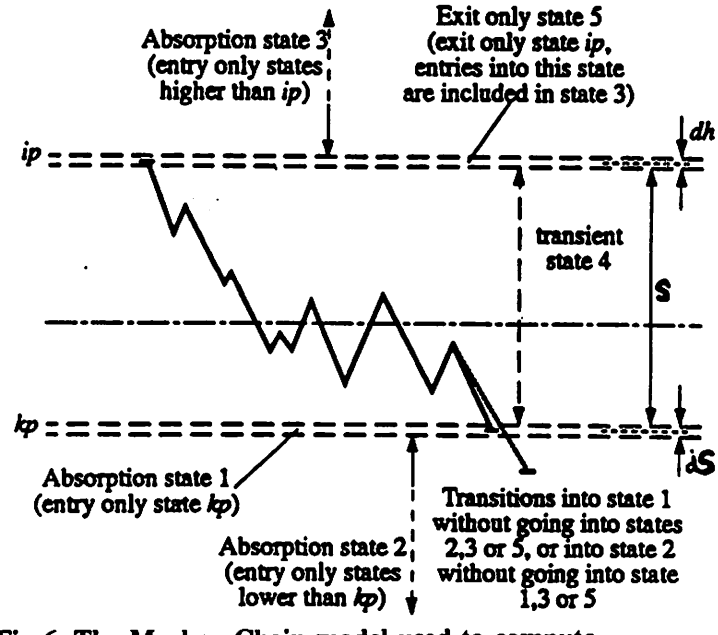

Fig 6. The Markov Chain model used to compute the pdf of rainflow ranges

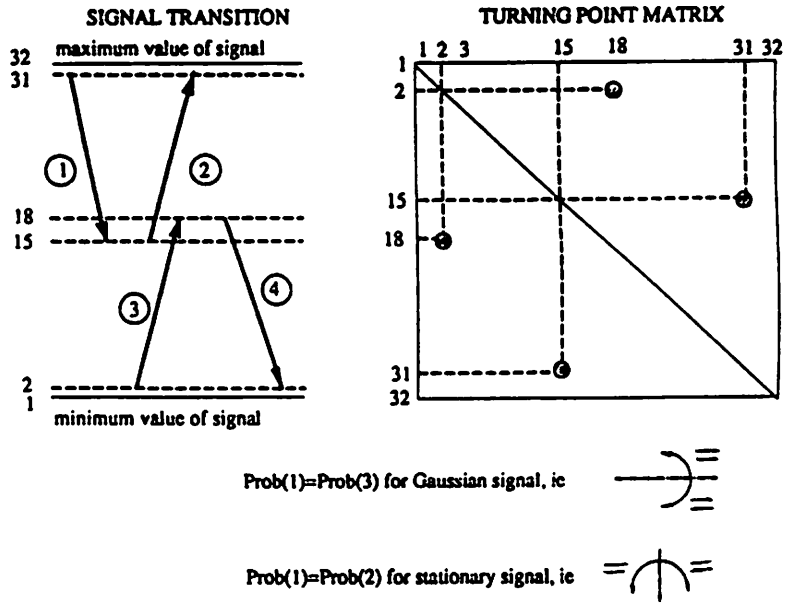

Fig 7. The assumptions of normality and stationarity which are used for the original Theoretical Solution

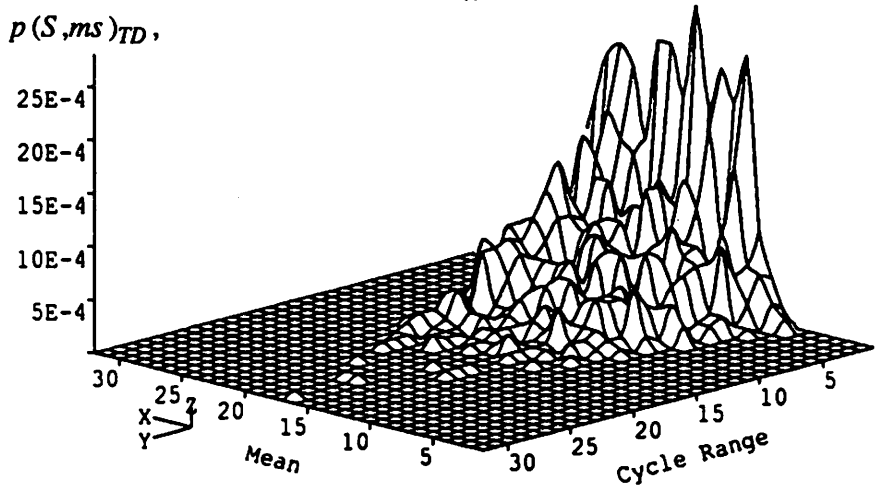

Fig 8(a). The joint pdf of rainflow ranges and means computed directly from the time sample of y27a

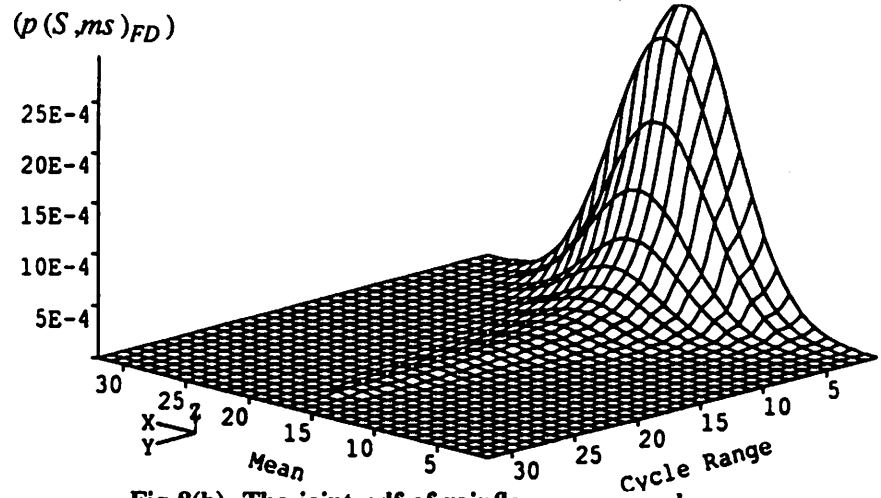

Fig 8(b). The joint pdf of rainflow ranges and means computed using the Theoretical Solution applied to y27a

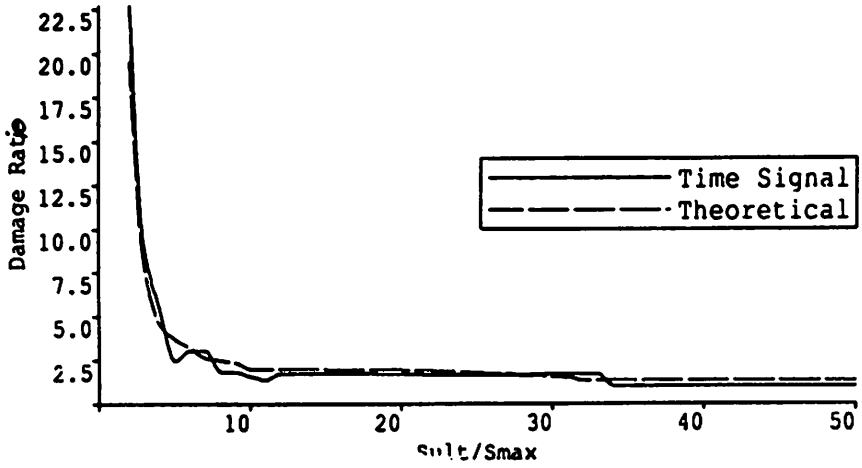

Fig 9. The effect on damage of different relative mean stress levels for y27a. Larger S_{ult}/S_{max} levels indicate a relatively lower mean stress level.

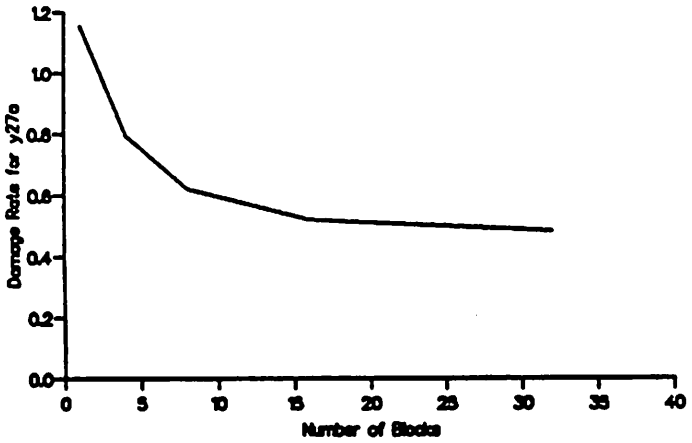

Fig 10(a). The effect of block length on average damage (using the time domain method) for y27a, normalised by the damage obtained directly from the whole time signal

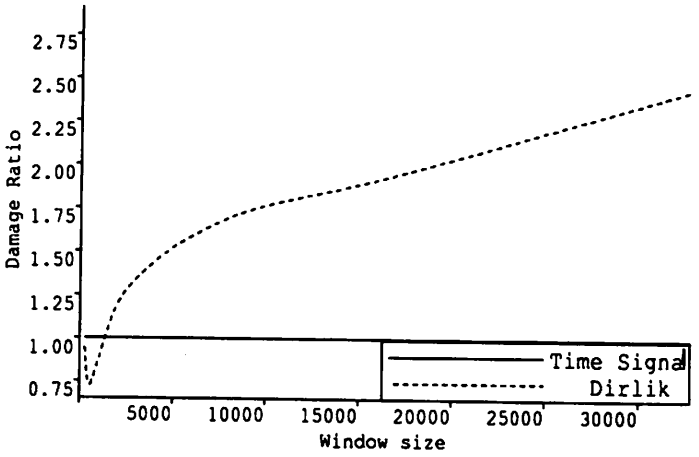

Fig 10(b). The effect of window size on average damage (using the frequency domain method) for y27a, normalised by the damage obtained directly from the whole time signal

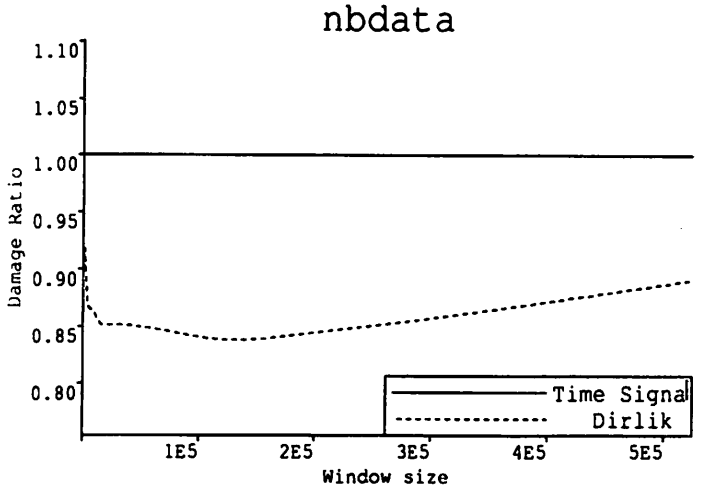

Fig 10(c). The effect of window size on average damage (using the frequency domain method) for a regenerated 'stationary', 'Gaussian' signal, normalised by the damage obtained directly from the whole time signal

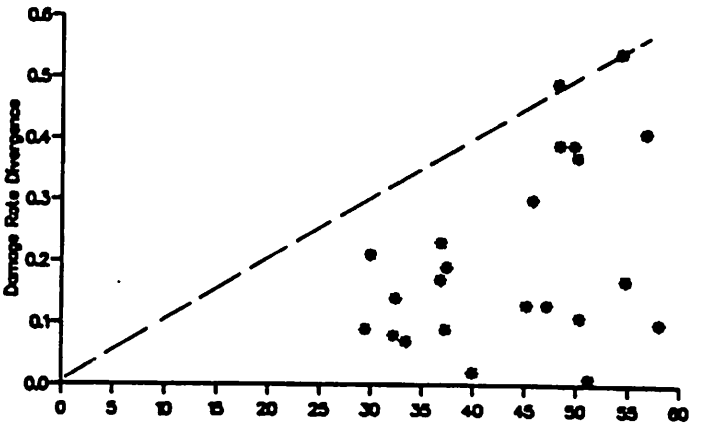

Fig 11. The damage rate divergence for the 24 MS1 load cases plotted against χ^2

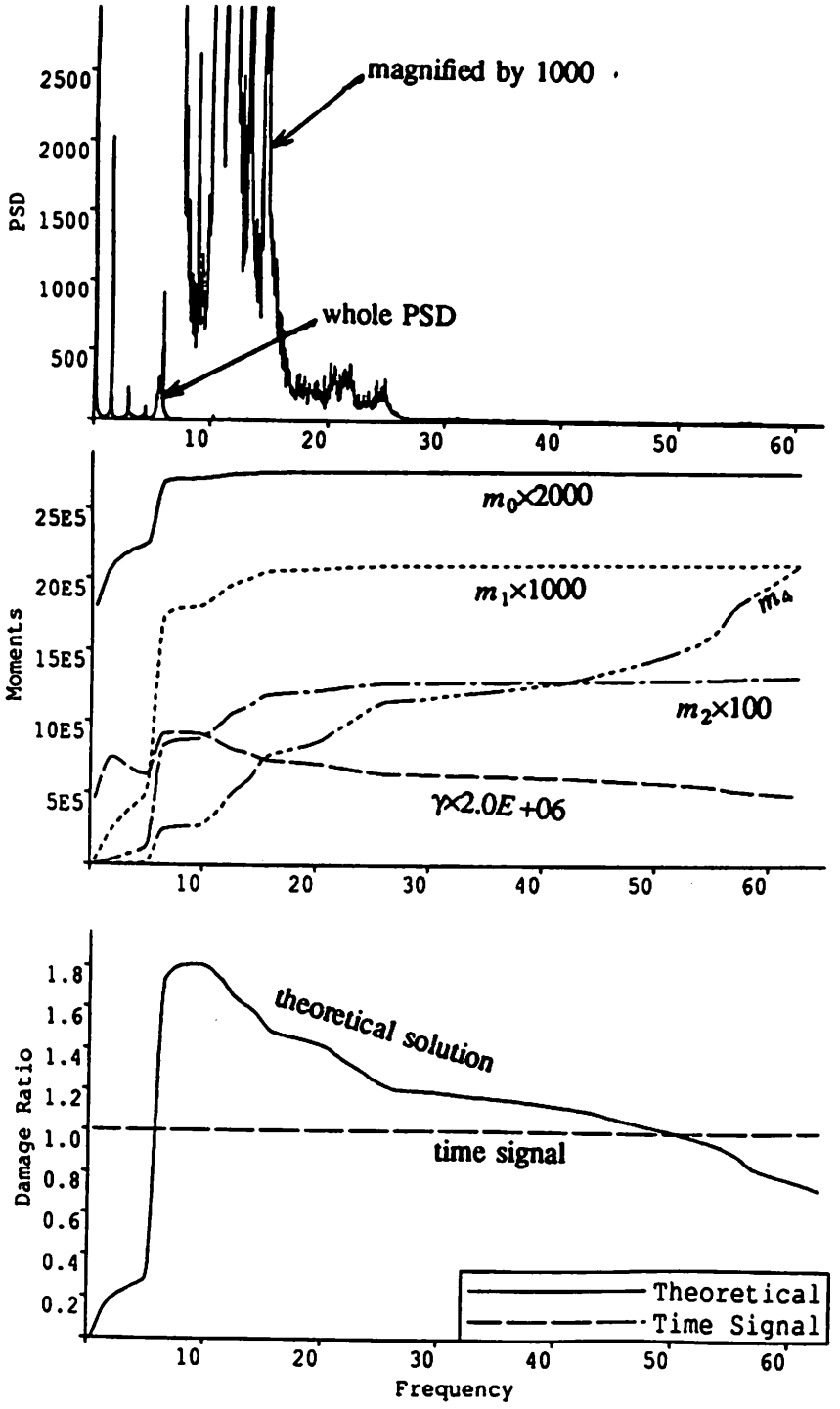

Fig 12. The variation of moments and damage with different cutoff points used for integrating the PSD plot.

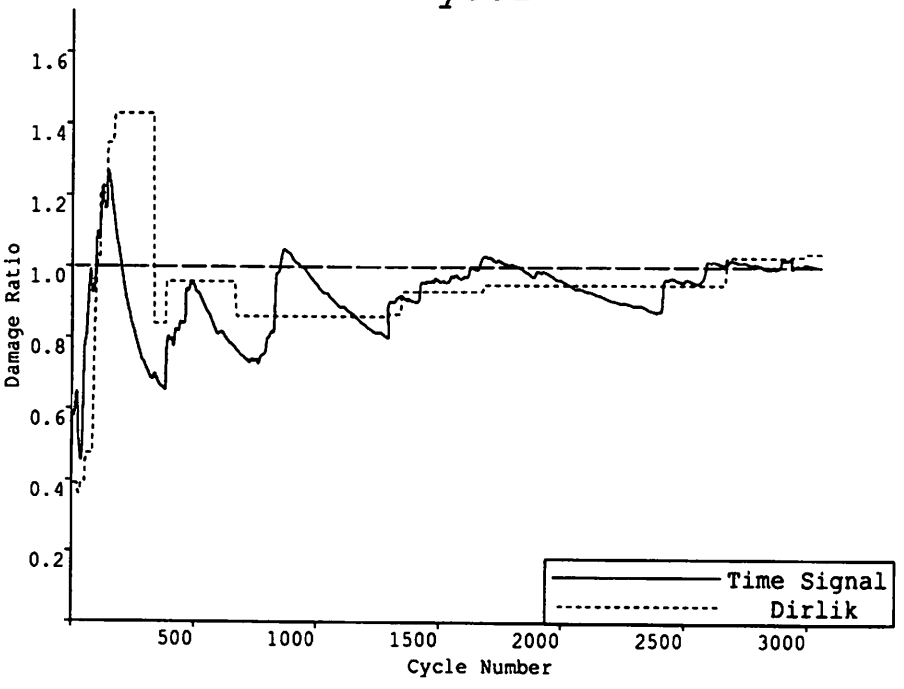

Fig 13. The variation of damage ratio plotted against increasing sample length.

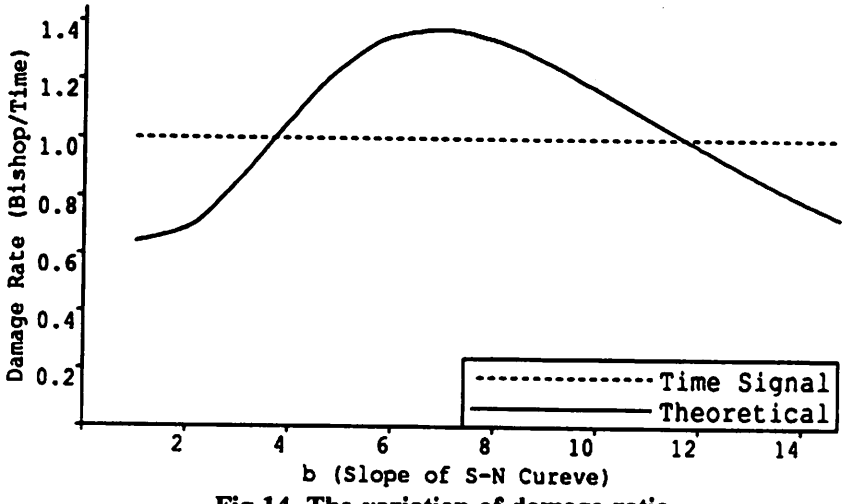

Fig 14. The variation of damage ratio plotted against S-N slope (b).

Extrapolation of Fatigue Loads

T. Haberle, T. Kramkowski, H. Sőker
Deutsches Windenergie-Institut

Presented at IEA Fatigue Experts Meeting
in Golden, Colorado

October 15-16, 1992

Introduction

When evaluating fatigue loads on a wind turbine a realistic estimation of its lifetime loads has to be found with the least effort. There are two alternatives: evaluation of time series of some minutes duration or on-line data reduction for several months with extrapolation to the intended lifetime in both cases. The uncertainty of the first method originates in the extreme extrapolation of time, while the second method is highly depending on the reliability of the measurement system.

DEWI is working on the verification of both methods. Time series measured at the DE-BRA 25 wind turbine are evaluated and new measurements using direct data reduction are performed.

Methodes of Fatigue Load Measurement

For the evaluation of fatigue loads on wind turbines two methods are proposed in the IEA recommendations [1].

The recommended method depends on measured time series of the loads at the rotor blade root, main shaft and tower. Measurements of some minutes duration characterize the loads of the modes of operation like start stop and emergency stop. For operational modes like power production, idling and yaw misalignment the loads are recorded in time series of 10 minutes duration and the power production mode is devided into wind speed intervals of 2 m/s additionally. For each mode of operation and wind speed interval at least three time series shall be collected, preferably at different turbulence conditions. With the statistics of mode of operation and wind speed for at least three months of automatic operation, the measured time series of the loads are extrapolated to the intended lifetime of the wind turbine.

Alternatively the fatigue loads can be evaluated by direct data reduction using the rainflow counting algorithm resulting in frequency matrices of load cycles. The measurement should

last for about 10% of the intended lifetime, to be representative. The evaluated frequency distributions are extrapolated linear to the intended lifetime as well, but the factor is about 1000 times smaller as with the time series extrapolation. This method is *not* recommended because of the following reasons.

Direct data reduction is highly depending on the reliability of the measurement system. Faulty Data can not be identified and removed.

Although the statistics for mode of operation and windspeed may be known for the measurement campaign it is very difficult to transfer the results to different wind conditions, because the relation to the measured load cycles is lost with direct data reduction.

If a wind turbine load has to be combined of measured load components this can only be done from measured time series, because the relation of the components is lost in the frequency matrices resulting from direct data reduction.

Description of Extrapolation Procedures

At DEWI a diploma thesis [2] was worked out, that deals with the extrapolation of time series in some detail.

When estimating fatigue loads from measured time series, a method is needed to extrapolate the frequency distribution resulting from the rainflow cycle counting with a sufficient accuracy. This is a main problem of the lifetime estimation, because no method is known up to now [3]. In the above mentioned diploma thesis the frequency distribution of the load cycles is extrapolated linear with and without previous statistical treatment. The resulting load spectra and fatigue damage are compared to show the influence of the different methods.

Time series of the flapwise and edgewise bending moments at the rotor blade root of the DEBRA 25 wind turbine were taken as a data base for the calculations. From this data the matrices, showing the frequency distributions of the load cycles for each mode of operation, were evaluated by rainflow counting. The matrices of the different operational modes are weighted according to the frequency distributions of the modes of operation and the wind speed, sumed up and extrapolated linear to one lifetime load spectrum.

Combining Method

For each mode of operation the individual time series are combined and evaluated by rainflow counting, Figure 1. The result is a frequency distribution of the load cycles in a matrix that represents the time of the measurement campaign. This matrix is extrapolated linear to the corresponding time of its operational mode to the intended lifetime.

Putting together the time series results in pseudo load cycles that did not take place in reality , Figure 2. Extrapolating some minutes measured to the intended lifetime increases this faulty load cycles (half cycles exactly) by the extrapolation factor. This results in about

10000 load cycles of accidental size in the lifetime load spectrum.

Statistical Method

The individual time series are evaluated for each mode of operation by rainflow cycle counting, Figure 3. In the following statistical analysis the mean value and standard deviation of each matrix element is calculated. To perform these calculations the matrices must represent the same measurement time and at least five individual matrices must be available. For a confidence factor of 99% two times the standard variation must be added to the mean value of each matrix element. Thus the number of the load cycles is clearly increased. It is assumed that the statistically analyzed matrix should contain as many load cycles as the sum of the matrices it was calculated from. For this purpose all matrix elements are multiplied by a scale factor. This considers the dependence of the sum of the load cycles on the duration of the measurement.

In the resulting matrix the elements are weighted depending on their variation. Elements showing large variation are emphasized and elements showing small variation are lowered, relative to their mean value. A redistribution of the frequency in favour of highly scattering load cycles takes place.

In the described procedure only already existing matrix elements are considered. Not any new elements with higher loads are created. This is a weakness of the method: with increasing duration of the measurement campaign the chance to record higher loads rises. It is assumed that the real lifetime load spectrum rises out of the time level like an iceberg out of the water, Figure 4. As the measurement duration rises so rise the recorded loads. The proposed method does not take account of this effect. A suitable method has to be found to extrapolate the number of the measured loads *and* their size.

For the development of a new method it is important to know the shape of the frequency distribution. In this first attempt it was assumed to be similar to the Gaussian type. This assumption will have to be approved.

Comparison of Fatigue Damage

For the fatigue damage calculation the lifetime load spectrum is converted to a range-mean type of matrix. The fatigue damage can be calculated then by means of the Palmgren-Miner linear damage rule in conjunction with material data for the GFRP-laminate used. The comparison of the calculated fatigue damage led to the following result:

The statistic method results in a 15% rise in fatigue damage compared to the combining method, that means a more conservative lifetime estimation. The effect is pronounced when the data base shows large variation. At least five time series should be measured for each mode of operation. A wide data base leads to less conservative results from the proposed statistical method.

Summary

The application of the proposed statistic method on the fatigue loads measured on a wind turbine can be an important factor for the estimated lifetime. This originates in the increased variation of rare load cycles measured in time series of some minutes duration. The method leads to a more conservative result for the estimated lifetime. To get a wider data base for the extrapolation of the fatigue loads the minimum number of time series measured per mode of operation and wind bin should be increased. Instead of three time series at least five should be demanded to get a statistically approved result. In further research work on the relation between fatigue loads extrapolated from short time series and such taken from long-time measurements, direct data reduction could be a useful tool despite of its disadvantages.

References

[1] P. H. Madsen e. a. *Recommended Practices for Wind Turbine Testing, 3. Fatigue Loads*, IEA, 2. Edition 1990.

[2] Till Haberle *Lebensdauerabschätzung an GFK-Rotorblättern für Windkraftanlagen auf der Basis von extrapolierten Lastkollektiven*, Lehrstuhl für Leichtbau, Technische Universität Műnchen, 1992

[3] Otto Buxbaum *Betriebsfestigkeit*, Verlag Stahleisen mbH, Düsseldorf, 1992

Figures

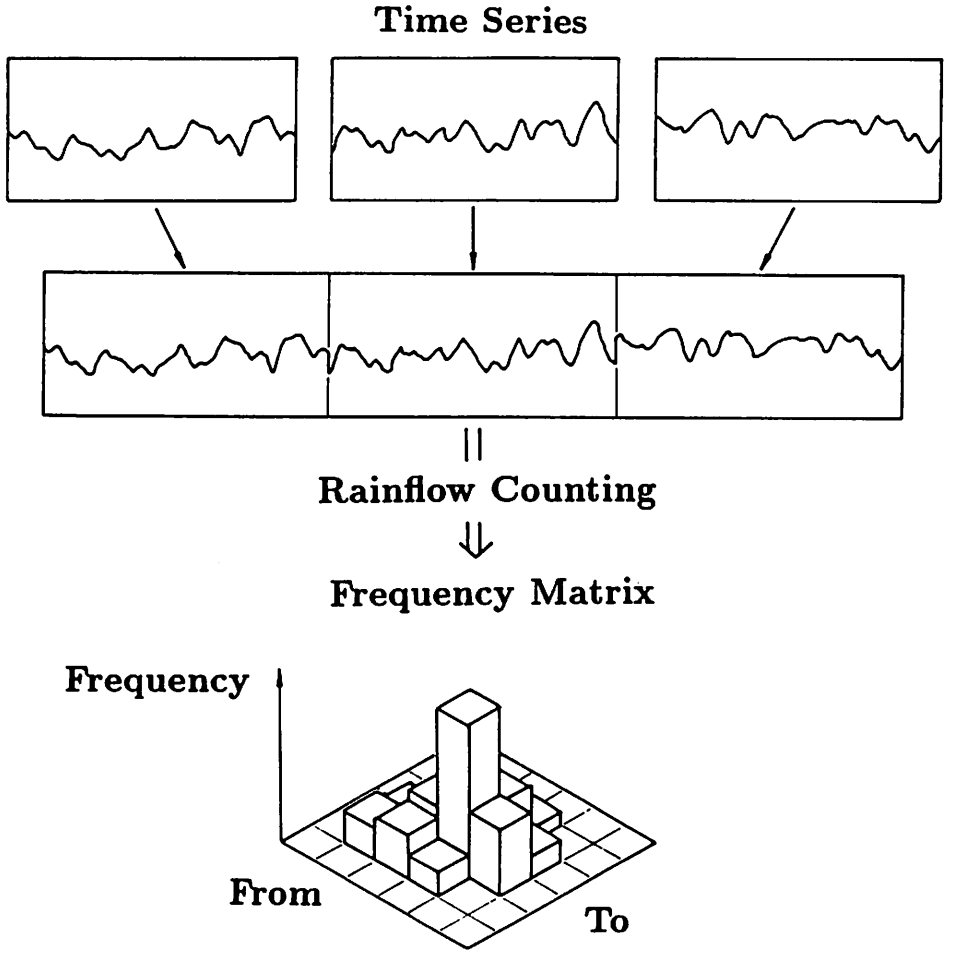

Figure 1: Combining Method

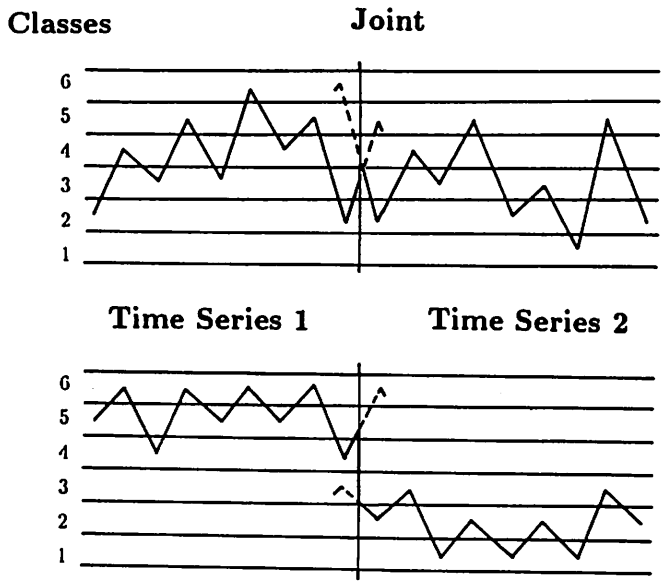

Figure 2: Generation of Pseudo Load Cycles

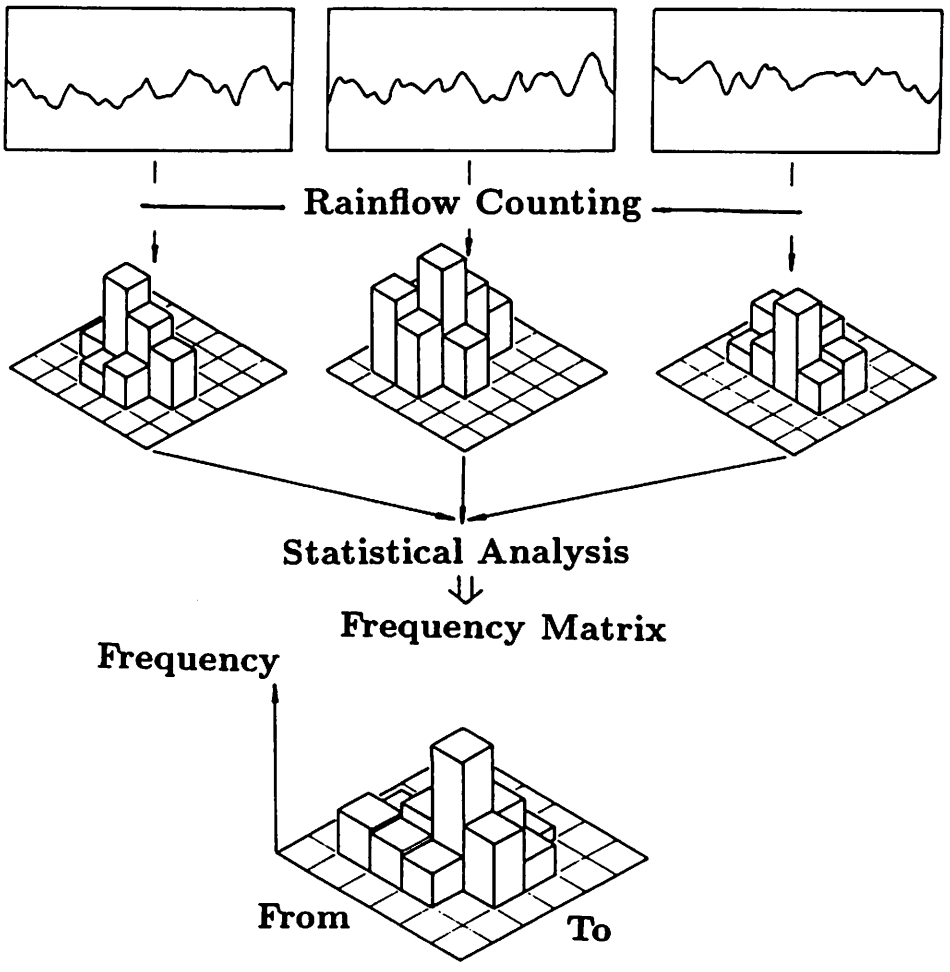

Figure 3: Statistical Method

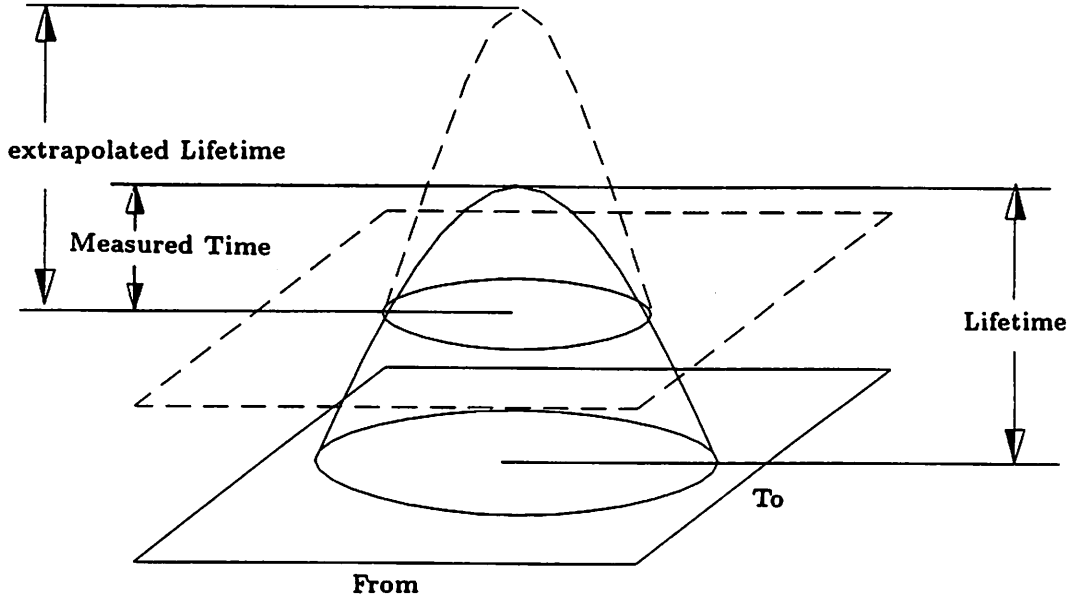

Figure 4: Iceberg Model of Lifetime Load Spectra

IEA Fatigue Expert Meeting
October 15–16, 1992
NREL, Golden Colorado, USA

The Strength and FATigue of large size Wind Turbine Rotors (SFAT) project

B.H. Bulder & H.J. van Grol
Netherlands Energy Research Foundation ECN
Unit Renewable Energies
P.O. Box 1, 1755 ZG Petten

October 1992

1 INTRODUCTION

If we want that wind energy will contribute to a greater extend to the electricity production in the future, the cost of one produced kWh has to be reduced. This can be achieved by a reduction in cost of a machine and the improvement of the (mechanical) reliability. Machines may become cheaper through system optimization and series manufacturing while reliability may be improved by thorough fatigue life analysis in the design phase.

One of the major cost factors of a wind turbine is among others the rotor. A sensible method of making turbine rotors cheaper is done by making them lighter [1]. This off course can't be done without increasing the effort put into the design. The optimization of a rotor can only be paid off when many items of one product are made. To prevent a rotor blade against early collapse, whether it be caused by a shortage of strength or reliability, is installed in great numbers, it is necessary to check the design by an approval test. Because the fatigue life analysis is still quite unrealiable [2], a specimen tested in laboratory conditions will fail quite often by Miner summations between 0.25 and 4 for constant amplitude test and between 0.6 and 1.6 for variable amplitude test. One method, and maybe the only method, to proof reliability and durability of the design can be done by performing a full scale strength and fatigue test. These test might also b required in future by the certification authorities to get a certificate.

Within the JOULE–II programme ECN proposed a project together with a number of European partners (see table 1) to investigate some aspects of full scale testing of rotor blades.

Table 1: The partners within the SFAT project

- Centro de Investigaciones Energeticas Medioambientales y Technologicas (CIEMAT)	[ES]
- Netherlands Energy Research Foundation (ECN)	[NL]
- Germanische Lloyd (GL)	[DE]
- Risø National Laboratories (RNL)	[DK]
- Stork Product Engineering (SPE)	[NL]
- Teknik Gruppen AB (TA)	[SE]

During this project many aspects of how to perform a fatigue and strength test on a full scale rotor blade will be assessed. Some of these aspects are:

- determination of design load spectrum, see also results of previous JOULE–I project REFSTRESS [3];
- determine technical criteria to what extend the different loading conditions and loads have to be taken into account for the fatigue load spectrum;
- determination of material properties (being not a main activity in this project but will be dealt with in a separate JOULE–II project[1]);
- determination of test procedures;

[1] Development of Advanced Blades for Integration into Wind Turbine Systems

2 OBJECTIVE OF THE PROJECT

The objective of the project consists of the following subjects:

- Determine requirements:
  - which or how many loads are to be simulated (number of cross-sections and which load per cross-section);
  - which material coupon tests are required to determine the fatigue test spectrum;
- Determine procedures :
  - how to perform a strength test;
  - how to perform a dynamic properties test;
  - how to perform a fatigue test;
  - how to make a test spectrum from a design load spectrum;
- Cost and benefit of strength and fatigue tests;
- Make recommendation for certification institutes.

3 DESCRIPTION OF ACTIVITIES

The following main activities are performed during the project:

- Establishment of procedures and criteria;
- Coupon test;
- Determination of design load spectrum;
- Determination of stress distribution,
  - static (strength) including stress reserve factors;
  - fatigue including fatigue stress reserve factors;
- Determination of fatigue test spectrum;
- Supply of rotor blade test specimen;
- Static strength tests;
- Dynamic properties tests;
- Fatigue test;
- Cost and benefit analysis;
- Evaluation.

4 SHARING OF TASK

The division of task among the participants is shown in table 2. ECN performs the project management.

Table 2: The task division

Participant	GL	CIE-MAT	ECN	RNL	SPE	TA
Procedures and criteria	+	(+)	+	+	(+)	(+)
Test specimen	Supplied by industrial partner					
Actual loads	-	+	+	+	-	+
Stress distr. and SRF, FRF	-	+	+	-	-	+
Fatigue test spectrum	-	(+)	+	+	-	+
Coupon test	performed by other JOULE project					
Dynamic test	-	+	-	-	-	-
and strength test	-	+	-	-	-	-
Fatigue test	-	-	+	-	-	-
Cost & benefit	-	-	(+)	-	+	+
Evaluation	+	+	+	+	+	+

(+) means a limited effort for the participant.

5 WORK PROCEDURE

5.1 Establishment of procedures and criteria

The following questions will be addressed as part of the SFAT procedures and criteria:

1. Should strength and fatigue test be performed and if so how are these test to be implemented and described within the frame work of wind turbine certification:
   - nominal strength test;

- ultimate strength test;
- failure strength test.

2. Ibid but now with regard to dynamic properties tests.
3. Ibid but now with regard to fatigue test.

5.2 Design load spectrum

A present ongoing JOULE–I project, REFSTRESS, is, among others, aimed at the establishment to what accuracy design load spectra and in particularly design life predictions can be calculated. A typical (preliminary) result, is shown in figure 1, showing the cumulative load range spectrum of the flatwise moment calculated by all participants. This spectrum covers only the normal design load case: energy production. The differences as shown are quite large certainly the first 10^4 cycles differ quite a lot. A good reason for this is that the curves N and S are the results of participants using a turbulence model including more extreme wind conditions than the other participants. Line I probably differs from the majority because they calculated the flatwise moment instead of the flapwise moment (chord direction – rotor plane).

5.3 Tests

5.3.1 Strength tests

In order to perform a limited number of meaningful strength test the following procedure might be performed. For say 5 cross-sections the critical load conditions are to be determined. A critical load condition can be expressed as that load condition which yields the lowest strength reserve factor (SRF), defined as

$$\mathrm{SRF} = \frac{\overline{\sigma}}{\sigma_{\mathrm{eff}}}.$$

In which

$\overline{\sigma}$: allowable stress;

σ_{eff} : effective stress.

It is expected that for each station different load combinations are critical, as along the concerned cross-sections the SRF values vary.

5.3.2 Dynamic tests

The dynamic tests will be performed to determine natural frequencies of the blade. To check the accuracy of the calculated natural frequencies and the aero - elastic model used to calculate the design load spectrum. As a basis the auto power spectral densities of the bending moments at the blade root will be used to determine the natural frequencies.

5.3.3 Fatigue test

The test load spectrum will be quite different from the design load spectrum because the design load spectrum consists of to many cycle for the test. The actual (design) load spectrum consist of 10^9 cycles in 25 years compared to a test spectrum of 2. or 3.10^6 cycles. The difference in number of cycles is a factor of 50. The number of cycles can be reduced by assuming an omission level (leaving the very low amplitude cycles out of the test spectrum). Increasing the loads with a Test Load Factor (TLF) in such a manner that at the concerned cross-sections the critical positions are subjected to the same damage as determined in the design analysis. A truncation level (cut off at high load range) might be applied because for metal structures the high ranges with a low probability of occurence might influence the test favourably and for composite structure the damage mode might be influenced unfavourable.

The need for accurate data of the material properties is of course critical in this part of the project. The data of coupon test will come from the already mentioned project concerned advanced blade materials.

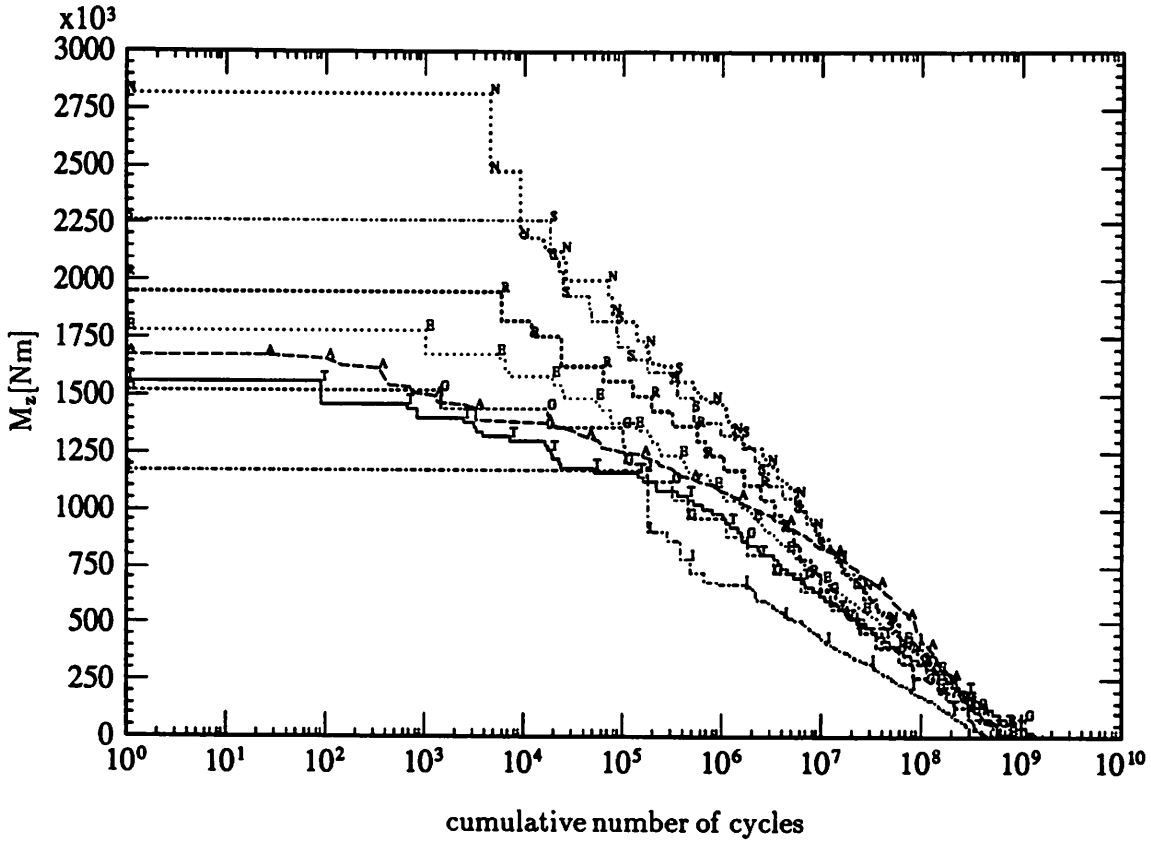

Figure 1: LOAD RANGE SPECTRUM OF THE FLATWISE MOMENT

6 OUTPUT AND RESULTS

The results aimed at are the following:

- recommendation on the procedures to perform full scale tests on large rotor blades;
- establishment of representative full scale static load tests
- establishment of representative dynamic tests;
- establishment of representative full scale fatigue tests, including the rationale on the performance of coupon test;

7 RELATED SUBJECTS OF THE PROJECT

The following subjects are still short of sufficient knowledge:

- Ultra high cycle data ($\geq 10^8$ cycles), to check design spectrum with test spectrum;
- Fatigue damage monitoring techniques.

References

[1] Snel H., Th. van Holten, and F. Fölings. "Study on the Next Generation of Large Wind Turbines.". In *Procedings of an International conference held at Madrid 10 – 14 September 1990*, pages 428 – 432, September 1990.

[2] Collins, J.A. *Failure of materials in mechanical design. Analyses - Prediction - Prevention.* John Wiley & Sons, 1981.

[3] Van Grol, H.J. and B.H. Bulder. "The REFSTRESS final report ". CR to be issued, ECN, 1992/93.

IEA - Workshop on Fatigue of Wind Turbines
NREL, Golden, Colorado, USA, 15-16th October 1992

NON-DESTRUCTIVE INSPECTION AND EVALUATION

Infra red condition monitoring of different joint geometry samples subjected to reversed (R=-1) fatigue loading.

I P BOND, C L HACKER, M P ANSELL
University of Bath, UK
A G DUTTON
Rutherford Appleton Laboratory, UK

The study of damage mechanisms in materials is often a difficult and complicated one. This is particularly so in the case of wood with its 3-D cellular structure and its distinct characteristic failure modes.

The use of wood/epoxy laminates in the construction of rotor blades for large scale commercial wind turbine generators (with rotor diameters up to 40m) has led to the need for a method of monitoring and understanding the various physical processes which occur in these blades during service. These blades are subjected to a complex combination of fatigue loading, the consequences of which are difficult to ascertain with regard to the structural integrity of the blade during its lifetime.

When a composite structure undergoes fatigue, heat is generated due to hysteresis and friction effects. This heat generation is likely to be related to the degree of damage in the composite. The surface manifestation of this heat can be detected using an infra red camera and analysed to give information about the underlying flaw.

Axial fatigue testing was carried out under load control on a Mayes 200kN servo-hydraulic test machine. Reversed or "R=-1" (R=min stress/max stress) loading was used as it is the most demanding condition to impose upon wood laminates. Different peak stress levels were used during the test of a sample, starting at one well below the static failure stress of the sample and increasing to consecutively higher levels once the temperature had stabilized, as indicated by the infra red thermographic image (i.e about 45-60 minutes). This accelerated fatigue testing was used to ensure that failure would occur after a relatively short number of cycles, thereby maximizing the number of tests that could be carried out over a two day period.

The four samples tested were all wood/epoxy/GRP composites consisting of 4mm

rotary cut *Khaya ivorensis* laid five ply thick using an epoxy adhesive and having a layer of +/- 45° woven glass fibre reinforced epoxy over the two outer joints and unidirectional glass fibre reinforced epoxy as an outer surface layer. All contained various joint geometries, representative of those likely to be found in commercial blades, e.g. scarfs, butts and imperfect joints.

Figure 1 is a schematic of a four scarf jointed sample, indicating the path along which failure occurred. Figure 2 is an I.R.T. image of the same sample at a point during fatigue testing when the peak stress had just been raised to 35MPa. A 'hot-spot' (temp. approx. 34°C) is clealy visible at the left hand side, lower, outer scarf joint.. Figure 3 is another I.R.T. image of the same sample but at a point just as failure occurred. This time the highest temperature region is over the left hand side, upper, inner scarf joint which showed a rapid increase in temperature after the peak stress level was raised to 35MPa. This joint region was the initiation site for failure.

Localised heat build-up in the form of 'hot-spots' occurred at joints in all the samples during fatigue testing with temperatures of 50°C-plus being observed at the onset of failure. The location of the highest temperature region indicated the joint at which failure would initiate. Different damage processes were competing during cyclic loading, an implication made by the movement of the 'hottest-spot' from joint to joint as damage mechanisms activated and became dominant upon the alteration of peak stress levels during testing.

Once a quantitative link has been established between the temperature increase and the corresponding damage seen by the wood, the effective "mapping of damage location and occurrence" will be very helpful in verifying and developing life prediction methods in addition to acting as a very good method of condition monitoring.

References

Infra Red Condition Monitoring of Wind Turbine Blade Fatigue Tests;
Dutton, A.G.; Irving, A.D.; Lipman, N.H.; Clayton, B.R.; Aftab, N.; Bond, L.J.. (1992). *Proc. of the 14th BWEA Wind Energy Conference - Wind Energy Conversion-1992.*, Ed. Clayton, B., Mechanical Engineering Publications., pp. 221-228.

Fatigue Testing of Wood Composites for Aerogenerator Blades. Part VII. Alternative Wood Species and Joints;
Bonfield, P.W.; Bond, I.P.; Hacker, C.L.; Ansell, M.P. (1992). *Proc. of the 14th BWEA Wind Energy Conference - Wind Energy Conversion-1992.*, Ed. Clayton, B., Mechanical Engineering Publications., pp. 243-249.

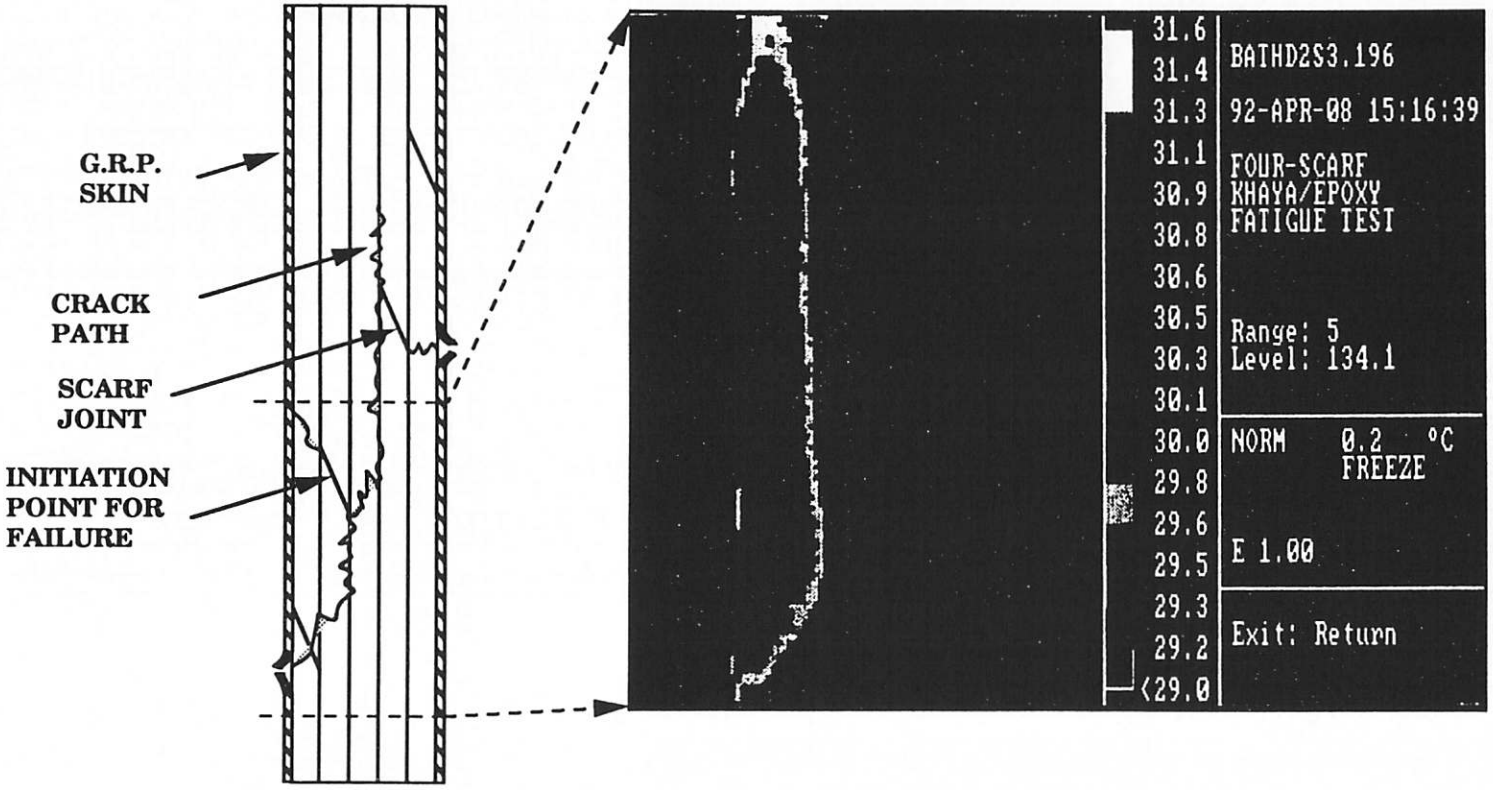

Figure 1 - Schematic of four scarf jointed sample indicating failure path.

Figure 2 - Infra red thermographic image of four scarf sample during testing.

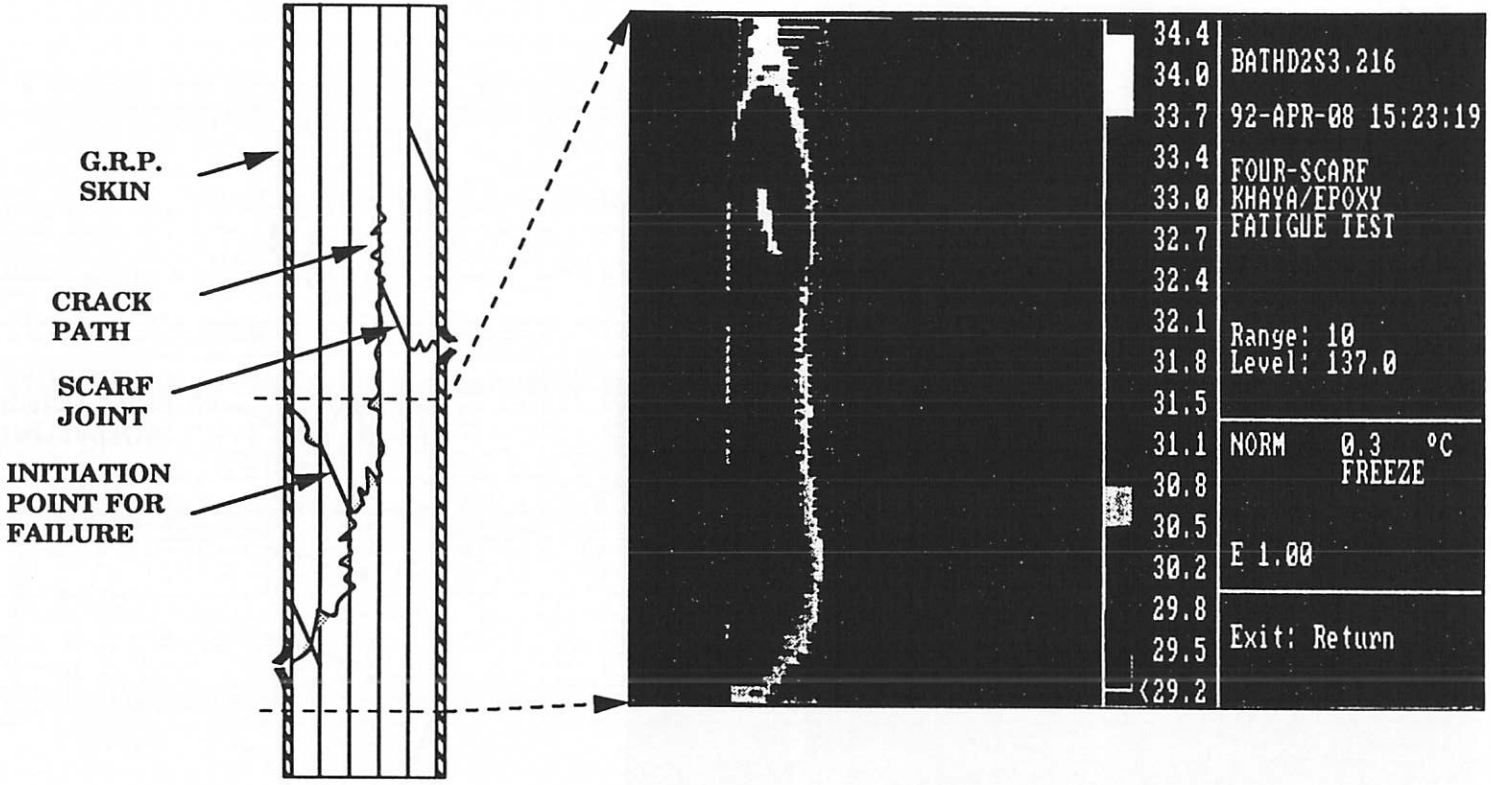

Figure 1 - Schematic of four scarf jointed sample indicating failure path.

Figure 3 - Infra red thermographic image of four scarf sample at a point just before failure.

Bengt Göransson
Kvaerner Turbin AB
Box 1005
S-681 29 Kristinehamn Tel: +46 550 848 44
Sweden. Fax: +46 550 189 98

EXPERIENCE FROM TESTING AND INSPECTION OF LARGE WIND TURBINE BLADES IN SWEDEN.

Presented at IEA Expert Meeting on Fatigue, Golden, Colorado 1992-10-15 — 16.

My acknowledgement to the FFA, Stockholm, Sweden who sponsered my trip.

Summary

This presentation givs a short review of the experience from the operation of the large Swedish wind turbine prototypes. First the inspection procedures and results from the two machines Näsudden I and Maglarp are described. Then there is a presentation of the new blade development of the new turbine Näsudden II.

The most important conclusion is that despite recent inspection and tracking techniques, suitable for large blades, the risk of missing severe damage is high. To cope with that the blades have to be fail safe designed, making it possible to detect imperfections more easily before they grow to a critical size.

Introduction

The development of wind energy in Sweden has to a great deal been in the field of very large machines (2 - 3 MW). It started in 1979 with orders for two turbines, Näsudden (I) and Maglarp. Kvaerner Turbin AB was the manufacturer of Näsudden under the former name of Kamewa. Blade development and manufacture was carried out by MBB of Germany. The Maglarp unit was delivered by Karlskrona-varvet whereas the blades were made by Hamilton Standard of the USA.

Näsudden was caracterized as a stiff concept with two blades, rigid hub, induction generator and a stiff concrete tower. Maglarp, on the other hand, is weak with two blades, teetered hub, soft drivetrain and a soft tower.

Both machines had constant rotor speed. The goal was to gain knowledge from two different designs for future development.

Experiencies from Inspection of Blades.

1. Näsudden I.

Blade data: length: 35.5 m
weight: 21 ton
material: welded steel

The blade consists of a welded steel spar with leading edge as a glass fibre/epoxy shell and the trailing edge as a glass fibre/epoxy/foam sandwich. These sections were screwed on to the steel box and all three parts form the aerodynamic profile.

Blades were manufactured under very high quality demands. They were dimensioned, mainly for fatigue, according to the old Swedish welding code StBk-N2.

Calculated strain, deformations and eigenfrequencies were verified at workshop tests.

The demand of 30 years life was not fully met for the blades and therefore it was decided to do regular inspections during operation. Inspection intervals were decided after crack propagation calculations. Visual and US-inspection technique was used. After a few thousand hours two small cracks originating from holes were found and repaired.

After 11400 h of operation a large crack was detected "acoustically", during an inching maneuvre, i e outside the inspection programme. The crack at R=6750 mm was covering almost 50% of the circumference. It was calculated that an 80 mm crack was missed at last visual inspection and a 2 mm crack was missed at the last US-inspection, which is not very unrealistic.

The crack was succesfully repaired meanwhile the discussion of how to carry on gave new inspection intervals for adequate safety:
- 1000 h for fillet welds
- 500 h for butt welds + holes.

This killed future operation of the machine as the maintenance costs became too high. It was decided to put the machine into a non-operative state and to use it only for demonstration. A few months later the decision was taken to scrap the machinery and to use the old tower for the new Näsudden II.

Conclusion: Despite inspection procedures a critical crack could not be detected. Safe procedures were found to be impossible to realize economically. The machine was shut down.

2. Maglarp.

Blade data: length: 37 m
weight: 13.5 ton
material: glass fibre/epoxy

Blades were manufactured with transverse filament winding technique using glass fibre roving/epoxy. The blade is built up from a D-spar and an aerodynamic shell for the trailing edge. To improve the surfasce finish a last layer of 90° fibre was wound on the mandrel and this has later caused problems as the longitudinal strength was too low.

Inspection includes search for delaminations, erosion damage and lightning strikes. L-profile at spar/shell connection and transition steel flange/GRP were tested thoroughly. Tap testing is mainly used but the steel flange has been tested with ultrasonics without any real success. Other areas have been covered visually and with tap testing. Four mandays/year have been the average time needed.

Inspection intervals were determined without theoretical investigation as crack propagation theory or similar for the laminate is unknown.

Cracks and delaminmations in the trailing edge have been repaired when necessary.

Conclusion: Visual annual inspections have protected the blades from critical damage. The drawback is the inexactness of the method. It can also be time consuming.

To get continuity in the development of wind energy two new design projects were decided in the late 1980s. One project is to design and build a totally new soft concept of 400 kW which has been developed by Nordic Windpower AB of Sweden. The other line is to continue the development of large machines with a new 3 MW machine manufactured by Kvaerner. This WTS is called Näsudden II. A sister unit is built in Germany, named Aeolus II.

3. Näsudden II

Blade data: length: 39 m
weight: 9 ton
material: carbon/glass fibre/epoxy, PVC-foam

Before the Aeolus II blades were built a full scale section of the root part was manufactured to be able to learn about the technique of wet hand layed-up CRP/GRP into a steel mould. As a separate task the laminate was equipped with "delaminations" i e teflon tape pieces bonded into the laminate at certain positions. At US-tests later, neither the errors nor the lower side of the laminate (both CRP and GRP) could be detected. Both reflection and transmission technique was evaluated.

Conclusion: US-technique can not be used for searching damages in fibre laminates without very large difficulties and complications.

The Näsudden II blade consists of three parts: upper and lower halves and one leading edge section. Carbon fibre stripes are put longitudinally to take flap and edge bending loads. Glass fibre laminate and sandwich is used for torsional loads. PVC-foam is used as webs to prevent from buckling.

At manufacturing the 1st blade was equipped with several strain gauges. Deflection line was measured at load and compared with theoretical model. Strain was measured and checked with allowed strain. Weight, centre of gravity and 1st and 2nd bending eigenfrequencies were also measured. The applied load is 1.2 - 1.3 times the dimensioning load case.

For the next three blades no strain gauges were applied. The deflection lines and the frequencies were measured and compared with the 1st blade.

Conclusion: This is probably a sufficient way of testing at delivery. Maybe it can also be used for testing the condition of the blade later. Loading condition shall preferably reflect real maximum loading. This of course requires using the same test rig as at workmanship test.

4. Overall conclusions.

- Visual inspection including tap testing of limited areas is quite easy to implement but is very inexact and can be time consuming.
- US-inspection or other surveyor techniques are very time intensive for large blades. Can be used for very small areas.
- Reference deflection line and eigenfrequency measurements can be used for follow up of blade properties but cannot detect single cracks.
- Blades shall be designed fail safe in a way that visual inspection can be used and cracks can be allowed for some time without detection.

5. List of Viewgraphs.

1. Blade design of Näsudden I
2. Crack near blad root, Näsudden I
3. Blade design of Maglarp
4. Inspection at Maglarp from special wire suspended platform
5. Blade design of Näsudden II
6. Teflon coupong for US-test of CRP/GRP laminate
7. Test rig at full scale test of Näsudden II blade
8. Conclusions
9. Recent development of large wind turbines: Aeolus II in Wilhelmshaven, Germany. Erected in August 1992.
10. Aeolus II: The nacelle is tilted on to the tower top.

WTS 75 BLADE

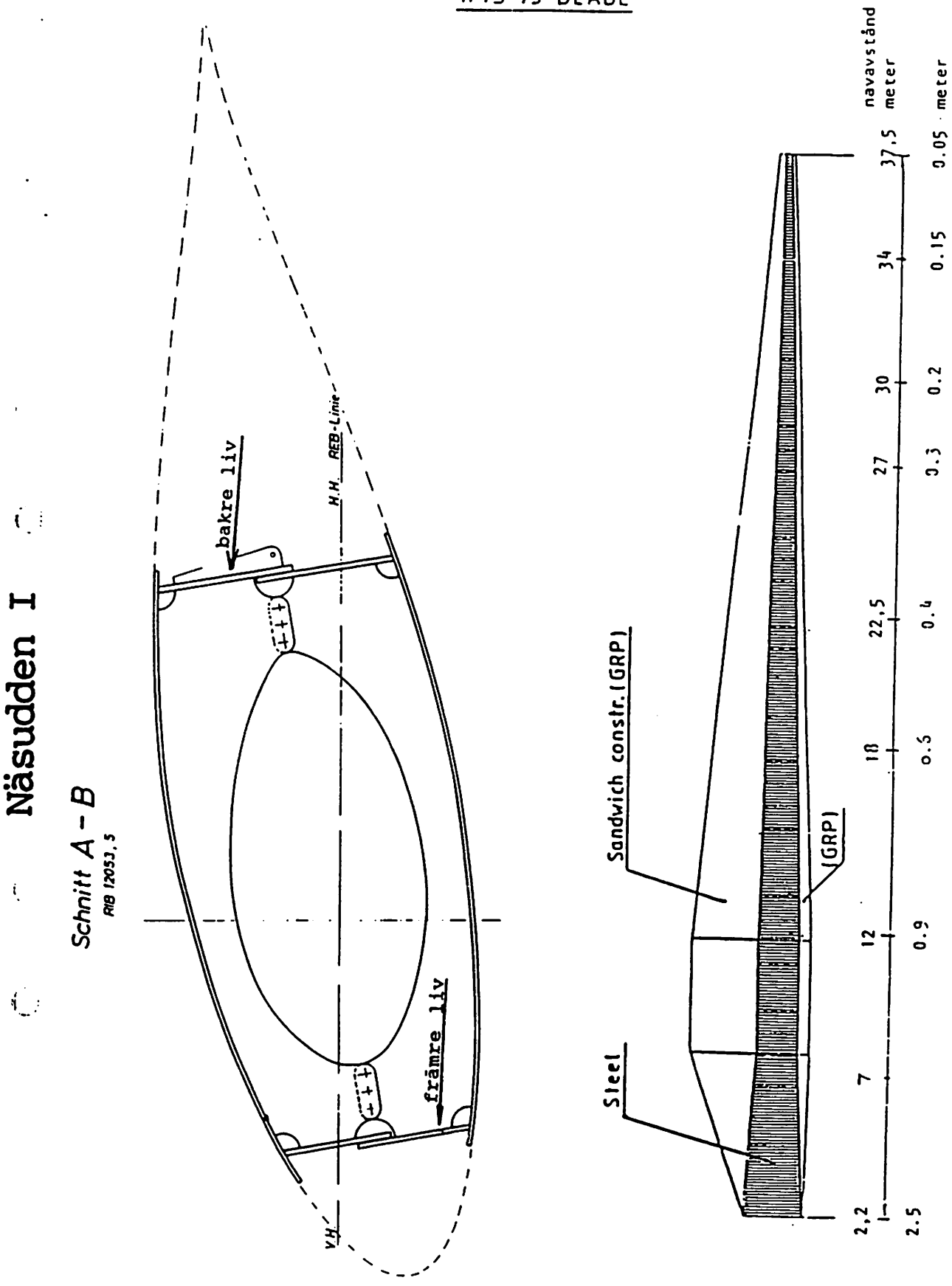

Figur 2. Bladutformning Näsudden.

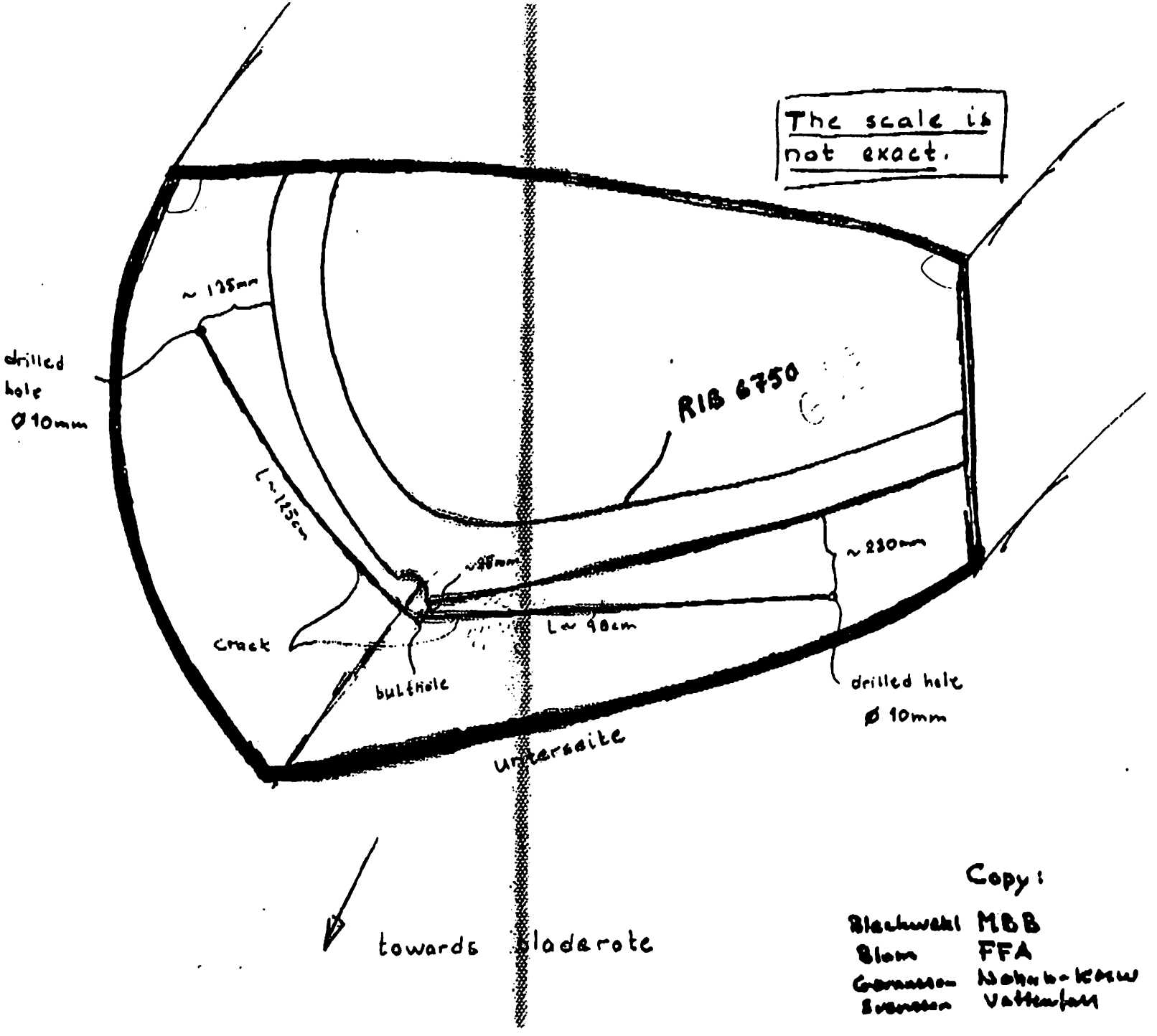

Copy:

Blackwell MBB
Blom FFA
Gamesa Nohab-Kaaw
Svenska Vattenfall

(2)

Bild 100-1
Underhåll

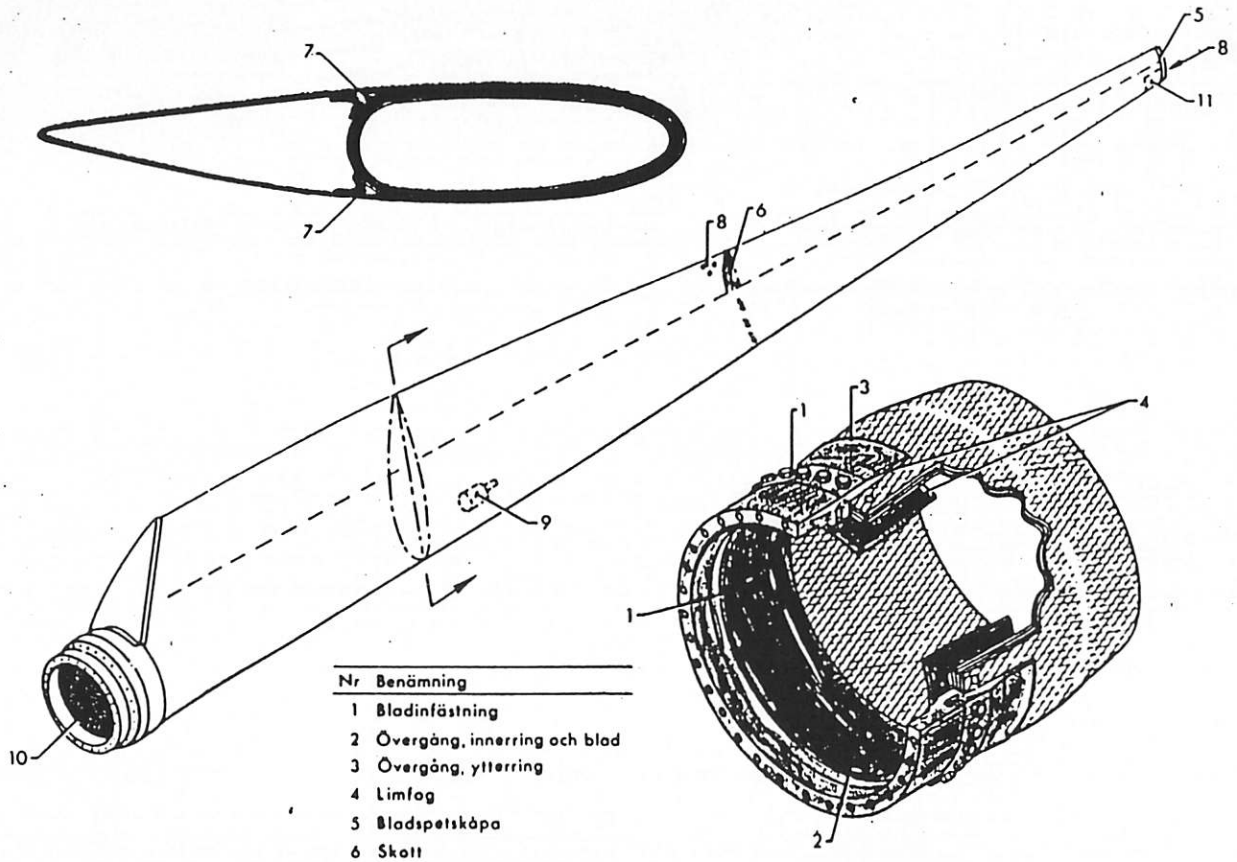

Nr	Benämning
1	Bladinfästning
2	Övergång, innerring och blad
3	Övergång, ytterring
4	Limfog
5	Bladspetskåpa
6	Skott
7	Övergång mellan bladbalk och bladprofil
8	Dräneringshål
9	Isdetektor
10	Fallskydd
11	Balanseringsvikt

KARLSKRONA VARVET AB
KARLSKRONA Sweden

WTS 3
Rotorblad

4

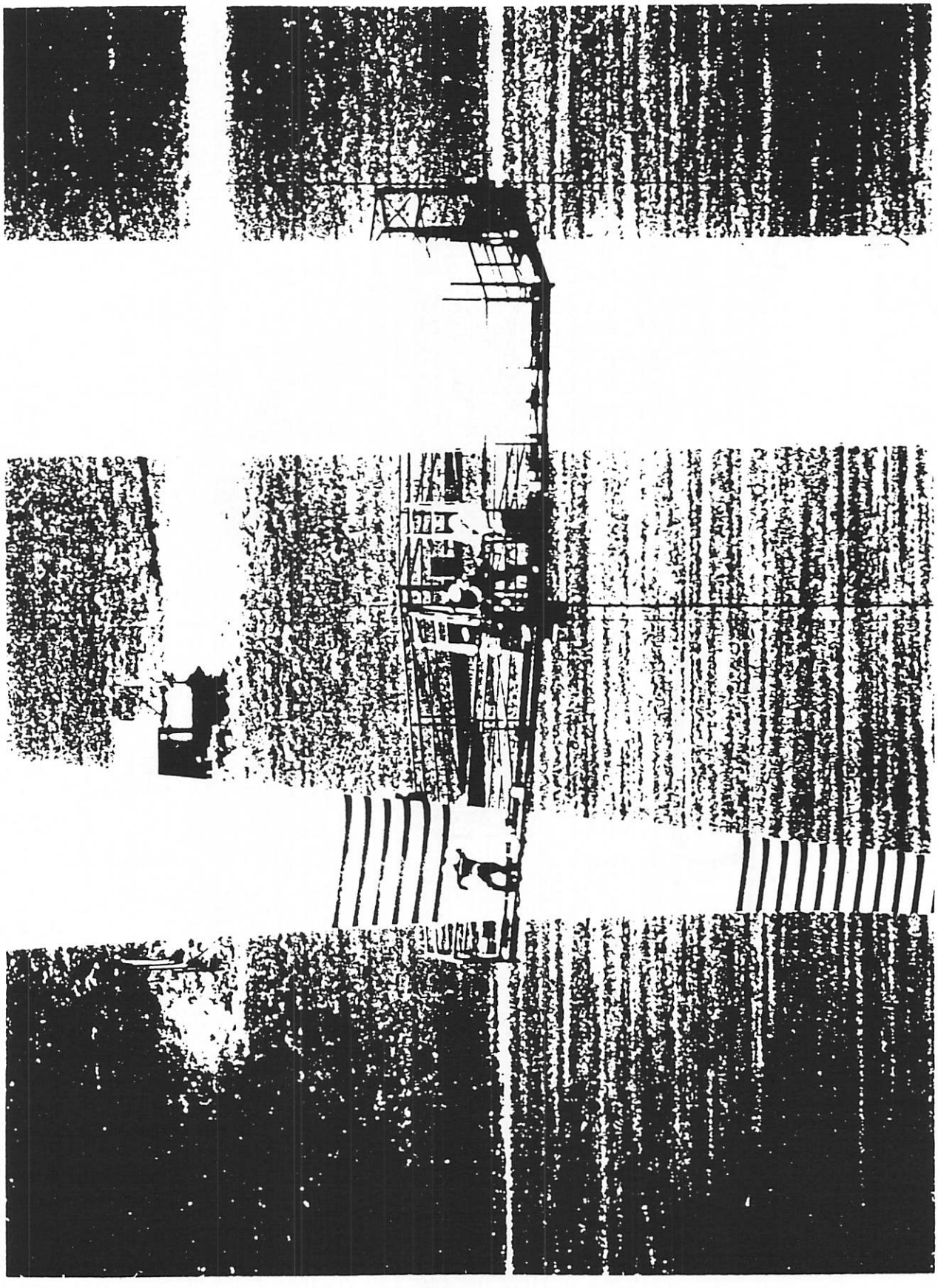

Näsudden II

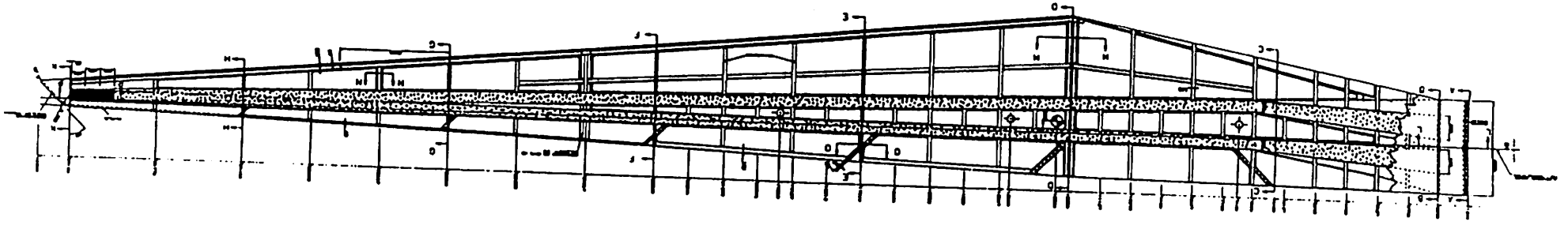

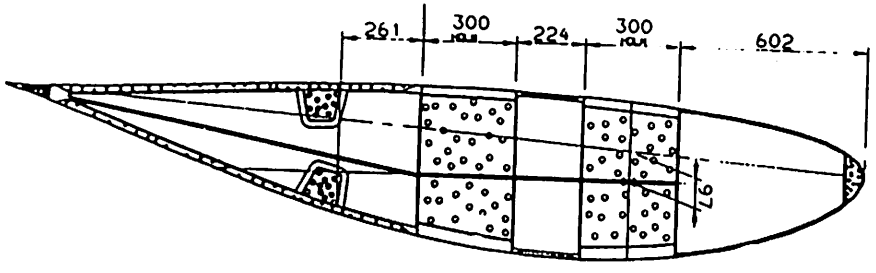

(6.)

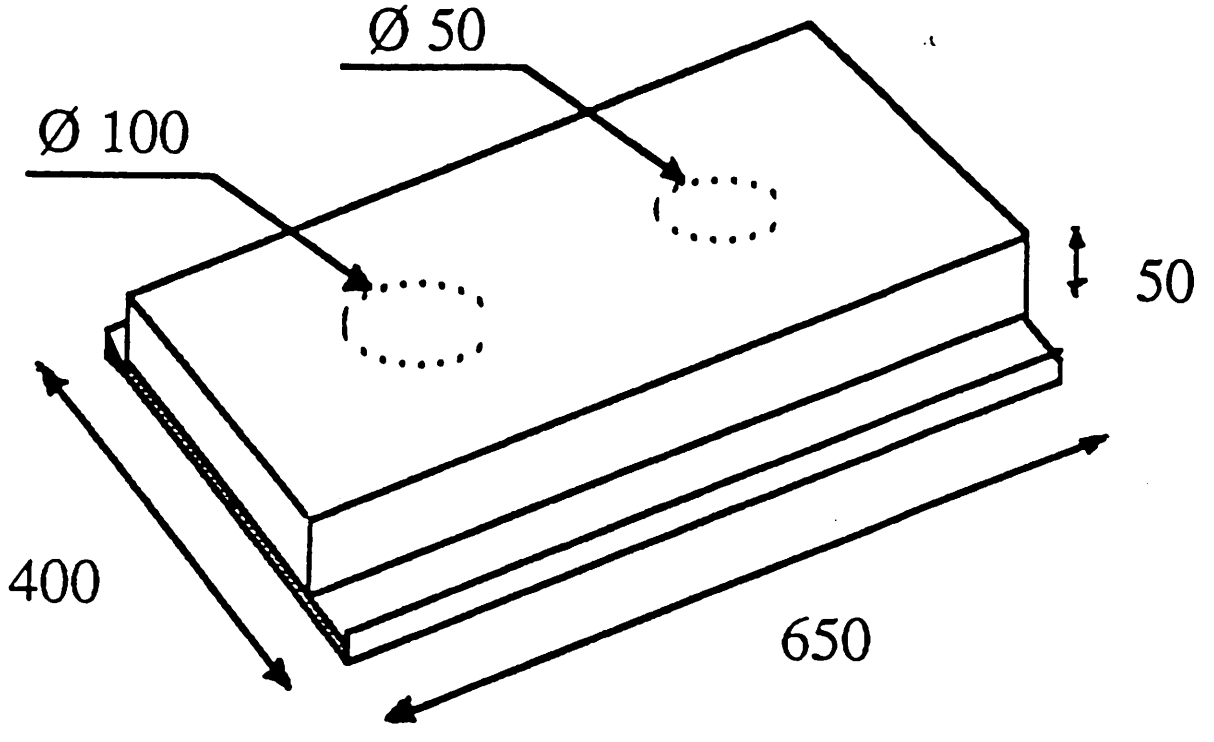

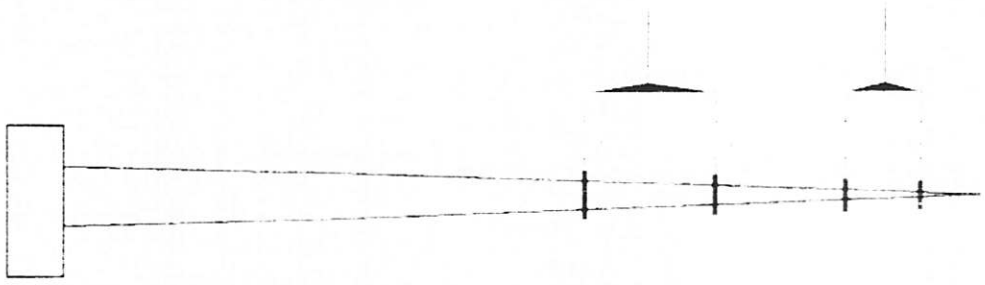

Bild 7: Lasteinleitung für Luvbiegung

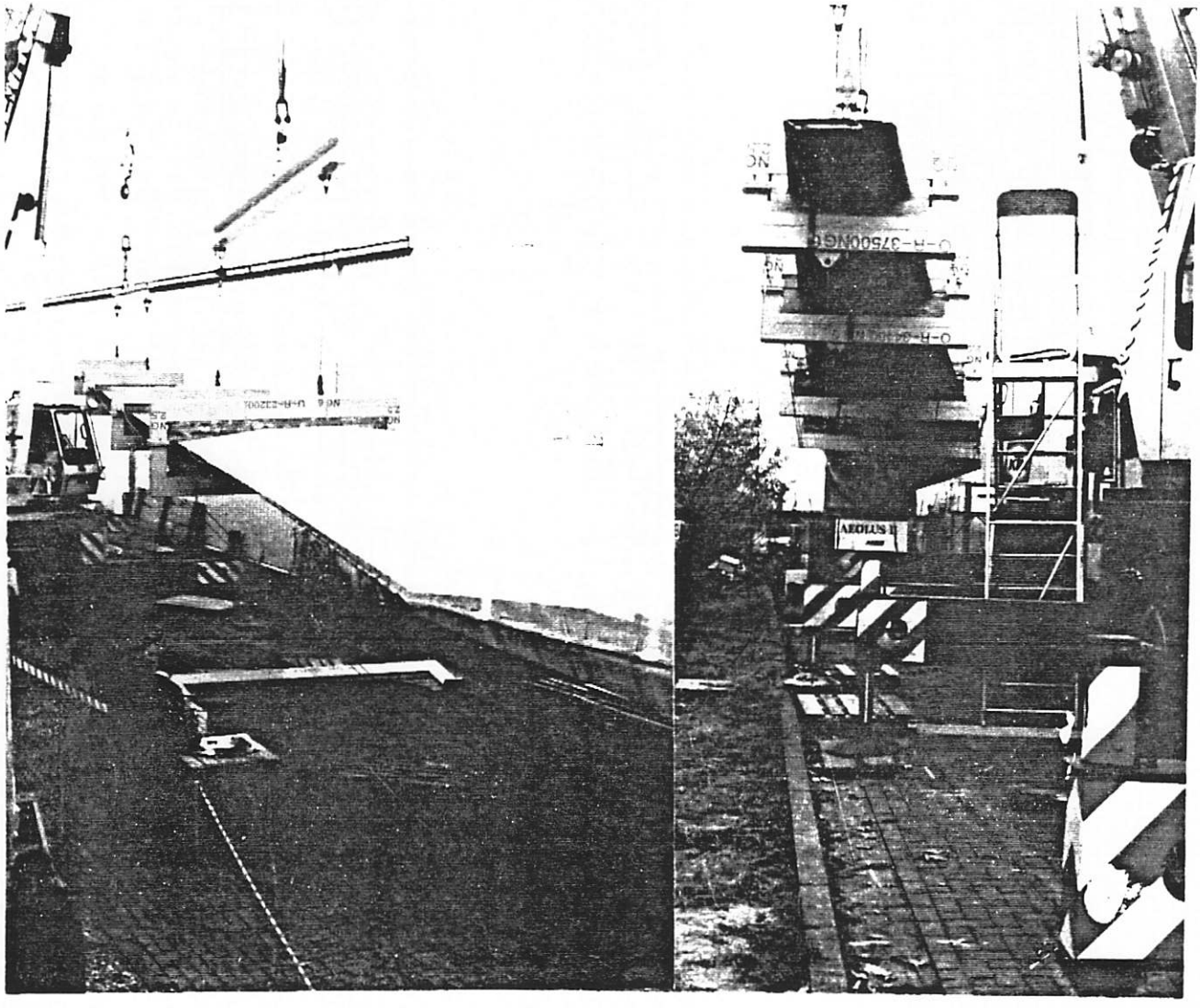

Bild 8 und 9: Versuchsaufbau für Biegung nach luv

7 cont'd

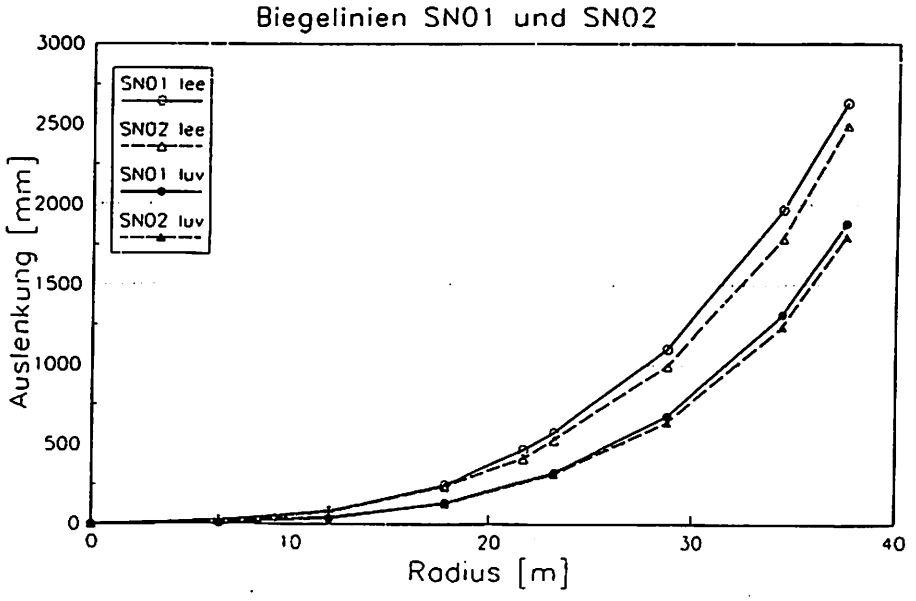
Biegelinien SN01 und SN02
SN01 lee
SN02 lee
SN01 luv
SN02 luv
Auslenkung [mm]
Radius [m]
0
500
1000
1500
2000
2500
3000
0
10
20
30
40

CONCLUSIONS

* VISUAL INSPECTION INCLUDING TAP TESTING IS EASY BUT INEXACT

* US-INSPECTION OR SIMILAR CAN BE USED FOR SMALL AREAS (BOLTS ETC)

* MEASURED VALUES FROM WORKSHOP TESTS MAYBE CAN BE USED FOR FOLLOW UP

* BLADES SHALL BE FAIL SAFE DESIGNED

* NEW INSPECTION TECHNIQUE IS A WISH

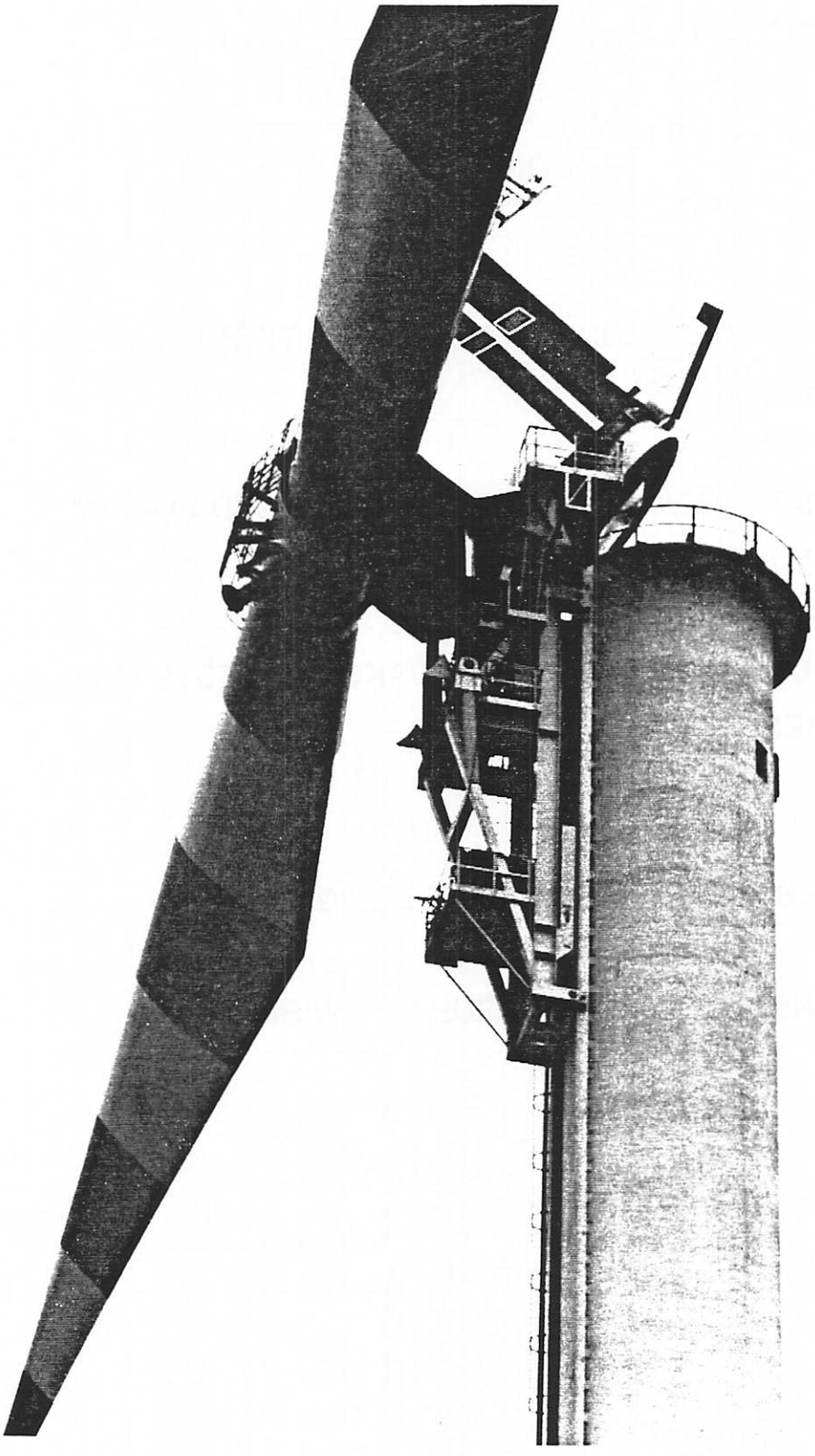

(10)

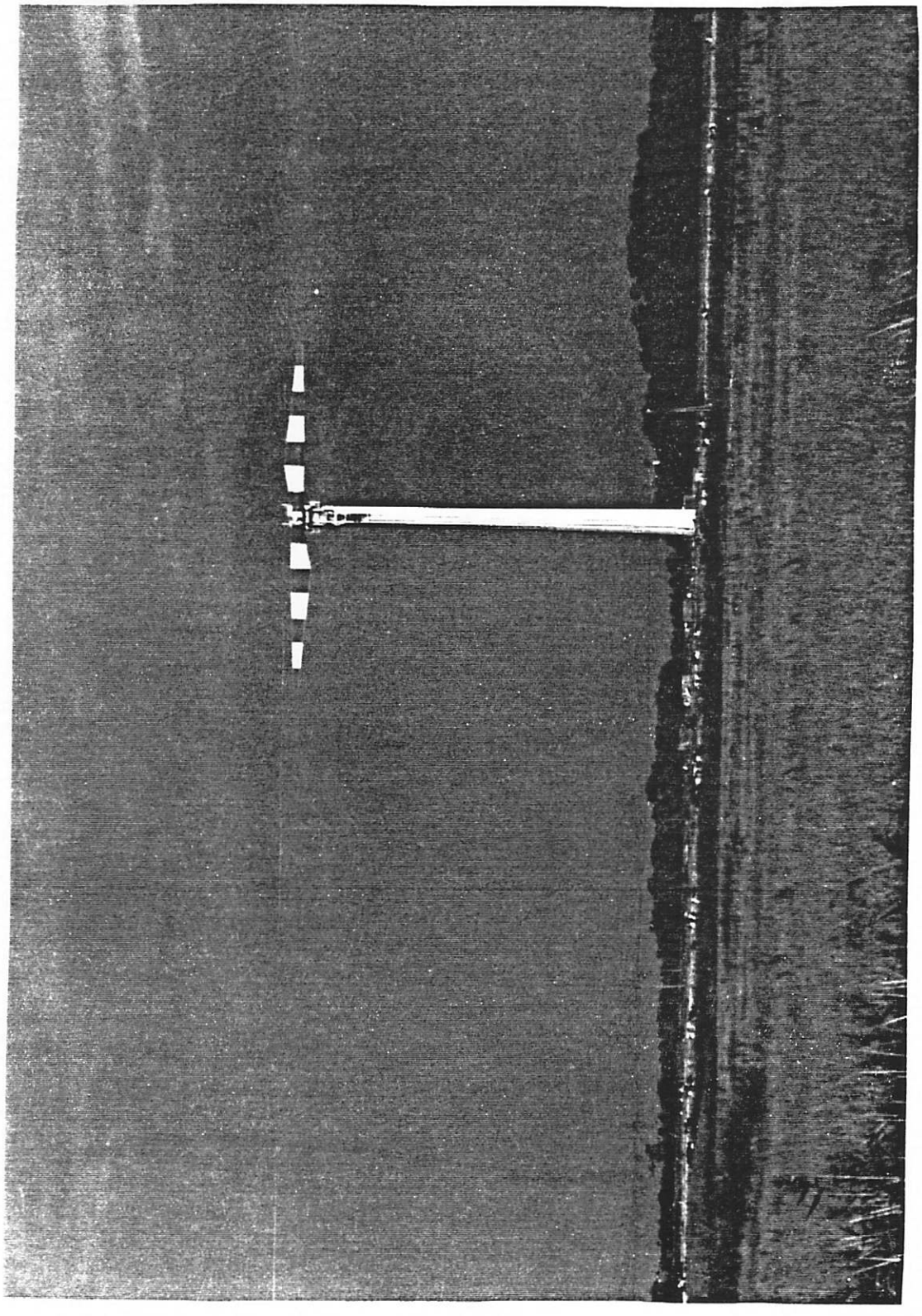

Summary

The 23rd IEA Expert Meeting on Fatigue National Renewable Energy Laboratory Golden Colorado 80401, USA October 15 - 16, 1992.

B.H. Bulder* A.J.P. van der Wekken*

Although the main subject, indicated by the IEA should be full scale test and non destructive inspection methods, the papers presented by the attendants of the meeting covered a wide range of subjects related to the fatigue of wind turbine components.

The subjects were

- material testing on coupons
  - glass fibre reinforced plastics;
  - wood;
- component (spar) fatigue test;
- full scale blade fatigue test;
- (non destructive) testing and inspection methods;
- measuring actual loads and extrapolation to a complete lifetime load spectra;
- a frequency domain method to predict fatigue life.

The authors describing material testing and the use of results of such tests in a design (I.P. Bond, D.R.V. van Delft, P. A. Joosse, G. A. Lowe and J. F. Mandell) showed many test results. G.A. Lowe and P. A. Joosse also discussed the discrepancy between coupon test and component test results. These inconsistent results can among others be caused by size or scale effects. The size effect was also discussed by M. Zuteck for the use of design data on wood from reports from e.g. building societies. Also the need to have reliable data at low stress levels as used in a real components was mentioned. This makes it necessary to perform fatigue test at a ultra high number of cycles (10^8 and more cycles). These tests are actually performed by D.R.V. van Delft and J.F. Mandell.

The authors describing component tests (G. Lowe and P.A. Joosse) reported the difficulties of performing representative test. It quite often happens that for instance the introduction of the load in the component causes the structure to behave differently compared to a real structure which make it fail much sooner than expected at forehand (using coupon data).

The authors describing full scale test (procedures) and the use of these test in the design process, (B. Bell, B.H. Bulder, D.R.V. van Delft, W. Musial and A.J.P. van der Wekken) described their facilities and

*Netherlands Energy Research Foundation ECN
Unit Renewable Energies
P.O. Box 1, 1755 ZG Petten

the test methods they use. The discussion at the end of the meeting was mainly focused on this part of the meeting. Some of the questions which arose were:

- are full scale fatigue test necessary (in the future) and for every new design;
- can these test be used to make design calculations less important or even redundant.

In general most of the participants thought it is not necessary to perform fatigue test on all new structures. If for example all concepts of which a design is built up are proven in other designs then it is not necessary to do so. Also when a design is not driven by fatigue but for instance by stiffness (stability) a fatigue test is probably superfluous.
All participants agreed that no test could make design calculations redundant.

The authors describing non destructive testing methods (I.P. Bond and B. Goransson) reported methods which can be used in laboratory surroundings and in the field. Especially the inspection in the field is very costly and difficult. The infra red condition monitoring to be used in laboratory surroundings are giving hopeful results although a good quantitative link between temperature increase and fatigue damage is still missing.

T. Kramkowski presented a paper on extrapolating relative short measurement campaigns to a lifetime load spectrum. A minimum of 5 time series of 10 minutes each for every wind speed interval is recommended. While every wind speed interval should have time series with different wind directions, to have measurements with different turbulence intensities.

H.J. Sutherland described a method to evaluate the reliability and fatigue analyses of wind turbines using a frequency synthesis method.

N.W. Bishop presented a frequency domain method to evaluate the fatigue damage. The method is based on calculating several (area) moments of different order of the power spectral density of the response spectrum. A discussion point was the cutoff frequency for calculating the moments. While in time domain the damage is relatively unsensitive to sampling at a higher frequency the result of the described method is quite sensitive to the small amounts of energy in the high frequency range.

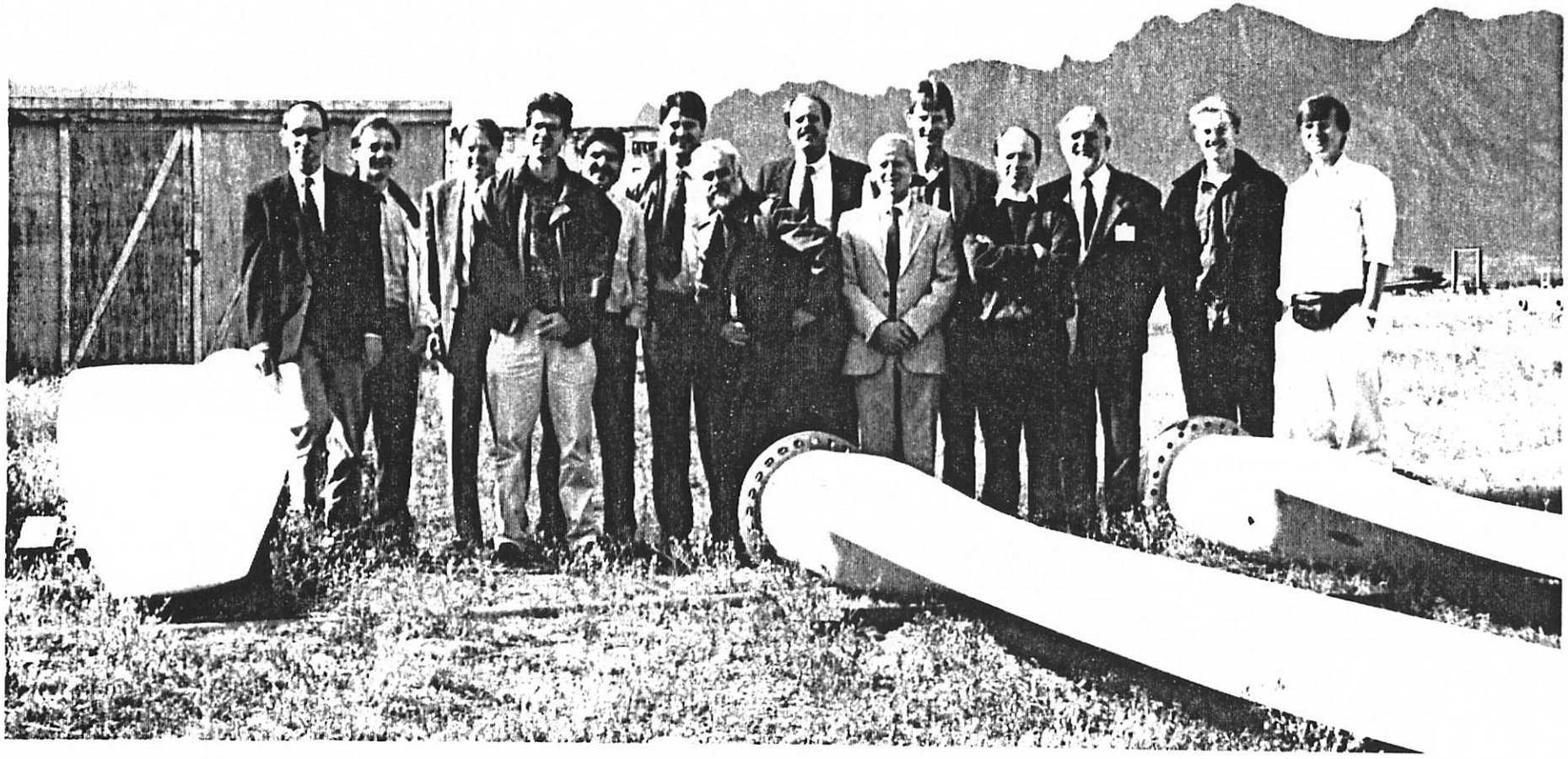

Site visit to the Structural Test Facility of the Wind Energy Test Centre in Golden.
Photograph of (most of) the delegates by N. W. M. Bishop.

LIST OF PARTICIPANTS

Ben Bill
U.S. Windpower
6952 Preston Avenue
Livermore, CA 94550
TEL: 415 455-6012
FAX: 415 443-3995

N.W. Bishop
Univ. of Sheffield
Dept. of Cicil & Structural Eng'g.
P.O. Box 600 Mappin St.
Sheffield, S1 4DU
England
Tel: 0742-768555
FAX: 0742-728910

Ian P. Bond
University of Bath
School of Materials Science
Claverton Down Bath BA2 7AY
United Kingdom
TEL: 0025-826826
FAX: 0025-826098

Bernard Bulder
Netherlands Energy Research
Foundation ECN
P.O. Box 1
1755 ZG Petten
The Netherlands
TEL: 31 2246-4482
FAX: 31 2246-3214

Sandy Butterfield
National Renewable Energy
Laboratory
1617 Cole Boulevard
Golden, CO 80401
TEL: 303 231-1171
FAX: 303 231-1199

Bengt Gransson
Kvaerner Turbin AB
P.O. Box 1005
S-681 29 Kristinehamn
Sweden
TEL: 46 550-84 800
FAX: 46 550-18 998

Susan Hock
National Renewable Energy
Laboratory
1617 Cole Boulevard
Golden, CO 80401
TEL: 303 231-7650
FAX: 303 231-1199

Peter Joose
Stork Product Engin. B.V.
Oostenburgevoorstraat 70
Postbus 379
1000 AJ Amsterdam
Holland
TEL: 20-6262011
FAX: 20-6260004

Theo Kramkowski
Deutsches Windenergie Inst.
Ebertstr. 96
D-26382 Wilhelmshaven
Germany
TEL: 49(0)4421-48080
FAX: 49(0)4421-480843

Geoff Lowe
Bristol Polytechnic
Faculty of Engineering
Coldharbour Lane
Frenchay
Bristol BS16 1QY
United Kingdom
TEL: 44(0) 272-763866
FAX: 44(0) 272-763873

John Mandell
Montana State University
Chemical Engineering Dept.
Bozemart, Montana 59717
TEL: 406 994-4543
FAX: 406 994-6098

A.J.P. van der Wekken
Netherlands Energy Research
Foundation ECN
P.O. Box 1, 1755 ZG Petten
The Netherlands
TEL: 31 2246 4482
FAX: 31 2246 3214

Walt Musical
National Renewable Energy
Laboratory
1617 Cole Boulevard
Golden, CO 80401
TEL: 303 231-1456
FAX: 303 231-1199

Michael Zuteck
MDZ Consulting
931 Grove
Kemah, TX 77565
TEL: 713 334-5681

Maribo Pedersen
Technical University of Denmark
Fluid Mechanics Dept.
Bldg. 404
Lundtoftevj 100
DK 2800 Lygby, Denmark
TEL: 45 45 93 2711
FAX: 45 42 88 2421

Herb Sutherland
Sandia National Laboratories
P.O. Box 5800
Div. 6214
Albuquerque, NM 87185-5800
TEL: 505 844-2037
FAX: 505 845-9500

Bob Thresher
National Renwable Energy
Laboratory
1617 Cole Boulevard
Golden, CO 80401
TEL: 303 231-7199
FAX: 303 231-1199

R.V. van Delft
Univ. of Technology Delft
Faculty of Civil Eng'g.
Stevinweg 1, 2628 CN Delft
The Netherlands
TEL: 31 15 783729
FAX: 31 15 782308

IEA-Implementing Agreement R+D WECS - Annex XI
Topical Expert Meetings

1. Seminar on Structural Dynamics, Munich, October 12, 1978
2. Control of LS-WECS and Adaptation of Wind Electricity to the Network, Copenhagen, April 4, 1979
3. Data Acquisition and Analysis for LS-WECS, Blowing Rock, North Carolina, Sept. 26-27, 1979
4. Rotor Blade Technology with Special Respect to Fatigue Design Problems, Stockholm, April 21-22, 1980
5. Environmental and Safety Aspects of the Present LS WECS, Munich, September 25-26, 1980
6. Reliabiltiy and Maintenance Problems of LS WECS, Aalborg, April 29-30, 1981
7. Costings for Wind Turbines, Copenhagen November 18-19, 1981
8. Safety Assurance and Quality Control of LS WECS during Assembly, Erection and Acceptance Testing, Stockholm, May 26-27, 1982
9. Structural Design Criteria for LS WECS, Greenford, March 7-8, 1983
10. Utility and Operational Experiences and Issues from Mayor Wind Installations, Palo Alto, October 12-14, 1983
11. General Environmental Aspects, Munich, May 7-9, 1984
12. Aerodynamic Calculational Methods for WECS, Copenhagen, October 29-30, 1984
13. Economic Aspects of Wind Turbines, Petten, May 30-31, 1985
14. Modelling of Atomospheric Turbulence for Use in WECS Rotor Loading Calculation, Stockholm, December 4-5, 1985
15. General Planning and Environmental Issues of LS WECS Installations, Hamburg, December 2, 1987
16. Requirements for Safety Systems for LS WECS, Rome, October 17-18, 1988
17. Integrating Wind Turbines into Utility Power Systems, Herndon (Virginia), April 11-12, 1989
18. Noise Generationg Mechanisms for Wind Turbines, Petten, November 27-28, 1989
19. Wind Turbine Control Systems, Strategy and Problems, London, May 3-4, 1990
20. Wind characteristics of Relevance for Wind Turbine Design, Stockholm, March 7-8, 1991
21. Elektrical Systems for Wind Turbines with Constant or Variable Speed, Göteborg, October 7-8, 1991

22. Effects of Environment on Wind Turbine Safety and Performance, Wilhelmshaven, June 16, 1992
23. Fatigue of Wind Turbines, Golden (Colorado), October 15 - 16, 1992
24. Wind Conditions for Wind Turbine Design, Risø, April 29 - 30, 1993
25. Increased Loads in Wind Power Stations, "Wind Farms", Göteborg, May 3 - 4, 1993

Note: Nr. 24-25 to be published